CHALMERS TEKNISKA HÖGSKOLA

CHALMERS UNIVERSITY OF TECHNOLOGY
GOTHENBURG
SWEDEN

Modelling of Turbulent Flow and Heat Transfer for Building Ventilation

Shia-Hui Peng

Department of Thermo and Fluid Dynamics

GOTHENBURG, 1998

ISBN 91-7197-646-9
ISSN 0346-718x

Vasastadens Bokbinderi AB
GOTHENBURG, 1998

CHALMERS UNIVERSITY OF TECHNOLOGY

Modelling of Turbulent Flow and Heat Transfer for Building Ventilation

by

Shia-Hui Peng

Thesis submitted for the degree of Doctor of Philosophy at the School of Mechanical and Vehicular Engineering, Chalmers University of Technology, Gothenburg, Sweden

Faculty opponent: Professor Kemo Hanjalić
Faculty of Applied Physics, Delft University of Technology, The Netherlands

Department of Thermo and Fluid Dynamics
Chalmers University of Technology
S-412 96, Gothenburg, Sweden

Gothenburg, May 1998

Errata

Page 1 (paragraph 2, line 9)
"Reynolds (1874) ..." should be "Reynolds (1884) ...".

Page 17 (equation (2.32), the last row in the ***F*** matrix)
"$f(n+e, s)$ $f(n+e, s)$ ... $f(n+e, n+e)$" should be "$f(n+e, s)$ $f(n+e, 1)$ ... $f(n+e, n+e)$".

Page 23 (equation (3.10), the last term)
"$\ldots+\nu\dfrac{\partial \overline{u_i' T'}}{\partial x_k}\Bigg]$" should be "$\ldots+\alpha\overline{u_i'\dfrac{\partial T'}{\partial x_k}}+\nu\overline{T'\dfrac{\partial u_i'}{\partial x_k}}\Bigg]$".

Page 33 (in both equations (3.41) and (3.43))
"$c_{\omega 2}$" should be replaced with "$(c_{\omega 2}-1)$"

Page 36 (equation (3.51))
" ..., $c_\omega = 1.35$" should be "..., $c_\omega = 0.75$"

Page 48 (equation (3.87))
"..., $\bar{\bar{f}} \neq 0$ and ..." should be "..., $\bar{\bar{f}} \neq \bar{f}$ and ..."

Page 68 (equation (4.29))
"$\varepsilon_w = \nu\left(\dfrac{\partial k^{1/2}}{\partial y}\right)_w^2$" should be "$\varepsilon_w = 2\nu\left(\dfrac{\partial k^{1/2}}{\partial y}\right)_w^2$"

Paper 7 (page 14, paragraph 3, line 5)
" ... in Eqs (12) and Eqs (13)." should be "... in Eqs (12) and (13)."

To

Bijun and Yifan

The thesis is based on the following papers

Paper 1
Peng, S-H., Holmberg, S. and Davidson, L. On the assessment of ventilation performance with the aid of numerical simulations. *Building and Environment*, Vol. 32, No. 6, pp. 497-508, 1997.

Paper 2
Peng, S-H. and Davidson, L. Towards the determination of regional purging flow rate. *Building and Environment*, Vol. 32, No. 6, pp. 513-525, 1997.

Paper 3
Peng, S-H., Davidson, L. and Holmberg, S. Performance of two-equation turbulence models for numerical simulation of ventilation flows. In *Proceedings of the 5th International Conference on Air Distribution in Rooms*, Vol. 2, pp. 153-160, Yokohama, Japan, 1996.

Paper 4
Peng, S-H., Davidson, L. and Holmberg, S. A Modified low-Reynolds-Number k-ω model for recirculating flows. ASME *Journal of Fluid Engineering*, Vol. 119, pp. 867-875, 1997.

Paper 5
Peng, S-H. and Davidson, L. Computation of turbulent buoyant flows in enclosures with low-Reynolds-number k-ω models. Submitted to *International Journal of Heat and Fluid Flow*, 1997 (in revision).

Paper 6
Peng, S-H. and Davidson, L. Comparison of subgrid-scale models in LES for turbulent convection flow with heat transfer. To be presented at *2nd EF Conference in Turbulent Heat Transfer*, Manchester, U. K., May 31-June 5, 1998.

Paper 7
Peng, S-H. and Davidson, L. Large eddy simulation for turbulent buoyant flows induced by differentially heated vertical walls. Report 98/8, Department of Thermo- and Fluid Dynamics, Chalmers University of Technology, Gothenburg, 1998.

Contents

Abstract

This thesis contributes to studies on the assessment of building ventilation performance and the development of turbulence models accounting for Low-Reynolds-number (LRN) effects and buoyant convection with heat transfer.

Assessments of building ventilation performance are discussed with respect to indoor air distribution and passive contaminant dispersion. Different concepts and methods for analyzing and assessing ventilation flow systems are addressed and re-examined. Several new ventilation scales have been developed, including the local purging effectiveness, the expected contaminant dispersion index and the local specific contaminant-accumulating index. Approaches for numerically exploring these scales are presented. The purging flow rate is re-formulated in several expressions different from its original and previous descriptions. Some scales defined from this quantity are discussed. Using stochastic theory in conjunction with the compartmental method, a Markov chain model is proposed to determine the transfer probability needed to compute the regional purging flow rate. This model contains extra and useful information that is not included in previous deterministic analyses. The new scales and methods are expected to be applicable for diagnosing problems and optimizing designs of ventilation systems.

The development of turbulence models based on the eddy viscosity concept is considered. For simulating turbulent recirculating flows, a comparison is made of the two-equation k-ε model, k-ω model and k-τ model. It is found that both the k-ω model and the k-τ model have relatively poor performance. Modifications are made for the k-ω model in which the model constants are re-established and the turbulent transport term in the ω-equation is re-modelled. On the basis of these modifications, a new LRN k-ω model is developed in which the damping functions are re-devised and the near-wall asymptotic behaviour is emphasized. The mechanism for simulating transition is preserved in the modified model. The LRN formulation is further extended for analyzing buoyant-driven flows in enclosures at moderate Rayleigh numbers. The model behaviour accounting for transition onset in the boundary layer along the vertical side wall is discussed, and some remarks are made for the LRN formulation. The new LRN model shows promising improvements in the predictions.

Large eddy simulation (LES) is implemented for turbulent convection flows with heat transfer. A modified subgrid-scale (SGS) buoyancy model is proposed, where the buoyant effect is explicitly accommodated in the SGS eddy viscosity/diffusivity formulation. The modification enables the model to avoid entailing no-real solutions for simulating thermal convection flows such as occurs in the original buoyancy model. Furthermore, the proposed model is able to account for some energy backscatter for flows with positive and significant thermal stratification. Comparisons and evaluations are made of several SGS models when applied to statistically stratified and unstratified buoyant flows. The performance of the SGS models is analyzed for natural convection boundary layer flows at moderate Rayleigh numbers, where laminar, transitional and fully developed turbulent flow features subsequently arise in the boundary layer. The behaviour of SGS models in accounting for energy backscatter is argued to be an essential ingredient for predicting natural transitional boundary layer flows. The failure and success of SGS models for handling this type of flow are analyzed and discussed.

Keywords

Building ventilation, ventilation performance assessment, purging flow rate, transfer probability, stochastic Markov chain model, ventilation flow, turbulence modelling, two-equation models, LRN k-ω model, turbulent buoyant convection, transition regime, large eddy simulation, SGS modelling, modified SGS buoyancy model, energy backscatter

Acknowledgements

This work was funded by the Swedish National Institute for Working Life, Stockholm (ALI, formerly the Swedish National Institute of Occupational Health), where I have been employed since March, 1995. The doctoral program was carried out in cooperation with the Department of Thermo- and Fluid Dynamics at Chalmers University of Technology (CTH), Gothenburg, under the supervision of Prof. Lars Davidson.

I am deeply indebted to Prof. Lars Davidson for his support and well-informed advice, for his encouragement and never-fading enthusiasm. Lars has read all the manuscripts and abstracts I have produced during the past three years and provided me with constructive criticism through which much knowledge has been gained. Lars has always had the time and patience to carry on discussions with me over the phone and during my visits in Gothenburg.

Dr. Sture Holmberg, who helped to initiate this program at ALI, deserves many thanks for his constant interest in and support of my work, and for sharing with me his interesting views on engineering research and Swedish social life. I also appreciate Sture as a good friend.

I am grateful to Prof. Lars Olander, Dr. Anders Jansson and Prof. Staffan Krantz, the leaders of the Ventilation Research Group and of the Technology Division at ALI, for their enthusiasm and support, and for providing me with favourable research conditions and a number of opportunities to attend international conferences, symposiums and courses. Lars and Anders have also kindly read a part of the chapter on ventilation performance, and offered me enlightening comments.

I should like to express my gratitude to Prof. Folke Peterson, the head of the Division of Heating and Ventilation, Department of Energy Technology at the Royal Institute of Technology, Stockholm. Folke initially invited me to work and study in his division, where I experienced different aspects in research of heating and ventilation and received my Licentiate in Engineering. I also wrote two computer codes (Vent2D and Vent3D) for the numerical simulation of ventilation flows. The experience gained through that course proved to be of great use. I particularly appreciate his understanding when I decided to leave for my present position and studies.

I would like to express my thanks to all my colleagues at ALI, for creating and sharing together a friendly working environment. Inger Wahlbeck, our group secretary, has always been patient and efficient, for which I am very thankful. I wish to thank Sten Lundström, our computer supporter, for providing me with help and information on a number of up-to-date computer software and hardware. My thanks also go to Sven Alenius, Andrzej Paprocki, Johan Johansson and Björn Nilsson for their friendship over the years. It has always been a joyful time to run together with Sture and Sven, and to break our own time records.

I wish to thank all the people at the Department of Thermo- and Fluid Dynamics, CTH, for their support in different ways. I would like to mention Prof. Erik Olsson, who supported and discussed my study program at CTH in the initial stage, and Mrs. Birgitta Hultman, the Department secretary, who kindly helped to arrange accommodations for my stay of two short terms in Gothenburg.

I am very grateful for the encouragement and support from my relatives in China. Finally, but foremost, I want to thank my wife, Bijun, and my son, Yifan, for their love, support and patience during these years of study. Without them, life would not be as rich and colorful.

Nomenclature

C	contaminant concentration, also model coefficient in SGS models
C_t	model coefficient in SGS models
$C(\infty)$	concentration at steady state
$C(t)$	transient concentration at time t
$\langle C \rangle$	room-averaged concentration
C_f	wall friction coefficient
c	turbulence model constant with various subscripts
c_p	specific heat at constant pressure
D	diffusivity in general form
E	constant in the wall function (4.23), $E = 9.0$
$f(i, j)$	transition probability from state i to state j
f	damping function with various subscripts
G	buoyant source term in the k-equation
g_j	gravitational vector, $g_j = (0, -g, 0)$
H	height of computational domain
h	height of step for backward-facing step flow
$\boldsymbol{I}$	initial state space
k	turbulence kinetic energy
L_t	turbulent length scale
n	number of compartments divided in a space
N_k	net production of k per unit dissipation term
N_ω	net production of ω per unit dissipation term
Nu	Nusselt number, $Nu = -(\partial T/\partial x)_w H/\Delta T$
p	pressure
p'	pressure fluctuation
P_{ij}	transfer probability from location i to location j
Pr	molecular Prandtl number, ν/α
Pr_t, σ_t	turbulent (or SGS) Prandtl number
Q	supply air flow rate
q	contaminant release rate or heat flux
R_p	residual turnover flow rate for region p
Ra	Rayleigh number, $Pr\,(g\beta\Delta T H^3/\nu^2)$
Re	Reynolds number
Re_τ	Reynolds number based on friction velocity, u_τ, for channel flow
R_t	turbulent Reynolds number
$\boldsymbol{S}$	state space
S_c	source term in the concentration equation
S_ϕ	source term in the thermal energy equation
T	temperature
T'	temperature fluctuation
U_p	purging flow rate for region p
$\mathbf{u}$	velocity vector
u_T	velocity scale for buoyant flow, $u_T = (g\beta\Delta T H)^{1/2}$
u_i	velocity components in the x_i directions
u_τ	friction velocity
u', v', w'	velocity fluctuations in x, y, z directions, respectively

V_t	turbulent velocity scale
V	volume of the flow system
W_p	turnover flow rate for region p
X	notation for the station visited by a passive tracking particle
x_i	Cartesian space coordinates
y_{tr}	location of transition onset

Greek letters

α	thermal diffusivity
α_t	turbulent (or SGS) thermal diffusivity
β	thermal expansion coefficient
Δ	width of grid filter
$\tilde{\Delta}$	width of test filter
ΔT	temperature difference
δ_{ij}	Kronecker delta
$\delta\tau$	variation of local mean air age
ε	dissipation rate of k
κ	von Kármán constant
μ	dynamic molecular viscosity
μ_t	turbulent (or SGS) viscosity
ν	kinematic viscosity, μ/ρ
ν_t	turbulent (or SGS) kinematic viscosity, μ_t/ρ
ρ	density of fluid
σ_k, σ_ε, σ_ω	turbulence model constants
τ	turbulent time scale or local mean air age
τ_n	nominal time constant, V/Q
ω	specific dissipation rate of k
ζ	similarity variable, (3.63)

Subscripts

b	buoyancy
e	exhaust
I	interior state
in	inlet
O	outlet
p	location/region or state p
rms	root-mean-square
s	supply or shear
sgs	subgrid scale
w	wall

Other symbols

∇	nabla operator
$< >$	averaging over time and/or space
$\bar{\phi}$	filtered variable on grid filtering level
$\tilde{\phi}$	filtered variable on test filtering level

Chapter 1

Introduction

Fluid flow and heat transfer are ubiquitous phenomena in nature and in engineering applications. Examples are air circulation and radiative heat transfer in the atmosphere, water eddies and fronts in oceans, blood flow in human bodies, combustion in engines of automobiles and aircraft, and heating and ventilation in buildings. The fluid motion in most cases does not hold a well-structured behaviour in terms of laminar flow. The flow will instead evolve further and eventually exhibit a chaotic type of motion known as turbulence. The reason that turbulence is so prevalent in fluids of low viscosity is that steady laminar flows tend to become unstable at high Reynolds numbers or Rayleigh numbers. Instability to small disturbances is an initial step in the process whereby a laminar flow becomes turbulent through transition.

Along with a turbulent thermal flow, convective heat transfer is naturally not separable from chaotic motion features therein. By contrast, it is closely correlated with random fluctuations of fluids in space and time and is embodied in physical transport processes of turbulence. Many turbulent flows of engineering interest are non-isothermal and are therefore accompanied by heat transfer; examples are chemical reacting flows in combustion chambers, flows in solar energy collectors and air flows in ventilated rooms. As heat transfer occurs in a turbulent flow, it always emerges as a chaotic turbulent type, where the temperature field, like the velocity and the pressure fields, is characterized by rapid and random fluctuations. Reynolds (1874) might have been the first to point out that, in turbulent flows, there must exist an intimate relation between the local shearing stress and the local heat flux since both depend upon the same basic mechanism. This has consequently opened the way for more than a century of modelling turbulent flows with heat transfer.

Experimental measurements have commonly been used and have contributed tremendously to the development of turbulence research, while theoretical analyses have greatly enhanced our understanding on turbulence mechanisms. Classical turbulence theories were generally set up through analytical deductive approaches in the work of several pioneering researchers, such as O. Reynolds, L. Prandtl, Th. von Kármán, G. Taylor and A. Kolmogorov. Their contributions have formed the cornerstone of modern turbulence theories.

During the last decades, the rapid development in digital computers has brought about another technique as an up-to-date tool for exploring turbulent flow and heat transfer, that is, computational fluid dynamics (CFD). CFD deals with the numerical solution of fluid dynamic equations. It is used for basic studies of fluid dynamics, for engineering designs of complex flow configurations, for basic and applied research into the nature and properties of turbulence and for extrapolation into parameter regimes that are relatively inaccessible or very costly to study experimentally (Boris, 1989). Applying direct numerical simulation (DNS) to the dynamic equations for a full resolution ranging from the smallest to the largest scales in a fluid motion, CFD has so far been able to give solutions only for turbulent flows at low Reynolds numbers owing to the prohibitive requirements for computer power. Alternative approaches have thus been developed in which the small scales or the fluctuating motions are ruled out so that the fluid dynamic equations represent only the evolution of large scales or the mean field. As a consequence, very few non-trivial predictions can be made on the resultant unclosed equation system. The equations for the nth order correlation contain unknowns in terms of the $(n+1)$th order and so on, *ad infinitum*. This in turn gives the so-called *closure problem*. It is important in numerical simulations of turbulent flow and heat transfer to model these un-

knowns on a certain level of order so that the equation system can be closed and is numerically solvable.

CFD has been widely applied to various engineering flow problems. A field in which CFD is becoming increasingly active for system design, optimization and diagnosis is heating and ventilation in buildings. One of the basic objectives of ventilation is to control and remove pollutants and/or excess heat to achieve the desirable indoor air quality and thermal environment. CFD has been proven to be an efficient approach for analyzing indoor air flow, heat transfer and contaminant dispersion processes. Particularly, it has often been employed to explore ventilation efficiency and effectiveness to indicate whether the air motion in a room is well organized.

The air motion in a ventilated room is generally of an incompressible, non-isothermal and turbulent type. Nonetheless, indoor air flow possesses some specific features stemming from practical requirements on building ventilation. In many cases, ventilation flows are characterized by low-Reynolds-number (LRN) turbulence with mixing and recirculating air motion. Such general and specific flow characteristics must be well accounted for in turbulence modelling in order to make reliable system analyses by means of numerical simulations.

This work contributes to the numerical simulation and modelling of incompressible turbulent flows with or without heat transfer, especially of flows in ventilated rooms. With the aid of numerical simulation, some new scales for assessing ventilation flow systems have been proposed. Stochastic theory, together with numerical methods, has been used to analyze passive scalar transport in ventilation flow or equivalent internal flow systems. When solving engineering flow problems, particularly ventilation flows, two-equation turbulence models remain the most frequently used. One part of this work has thus been directed towards a development based on two-equation models which are capable of dealing with low-Reynolds-number turbulent recirculating flows and turbulent buoyant flows with convective heat transfer. To further examine and evaluate more advanced turbulence models, large eddy simulation (LES) has been implemented and formed a part of the modelling work. This has been aimed primarily at evaluations of subgrid-scale (SGS) models for handling turbulent buoyant flows.

Since, as mentioned above, the application is especially emphasized for building ventilation, a general description of indoor airflow characteristics is first given in Chapter 2, whereafter some new development and methods on the assessment of ventilation flow systems are presented. Chapter 3 discusses the modelling of turbulent flow and heat transfer, including analyses of the behaviour of LRN two-equation models and some SGS models in LES. The methodology used in numerical simulations, including numerical methods and boundary conditions, is addressed in Chapter 4. General findings and new development have also been included in these chapters. In Chapter 5, conclusions are derived from this study, and the papers on which this thesis is based are briefly reviewed in a short summary.

Chapter 2

On the Assessment of Ventilation Flow Systems

The flow pattern in a ventilated room is created in accordance with practical purposes that may vary largely for different ventilation applications. Bearing this in mind, it is then recognized that the flow field varies from case to case owing to various requirements on ventilation. Basically, ventilation means the exchange of contaminated and/or over-heated/cooled indoor air with make-up fresh air. In practice, the role of ventilation in the creation of a healthy and comfortable indoor environment involves a number of other aspects, e.g., room geometry, outdoor climate and indoor heat and/or contaminant sources and sinks. Using either experimental methods or CFD techniques, all these and other factors must be considered in studies of flow behaviours and heat and mass transfer processes in ventilated spaces. To set up a background, we start with a brief description of general requirements on building ventilation.

2.1 General Requirements on Ventilation

In general, the objective of building ventilation is, with as low an energy cost as possible, to create an indoor air quality and thermal condition more suitable for people and processes than what naturally occurs in the unventilated building. The value of ventilation thus lies in how well basic needs are fulfilled, such as an indoor environment that does not endanger health and is comfortable and promotes productivity. General requirements for advanced ventilation can thus be summarized as: to create a healthy *indoor air quality* and a comfortable *indoor thermal condition* with as low as possible *energy consumption*.

2.1.1 Indoor Air Quality

The basic objective of a ventilation system is to achieve acceptable indoor air quality. This concerns the effectiveness of a system in removing/diluting contaminants and smell and involves the properties of contaminant sources. Studies on the so-called *sick-building syndrome* (SBS) have been very extensive in recent years, see e.g. Sundell (1994) for details. A sick-building causes occupants to complain of illness symptoms such as headache, fatigue, and irritation to skin, eyes, mucous membranes or airways.

It is admitted that there are close connections between building ventilation and SBS symptoms. Inadequate ventilation is a common denominator in buildings with SBS problems (NIOSH, 1987; Turnner and Binnie, 1990). It has been argued that the prevalence of SBS symptoms is related to ventilation air flow rate, type of ventilation system and room air motion. The distribution of room contaminants is ordinarily a function of source properties and ventilation. Contaminants in a room are transported either passively or dynamically. This makes it possible to study contaminant dispersion by means of CFD techniques. For passive contaminants, the scalar mass transport equation coupled with the equations governing the air motion can be numerically solved to reveal pollutant distributions, see e.g. Gan *et al.* (1991) and Peng and Davidson (1998c). For particulate contaminants that are dynamically transported with air motion, particle deposition and dispersion can be studied by a stochastic treatment of the particle-turbulence interaction in which the trajectories of particles of representative sizes can be tracked and computed in numerical simulations, see e.g. Lu and Howarth (1995) and Riffat *et al.* (1995). Other advanced methods are also applicable for this purpose, e.g., using a probability density function (PDF) evolution equation to determine the PDFs of the particle velocities and positions (Lockwood and Papadopoulos, 1989).

2.1.2 Thermal Comfort

Thermal comfort is another important aspect closely related to building ventilation. It concerns the thermal sensation of the occupants in ventilated rooms. A number of indices have been introduced to quantitatively describe the thermal environmental conditions and are used in guidelines for design and evaluation of thermal comfort. Fanger and co-workers (Fanger, 1982; Fanger *et al.*, 1988) proposed a set of empirical and comprehensive thermal sensation indices, including the predicted mean vote (PMV), the predicted percentage of dissatisfied (PPD) and the percentage of dissatisfied due to local draught (PD).

These indices are related to indoor air velocity, air temperature, air humidity, turbulence intensity, mean radiant temperature and the human body's conditions of clothing and activity. Thermal comfort is thus essentially influenced by indoor air flow and heat transfer processes. It can be achieved by many different combinations of the above variables, which will create an optimal thermal environment for occupants. Using empirically formulated expressions, local thermal sensation indices are predictable, as they are incorporated into numerical simulations for indoor air flow and heat transfer in ventilated rooms, see e.g. Kaizuka and Iwamoto (1987) and Gan (1994).

2.1.3 Energy Consumption

Energy consumption concerns the energy cost effectiveness and efficiency in buildings with heating, ventilation and air-conditioning systems. The computation of thermal loads, i.e. heating load and cooling load, is related to convective heat transfer over the building enclosures, radiative heat transfer between enclosure surfaces with temperature differences, and conductive heat transfer through enclosures. All these heat transfer processes can in principle be modelled and predicted by means of numerical simulations.

Convective heat transfer is regarded as one of the most important processes, where heat is exchanged through air-to-wall and air-to-air convection. The determination of a wall convective heat transfer coefficient relies essentially on the air flow pattern created by a ventilation system. An erroneous determination of this coefficient will lead to significant inaccuracy in calculated thermal loads, see Bauman *et al.* (1983). Convective heat transfer over a cold window, for example, may differ from that along an infinite flat plate (Peng and Peterson, 1995). Conductive heat transfer is related to a changeable outdoor climate, usually entailing heat gain in summer and heat loss in winter. Its determination thus depends on outdoor climate data and requires a long time period of transient simulation to perform an extensive analysis. In traditional designs, thermal loads are often calculated by assuming a uniform indoor air temperature. With numerical simulations, local indoor air temperatures can be used to improve computations of heating and cooling loads (Chen, 1988). Radiative heat transfer within buildings occurs between wall surfaces with a temperature difference, as well as through fenestration areas owing to solar radiation, see e.g. Chen (1988) and Li (1992). The heat sources in a room, e.g. heating radiators and cooled ceiling air-conditioning devices, often entail radiative heat transfer and thus affect the ventilation flow pattern.

In general, indoor air quality, thermal comfort and energy consumption form the basic disciplines in ventilation system designs. They are therefore the virtual starting points for assessing system performance. These three aspects can be explored in detail with the aid of numerical simulations. In ventilation practice, CFD has come to be a powerful technique and is used to investigate system performance, diagnose system problems and improve system designs. The development of CFD as a reliable alternative and complement to conventional experimental measurements is thus of practical importance in building research to realize basic requirements on building ventilation.

2.2 Features of Ventilation Flow

To achieve an acceptable indoor environment with low energy consumption, the principal task of building ventilation is to control mass and heat transfer processes through well-organized air movements. With only the ventilation device, such control is achieved through air supply and exhaust by alteration of the supply air flow rate and air temperature and the location and shape of supply and exhaust openings. This is however insufficient to control room transport phenomena that may also be significantly affected by other factors, including the arrangement of indoor heat and/or contaminant sources and obstacles, the type and geometry of room enclosures and so on. Building ventilation is thus far more complicated than a supply-and-exhaust flow system.

Ventilation flow is often internal air motion arising in enclosures. Most ventilation flows encountered in practice are of an incompressible, non-isothermal type with significant heat transfer. Usually, ventilation is used to decrease occupants' exposure to pollutants by supplying fresh air to contaminated spaces. The contaminant is diluted through efficient mixture with local or global recirculating and mixing air motion, whereupon turbulence is generated. Therefore, ventilation flow is often turbulent flow. Further, to avoid draft risk caused by low air temperatures and high air velocities and turbulent fluctuations, air motion in the occupied zone must be controlled so that it is characterized by low-velocity and low-Reynolds-number turbulence. Moreover, boundary layer flows often occur along solid wall surfaces. As non-adiabatic walls are exposed to a colder or warmer outdoor climate, the boundary layer flow is then of a natural convection type induced by buoyancy, owing to a temperature difference between the wall surface and ambient indoor air.

In addition to these generally viewed flow features, ventilation flow exhibits other flow behaviours in different regions of a ventilated space (Peng, 1994). Typical flow characteristics include wakes and vortex shedding behind obstacles, potential flows near exhaust openings, thermal jets or plumes arising above heat sources, and laminar and transitional flows in near-wall boundary layers and in regions far from walls due to dampened turbulence with thermal stratification. These and other flow phenomena are associated with the ventilation system used: they may appear when using one system, and may not with another.

According to the approach of withdrawing air from a space, ventilation systems are classified into two types: *local ventilation* and *general ventilation*. The former, which is widely used in industrial ventilation, exhausts air and contaminants from a limited region where pollution sources are located. Some local equipment is thus used, such as a laboratory fume hood, glove box and canopy hood etc. (Heinsohn, 1991). With the latter type, the air is extracted from the entire space and replaced with make-up fresh air. General ventilation of different types is the main consideration in this work.

According to the approach of supplying air to a space, general ventilation is further classified into *natural ventilation*, *mixing ventilation* and *displacement ventilation*. Natural ventilation does not rely on any mechanical system. Instead, room air motion is created by indoor and outdoor temperature or pressure differences through infiltration and exfiltration. Mixing and displacement ventilation systems are the most used types, which rely on mechanically driven systems built with fans, ducts, filters and air diffusers etc.. These two systems are briefly described here.

2.2.1 Mixing Ventilation

In mixing ventilation, fresh air is supplied at a high momentum to induce overall recirculation and promote sufficient mixture of contaminants and fresh air. It thus aims at diluting the contamination level down to an acceptable level. To avoid sensible air draught in the occupied

zone, the supply opening (usually a slot) is often installed at ceiling level. The inflow is in most cases a wall jet. As the initial momentum is large enough (often, it is), the wall jet is then able to reach the opposite wall and consequently becomes an impinging jet.

Although the wall jet is generally characterized by fully developed turbulence, the air motion in the occupied zone is often characterized by low velocities induced as a result of jet entrainment and air recirculation. Nielsen (1989) showed that the maximum velocity in the occupied zone is linearly proportional to supply air flow rate for isothermal mixing ventilation flows. If the ventilation air flow rate is lower than four air changes per hour (ACH), however, this proportionality no longer holds and the velocity decays more sharply. Using relatively small supply air flow rates ($\leq$ 3 ACH), Sandberg *et al.* (1991) measured near-wall velocity distributions in a room with mixing ventilation. An interesting finding is that the conventional *log-law* of walls, widely used as a wall function for velocity in indoor air flow simulations, is altered.

Ventilation flow is in most cases non-isothermal. As the wall function for velocity differs from the conventional one, there is reason to worry about predictions of near-wall convective heat transfer. Furthermore, the wall function for temperature that remains in common use is empirically derived from experimental data for pipe flow. For natural convection boundary layers, where the flow is dominated by buoyancy, this wall function, as well as that for velocity, should not be expected to perform well. In a measurement on natural convection boundary layer flows along a cold window with simulated floor heating, Peng and Peterson (1995) showed that the convective heat transfer coefficient over the window surface even possesses a behaviour different from that along an infinite, heated/cooled vertical flat plate.

2.2.2 Displacement Ventilation

In displacement ventilation, cooled fresh air is supplied at floor level with a low momentum. Upward buoyant convection created by indoor heat sources carries contaminants into the upper zone, where recirculation and mixture occur and contaminated air and/or excess heat are exhausted. This system thus aims at directly delivering fresh air into the occupied zone without inducing (or with insignificant) mixture with contaminants. The buoyancy thus becomes the virtual origin of air motion. The mechanism of inducing buoyancy relies on the behaviour of both air supply and heat sources. To investigation the performance of this system, special attention must be paid to air supply, buoyant convection, and their interaction (Peng, 1998c).

A comprehensive description of this ventilation system can be found in, e.g., Nielsen (1993) and Mundt (1996). Since the air is supplied at a low velocity and at a temperature of usually 2–4 ^{o}C lower than the mean room air temperature, the inflow forms a gravity current due to buoyancy and spreads over the floor surface. Heat sources (e.g. people, lamps and computers etc.), on the other hand, create upward thermal plumes, entraining surrounding ambient air and rising to the upper zone. The flow is thus characterized by stable thermal stratification with nearly linear vertical temperature distribution in the room. Nevertheless, recirculating and mixing air motions often occur locally, owing to the entrainment of thermal plumes and the downwards natural convection along non-adiabatic cold wall surfaces. Furthermore, the plumes created by heat sources may entail local turbulence damping in the vertical direction and trigger locally anisotropic turbulence. In the lower zone, weak turbulence often tends to be relaminarized. In numerical simulations, displacement ventilation flows are generally more difficult to handle than mixing ventilation flows. Davidson (1989) showed that a low-Reynolds-number (LRN) turbulence k-ε model often fails to give a turbulent solution when it is applied to this type of flow. Instead, an unrealistic laminar solution is recovered in the whole flow domain without predicting any turbulent transport, as it actually should.

2.2.3 General Problems in Modelling Ventilation Flows

Numerical simulation has been applied to ventilation flows for more than twenty years. A brief historical review can be found in, e.g., Peng (1994). The current status and potential capabilities and limitations of using CFD for analyzing indoor air flows were discussed by, e.g., IMechE (1991), Jones and Whittle (1992), Peng (1994) and Chow (1996). Among the existing turbulence models, two-equation type closures, particularly the conventional k-ε model (Launder and Spalding, 1974) and its variants, have been the most used approach in numerical simulations of indoor air flow and heat transfer. Due to the complex flow characteristics in a ventilated space, three principal and problematic aspects must be well accounted for when carrying out numerical simulations with a two-equation model to achieve reliable predictions.

- Using the conventional wall functions might be an inappropriate approach for near-wall treatment, particularly when the flow is not fully developed turbulence (e.g. with low supply air flow rate) and when the flow is characterized by separation and affected by thermal buoyancy force.
- Using turbulence models without incorporating LRN formulation, for example the standard high-Reynolds-number k-ε turbulence model, might be one of the main sources of error in predictions since most ventilation flows are characterized by LRN turbulence.
- Using LRN turbulence models that cannot accommodate well near-wall turbulence behaviour associated with buoyancy effects and laminar-turbulence transition might result in predictions deviating far from reality in air-to-wall convective heat transfer and in computed mean flow field.

The first aspect has attracted some attention and attempts have been made to develop new wall functions from analyses of natural convection boundary layer flows along vertical flat plates, see e.g. Yuan *et al.* (1993) and Peng and Peterson (1994). The applicability of such wall functions is however questionable in regions near horizontal walls. The second aspect is a consequence of the first since the wall-function method is often used together with a high-Reynolds-number (or the standard) turbulence model to serve as a bridge between the near-wall viscous sublayer and the outer layer where turbulence is fully developed. On the other hand, as stated above, low-Reynolds-number turbulent flows and even laminar flows not only occur in near-wall regions, but can also exist in regions far away from walls in a ventilated room. A high-*Re* turbulence model will apparently mislead the simulation when handling such flows. Furthermore, local relaminarization and transitional phenomena in particular require appropriate modelling that is able to account for flows that develop from laminar to turbulence through transition, which often occurs in natural convection boundary layers along non-adiabatic wall surfaces. The third aspect concerns LRN modelling for buoyancy-driven (or significantly affected) ventilation flows where thermal stratification is of importance for turbulence generation or destruction.

These general problems thus call for advanced turbulence models that are capable of handling ventilation flows of different types, different flow features existing in one flow, particularly for flows with low-Reynolds-number turbulence and with heat transfer, and flows in which laminar, transitional and turbulent phenomena co-exist. This has motivated the devotion of a large part of this work to the development and investigation of LRN-type models and of advanced modelling methodology based on large eddy simulations. In addition, it is worth mentioning that turbulence modelling for indoor air flows needs also to consider non-isotropic effects caused by thermal plumes arising in stratified surroundings, which have been often encountered in rooms with displacement ventilation, see e.g. Davidson (1990).

2.3 Assessment of Ventilation Performance

As a flow system is set up, some relevant measures are needed to quantify heat and mass transfer processes occurring in the system for engineering purposes, such as diagnosing system problems and optimizing system designs. With a ventilation system aiming at improving indoor environment, such a measure is often devised to indicate the efficiency of delivering make-up (filtered, heated or cooled) fresh air and the effectiveness of removing contaminants and/or excess heating/cooling load. It is usually termed as a *scale* for assessing ventilation performance. For ventilation flows, nearly all the flow quantities can have individual effects on the assessment of the indoor environment. These may include mean air velocity, temperature, pressure, air humidity, turbulence quantities, heat transfer coefficient, contaminant concentration and so on. When applied to an assessment of ventilation performance, such a large category would be a tiring list for practical use. In principle, numerical simulation is indeed able to provide detailed figures for a number of individual quantities, but they are often not standardized or constructed as independent scales for ventilation performance assessment.

Processes arising in some specific zones/regions are usually more interesting than in the whole ventilated space. A typical example is the occupied zone since ventilation is essentially used for the comfort of the occupants. When analyzing risk of exposure to contaminants, the breathing zone of the occupant is another specific region. This suggests that zonal or local scales are more relevant than global ones. Using only globally-averaged simple scales, for example the mean room concentration and the turnover time of contaminants, is obviously not enough to assess a ventilation flow system. Moreover, owing to complex ventilation flow phenomena, a simple global scale could fail to explore and indicate the effect of some local, substantial mass/heat transfer processes. When exploring local/zonal scales, it may be noted that the characteristics of mean flow resulting from the action of turbulence is often emphasized more than the turbulent motions themselves. This is particularly true when the scales are constructed by means of the mean flow field to quantify ventilation performance in supplying fresh air and removing contaminants.

2.3.1 Basic Aspects of Assessing Ventilation Performance

Scales used to assess a ventilation flow system can be classified into the following three groups (Peng *et al*., 1997a):

a) *Ventilation air diffusing efficiency*. This includes scales that evaluate ventilation performance by indicating how efficiently fresh air has been supplied and delivered to a space;
b) *Ventilation effectiveness*. This includes scales that evaluate ventilation performance by indicating how effectively passive contaminants in a space can be removed or diluted by ventilating air flows;
c) *Specific ventilation effectiveness*. This includes scales that evaluate the ability of ventilating air to remove or dilute contaminants for a specific application.

A number of scales have been proposed to accommodate these aspects. Comprehensive reviews on different scales have been given by e.g. Skåret (1984), Etheridge and Sandberg (1996). In the construction of these scales, two basic quantities have often been used, i.e., the contaminant concentration, C, and the local mean age of air, τ. The concentration is a well-known quantity that indicates the amount of contaminants residing in a unit volume of air. Its distribution in an air flow follows the mass transport equation, given by

$$\frac{\partial C}{\partial t} + \nabla \cdot (\mathbf{u}C) = \nabla \cdot (D \nabla C) + S_c \qquad (2.1)$$

The local mean age of air *statistically* expresses the mean time it takes for air to reach an arbitrary point after entering a system. It represents the *freshness* of the air at the location. It is a passive scalar quantity and is governed by a transport equation (Spalding, 1972),

$$\nabla \cdot (\mathbf{u}\tau) = \nabla \cdot (D \nabla \tau) + 1 \qquad (2.2)$$

This parameter can be used to passively *track* the air flow. Other important scales include the purging flow rate, the contribution ratio of supply openings and the residence time distribution (RTD), see e.g. Peng *et al*. (1997a). The origin of some ventilation scales can be found in chemical engineering where analyses of mixture are essential for chemical reactors, see e.g. Danckwerts (1952), Levenspiel (1962), Zvirin and Shinnar (1976), Nauman (1981) and Robinson and Tester (1986).

Three methods have been commonly used to quantitatively determine ventilation scales, including the *experimental method*, the *compartmental/zonal method* and the *numerical method*. In experiments, passive tracer measurements have usually been employed to characterize and track air flow patterns. With the compartmental or zonal method, a flow system is divided into a number of compartments/zones. Using mass and/or energy conservation, this method can be effectively used to analyze passive mass and heat transfer in various zones. The compartmental method is usually applied with the aid of measurements or numerical calculations to determine interchanging flow rates between different zones. Stochastic theory can also be used and incorporated into this method to explore the regional purging flow rate and other useful ventilation scales, see Peng and Davidson (1997b).

The numerical method has gained increasing attention in analyses of ventilation performance. This approach appears to be the most efficient one and is able to provide detailed figures of air flow and contaminant distributions. Liddament (1992) concluded that the prediction from numerical methods has enabled the concepts of ventilation efficiency and contaminant removal effectiveness to be applied at the design stage, while the value of the experimental method has been restricted to evaluation and diagnostic studies on existing structures. With the aid of numerical simulation, effort has been made in this work to develop new ventilation scales (Peng *et al*., 1997a), which are expected to be applicable in ventilation practice.

2.3.2 New Scales for Assessing Ventilation Flow Systems

As numerical simulation is used to explore ventilation scales, the new scale must be calculable either through indirect manipulation with predictable transport quantities or through direct solutions of a transport equation for this scale itself. It should be noted that the new scales were devised for ventilation applications, but they may also be applicable for other equivalent flow systems when the same or a similar assessment is required.

Local Purging Effectiveness of Inlet

This scale is proposed for assessing flow systems with multiple inlets, where the contribution from an individual supply opening needs to be distinguished. The openings are denoted *s*1, *s*2, ..., *sp*, ..., *sm*. For an arbitrary opening, say *sp*, its contribution to an arbitrary location within this system can be analyzed by the variation in local mean air age, $\delta\tau$, induced by supplying different aged air through *sp*. A detailed procedure for obtaining $\delta\tau$ was described in Peng *et*

al. (1997a). Denoting τ_{old} as the local age with old air supplied through *sp* (e.g. $\tau_{sp} = \tau_n = V/Q$) and τ_{new} as the local age with fresh air supplied ($\tau_{sp} = 0$), the *local purging effectiveness* of supply opening *sp*, A_{sp}, is defined as

$$A_{sp} = \frac{\delta\tau}{\tau_{old}} = \frac{(\tau_{old} - \tau_{new})}{\tau_{old}} \tag{2.3}$$

At an arbitrary point, the decrease in local mean air age, i.e. $\delta\tau = (\tau_{old} - \tau_{new})$, indicates the capability of the system to purge the *old air* by supplying fresh air through inlet *sp*. This age variation can readily be computed by using the following equation

$$\nabla \cdot [\mathbf{u}(\delta\tau)] = \nabla \cdot [D\nabla(\delta\tau)] \tag{2.4}$$

The boundary condition for the inlet considered, say *sp*, is $\delta\tau_{sp} = \tau_n$ and is zero for all the other inlets. At the inlet, *sp*, the local purging effectiveness is thus equal to unity and is zero at other inlets. A large A_{sp} means a large capability of a supply opening, *sp*, to deliver fresh air to a location for purging or diluting the contaminant there. This scale is measurable in tracer experiments by varying the tracer concentration at the inlet considered.

Expected Contaminant Dispersion Index

This scale is proposed for "*what if*" purposes in ventilation applications. In practice, without knowing the strength of a passive contaminant source, one is often eager to know what the possible contaminant distribution will be if this source is located at some specific locations. In other words, a source-independent index is needed for quantifying *ventilation flows* to forecast the dispersion of passive contaminants produced at specific locations. The local *Expected Contaminant Dispersion Index* (*ECDI*) is also derived from the age variation analysis, and is defined as

$$ECDI = \frac{(\tau_{c2} - \tau_{c1})}{\tau_{c2}} \tag{2.5}$$

where τ_{c2} is the local age calculated by specifying an age, τ_n, at the specific location and zero age at the supply opening; τ_{c1} is the local age calculated by specifying zero age at both the specific location and the supply opening.

Local Specific Contaminant-Accumulating Index

This scale can be used as a bridge index between the general scale and the specific scale. It is able to reflect how a set-up ventilation air flow and a specific contaminant source interact on each other. An index, termed the *local age-integrated exposure*, γ, is first defined as

$$\gamma = \int_0^{\tau} C(t)dt \tag{2.6}$$

This index expresses the local accumulation or dose of contaminants at an arbitrary position over a time equal to the local mean age of the air passing this position. By comparing this index with a value specified for limiting the time-integrated exposure, a scale can be obtained for evaluating the capacity of an air flow to dilute/remove the contaminant. A small value of γ

implies either that a small amount of contaminants has been dispersed to the position in question or that the air flow has been quickly supplied to this position, or both. A transport equation for γ can be readily derived (Peng *et al.*, 1997a) as

$$\nabla \cdot (\mathbf{u}\gamma) = \nabla \cdot (D\nabla\gamma) - 2D[\nabla\tau \cdot \nabla C(\tau)] + S_c\tau \tag{2.7}$$

where $C(\tau)$ is the concentration at the time equal to the local mean age of the air, τ. Note that the local age-integrated exposure is a measurable index. In practice, the accumulation at steady state is of more importance and interest. Equation (2.6) therefore becomes $\gamma = C(\infty)\tau$, and the corresponding transport equation takes the following form

$$\nabla \cdot (\mathbf{u}\gamma) = \nabla \cdot (D\nabla\gamma) - 2D[\nabla\tau \cdot \nabla C(\infty)] + C(\infty) + S_c\tau \tag{2.8}$$

This equation can be solved by coupling with Equations (2.1) and (2.2) at steady state. The boundary condition of γ at the inlet is zero.

The mean nominal time-integrated exposure is then used to normalize γ, leading to the *local specific contaminant-accumulating index*, α, i.e.,

$$\alpha = \log\left(\frac{\gamma}{\tau_n < C >}\right) \tag{2.9}$$

A negative α indicates a small amount of contaminant accumulation and thus a large contaminant-diluting capability at the location considered. For complete mixing, α is zero, which forms the basic scale of this quantity. When the steady-state concentration is used for γ in (2.6), Equation (2.9) can be rewritten as

$$\alpha = \log\left(\frac{\varepsilon_c}{\varepsilon_p \varepsilon_{ap}}\right) \tag{2.10}$$

where ε_c is the contaminant-removal effectiveness, $\varepsilon_c = C_e/<C>$, ε_p is the local air change index, $\varepsilon_p = \tau_n/\tau_p$, and ε_{ap} is the local air quality index, $\varepsilon_{ap} = C_e/C_p$. Equation (2.10) shows that α refers to both the delivering of fresh air to a location and the removal of contaminants from this location. The use of the new scales has been demonstrated by Peng *et al.* (1997a).

2.4 On the Purging Flow Rate

The purging flow rate describes the nature of the purging process in a flow system. It was originally proposed by Zvirin and Shinnar (1976) for analyzing two-phase flow systems and was used to distinguish between well-purged and stagnant regions. This concept is defined for the local continuum motion in a flow system. A small purging flow rate for a region means that this region is weakly connected with the rest of the system. Such a region is stagnant. The purging flow rate expresses the *net* fraction of the total flow through the system that passes one location in the system on its way to the outlets. In other words, it represents the net flow rate at which the passive contaminant at this location is flushed towards the exhaust opening. This concept is originally defined through a pulse or step tracer experiment. When a pulse tracer (m_p) is released at an arbitrary location p, the purging flow rate, U_p, is expressed as

$$U_p = \frac{m_p}{\int_0^\infty C_p(t)\,dt} \tag{2.11}$$

With a step tracer release (q_p), U_p is defined as

$$U_p = \frac{q_p}{C_p(\infty)} \tag{2.12}$$

It is emphasized here that the purging flow rate is a quantity for a sub-region in a flow system. Addressing U_p for a point will make this concept misleading and useless, since a flow rate at a *point* is zero. It is thus termed in this work the *regional purging flow rate*. So far, there is no available means proposed in experiments to measure this quantity. Numerical and compartmental methods have often been used to determine it, see e.g. Sandberg (1984) and Davidson and Olsson (1987).

2.4.1 Mathematical Derivations of the Purging Flow Rate

The original definition in (2.11) or (2.12) has commonly been used in theoretical determination of the purging flow rate. Although these definitions originate from *imaginary* tracer experiments, it seems impossible to measure the purging flow rate through experiments. The problem is that this quantity is associated with the volume (rather than the point) of the source-bearing location. The concentration used in (2.11) or (2.12) would be pointless in measurements for *a volume* containing the tracer source. If the concentration is measured at the tracer-release point, on the other hand, the resultant purging flow rate becomes pointless for representing a volume around the measured point.

Instead of relying on the original expressions in (2.11) and (2.12), the purging flow rate is reformulated here by means of a straightforward description. This new formulation is obtained by using the turnover flow rate, which is the total local flow rate passing through the region considered. The turnover flow rate for region p, W_p, includes two parts: the net flow rate at which the air leaving p flows towards the outlet, i.e. U_p; and the remaining flow rate (termed here the *residual turnover flow rate*), R_p, at which the air may recirculate and rejoin p after leaving it. The regional purging flow rate can then be simply expressed as

$$U_p = W_p - R_p \tag{2.13}$$

From Equation (2.13), one always has $U_p \le W_p$. This formulation shows that the purging flow rate for a flow system as a whole is therefore the total supply or exhaust air flow rate through the inlet or outlet.

General Mathematical Expressions

In compartmental analyses, the flow space is divided into n parts and each has a volume, δV_p (p = 1, 2, ..., n). With a step tracer experiment, at time $t = 0$, a passive contaminant is continuously released at a rate q_r at location r ($0 < r \le n$). The released passive contaminant follows the air flow, undergoing diffusion and convection. A fraction of contaminants, P_{rp}, is brought into an arbitrary location p (p = 1, 2, ..., n), with p as a receiver. The total amount of contaminants ever reaching location p after time t, from all contaminant sources in the system, is then

$$\Sigma m_p = \sum_r \left(P_{rp} \int_{t_{0r}}^{t} q_r dt \right) \tag{2.14}$$

where P_{rp} is termed the transfer probability. It reflects the transport ability possessed by the flow and represents the fraction of passive contaminants transported from the source-bearing location, r, to an arbitrary location p; t_{0r} is the time when the first fraction of contaminants emerges at location p after its release at r. As $t \to \infty$, according to the mass conservation principle, the total amount of contaminants ever reaching p after its release, Σm_p (as $t \to \infty$), must be balanced by an amount of contaminants, M_p, carried in the net air flow passing through p and flushing out of the system, to eventually make the concentration at p steady. Thus, in general,

$$M_p = \Sigma m_p \quad \text{as } t \to \infty \tag{2.15}$$

The net flow rate needed to hold the contaminant at location p and to carry it towards the outlet is the purging flow rate, U_p. At time t after release, M_p can be written as

$$M_p = U_p \int_{t_0}^{t} C_p(t)\, dt \tag{2.16}$$

where t_0 is the time at which the first fraction of contaminants appears at location p, $C_p(t)$ is the mean transient concentration at location p and $C_p(t) \equiv 0$ for $t \le t_0$. Substituting Equations (2.14) and (2.16) into Equation (2.15) yields

$$U_p = \lim_{t\to\infty} \frac{\sum_r P_{rp} \int_{t_{0r}}^{t} q_r dt}{\int_{t_0}^{t} C_p(t) dt} \tag{2.17}$$

With a pulse release, Equation (2.15) can also be used to give an expression for U_p, yielding

$$U_p = \frac{\sum_r (P_{rp} m_r)}{\int_0^{\infty} C_p(t)\, dt} \tag{2.18}$$

where m_r is the amount of contaminant released at location r by a short burst.

With a constant release rate for each source, i.e. $q_r \equiv constant$ at any time for all r ($r \le n$), Equation (2.17) can be rewritten in terms of a steady mean concentration, $C_p(\infty)$, as

$$U_p = \frac{\sum_r (P_{rp} q_r)}{C_p(\infty)} \tag{2.19}$$

Particularly, when a single passive contaminant source is located at p, then $P_{pp} \equiv 1$. Equations

(2.18) and (2.19) then take the same forms as the original definitions in (2.11) and (2.12), respectively. The mass conservation principle, expressed in Equation (2.15), thus forms the physical basis for deducing U_p. This enables us to formulate U_p through various tracer experiments.

Expressions Derived from Two Tracer Experiments

Step-up Tracer Release at the Inlet. For a situation with continuous tracer release, after a steady state is reached, the amount of purged passive contaminants from an arbitrary location p, M_p, over a time period of Δt can be written as

$$M_p = U_p C_p(\infty)\Delta t \tag{2.20}$$

With a step-up release at the inlet, the passive contaminant is released at time $t = 0$ at a constant rate q_s. The transfer probability from the inlet to an arbitrary interior location p is P_{sp}. The total amount of contaminant ever reaching p over a time period of Δt, at a steady state, is then $\Sigma m_p = P_{sp}\, q_s\, \Delta t$. This amount is balanced by M_p in Equation (2.20). This gives

$$U_p = \frac{P_{sp} q_s}{C_p(\infty)} \tag{2.21}$$

A continuous release at the inlet will eventually give a uniform concentration in the whole system as $t \rightarrow \infty$. This concentration equals the concentration at the inlet, i.e. $C_p(\infty) \equiv q_s/Q$ for all locations. Equation (2.21) thus becomes

$$U_p = P_{sp} Q \tag{2.22}$$

Equation (2.22) provides a convenient method for obtaining U_p in terms of the transfer probability from the inlet to an arbitrary interior region without requiring the transfer probabilities between different interior locations. This expression indicates that the purging flow rate also represents the *net* flow rate at which the fresh air is supplied to a location p.

Overall Step-up Tracer Release. In an overall step-up release within a flow system, the passive contaminant is released at each region. The release rate, δq_p (p = 1, 2, ..., n), is the amount of contaminant released per unit time and unit volume. When $i \neq j$ (i, j = 1, 2, ..., n), δq_i need not be equal to δq_j. In an arbitrary region p, the total amount of contaminant during a time period of Δt includes two parts: the amount released from the source in this region and the total amount during Δt from other sources in the rest of the system. This gives

$$\Sigma m_p = \sum_{i=1}^{n} (P_{ip}\, \delta q_i\, \Delta t\, \delta V_i) = \Delta t[\delta q_p \delta V_p + \sum_{i=1(i\neq p)}^{n} (P_{ip}\, \delta q_i \delta V_i)] \tag{2.23}$$

This amount is equal to M_p in Equation (2.20). Consequently, one gets

$$U_p = \frac{\delta q_p \delta V_p + \sum_{i=1(i\neq p)}^{n} (P_{ip}\, \delta q_i \delta V_i)}{C_p(\infty)} \tag{2.24}$$

When continuous release occurs in only a few regions, Equation (2.24) turns out to be Equation (2.19). If the source distribution is spatially homogeneous, i.e. $\delta q_i \equiv constant$ everywhere, the local mean age of air, τ_i, can then be expressed in terms of δq_i and $C_i(\infty)$, i.e. $\tau_i \equiv C_i(\infty)/\delta q_i$. Introducing this relation into Equation (2.24) gives

$$U_p = \frac{\delta V_p + \sum_{i=1(i\neq p)}^{n} (P_{ip}\delta V_i)}{\tau_p} = \frac{V_{sp}}{\tau_p} \tag{2.25}$$

where V_{sp} is the volume swept by the purging flow on its way from the supply opening to region p. The same equation was derived by Sandberg (1984) by means of matrix analyses. This equation shows that the regional purging flow rate is related to the volume of the region.

Some Scales Defined in Terms of the Purging Flow Rate

Several useful scales can be defined by using the purging flow rate to quantify ventilation performance. A *back-mixing index or probability*, β_p, is defined in terms of R_p and W_p, see (2.13), giving

$$\beta_p = \frac{R_p}{W_p} = 1 - \frac{U_p}{W_p} \tag{2.26}$$

The back-mixing index indicates the probability that the air will rejoin p after leaving it. This index, therefore, reflects the degree of air recirculation for region p. It is thus applicable for evaluating the air mixing degree. The *equivalent regional Peclet number*, Pe_p, for region p can be expressed as

$$Pe_p = \frac{2V}{\delta V_p}\frac{U_p}{W_p} = \frac{2V}{\delta V_p}(1-\beta_p) \tag{2.27}$$

Pe_p can be used as an indication of the uniformity of mixing. It can also be used to represent the segregation between the flow in the region considered and the ideal plug flow. Some other U_p-related scales were also discussed in Peng and Davidson (1997b).

2.4.2 A Markov Chain Model for Transfer Probabilities

To compute the regional purging flow rate, the key is to determine the transfer probabilities between different regions within a system. Equation (2.22) appears to be the most convenient expression, where only the transfer probability from the inlet to the interior region in question is needed. Sandberg (1984) used matrix analyses to find the transfer probabilities between different interior regions, without including the transfer probabilities from the inlet to the interior regions and those from the interior regions to the outlet. These parameters are important estimators to indicate the contribution of the inlet and the outlet and are particularly useful when using multi-inlet/outlet flow systems. A stochastic analysis was carried out by Peng and Davidson (1997b), in which a Markov chain model was developed to determine the transfer probabilities. This model is used in combination with the compartmental method to calculate the desired transfer probabilities mentioned above.

Transition Probability

Stochastic theory can be found in, e.g., textbooks by Feller (1971), Cinlar (1975) and Chiang (1980). It has been used in chemical engineering for many years, mainly in analyses of mixture and residence time distributions in chemical reactors, see e.g. Krambeck *et al.* (1967).

The flow is *tracked* by an imaginary fluid element (or a passive particle) within a flow field that is divided into a number of regions. The flow field is assumed to be steady and divided into n regions with interconnecting flows. The flow system has one inlet and multiple outlets (the multi-inlet system will be analyzed later). The interior regions are numbered continuously from 1 to n. Let the inlet be denoted by the letter s and the outlets numbered as $n + 1, n + 2, ..., n + e$, where e is the total number of the outlets. The inlet and outlets are treated as special regions with zero volume (i.e. $\delta V_s = \delta V_{n+1} = ... = \delta V_{n+e} \equiv 0$, and $V = \delta V_1 + \delta V_2 + ... + \delta V_n$). Each region (including the inlet and outlets) represents a state of the particle. A state space $\boldsymbol{S}$ is then formed, and

$$\boldsymbol{S} = \{s,\ 1,\ 2,\ \ldots,\ n,\ n+1,\ n+2,\ \ldots,\ n+e\} \tag{2.28}$$

$\boldsymbol{S}$ consists of two sub-spaces: the interior states (including the inlet and interior regions) form $\boldsymbol{S}_I$, and the outlet states (recurrent states) form $\boldsymbol{S}_O$, i.e. $\boldsymbol{S} = \boldsymbol{S}_I \cup \boldsymbol{S}_O$ ($\boldsymbol{S}_I \subset \boldsymbol{S}$ and $\boldsymbol{S}_O \subset \boldsymbol{S}$).

When the particle is released at a state p ($p \in \boldsymbol{S}$) in the beginning of the tracking, its initial state is denoted by $X_0 = p$. Let $I(p) = P\{X_0 = p, \exists\ p \in \boldsymbol{S}\}$. A set for the initial states is then formed

$$\boldsymbol{I} = \{I(s),\ I(1),\ \ldots\ ,\ I(n+e)\} \tag{2.29}$$

With one particle, $\Sigma I(i) \equiv 1$. To reveal the contribution of the inflow to different interior regions, the particle is released at the inlet, i.e. $I(s) = P\{X_0 = s\}$. After entering the room, the particle follows the air flow and visits a set of regions before leaving through an outlet. Each visit to a region is counted as a station X_i, where i denotes the number of stations the particle has ever visited since its release at initial state $I(s)$. The station $X_i = k$, when $k \geq n + 1$, means that the particle leaves the system. The sequence $\{X_i;\ i = 0, 1, 2, ...\}$ is thus a discrete space and a stochastic process. Its trajectories give a complete picture of the particle's movement in terms of the flow regions it visits. Since all the possible states in the system are covered by the state space $\boldsymbol{S}$, and the flow pattern is assumed to be steady, the state for the particle's current station X_i is affected only by its state at the last station, X_{i-1}. This is thus a typical Markov process. Its present state alone is therefore all that is needed to forecast its future, see Krambeck *et al.* (1967) and Feller (1971). The statistical sequence of a Markov process is governed entirely by the probabilities of transition from one state to another. In the parlance of statistics, for $i \geq 0$,

$$f\{X_i = p | X_0,\ X_1,\ \ldots,\ X_{i-1}\} = f\{X_i = p | X_{i-1}\} \quad (\forall\ p \in \boldsymbol{S}) \tag{2.30}$$

Furthermore, it is assumed that the particle's movement is a Markov chain with stationary transition probabilities. Then for all $i \geq 0$,

$$f(j,\ p) = f\{X_i = p | X_{i-1} = j\} = f\{X_1 = p | X_0 = j\} \quad (\forall\ j,\ p \in \boldsymbol{S}) \tag{2.31}$$

where $f(j, p)$ is the transition probability from state j to state p. With all members in the state space, $\boldsymbol{S}$, the transition probabilities between any two states form the entries of a matrix. This is

here called the $\boldsymbol{F}$ matrix, giving

$$\boldsymbol{F} = \begin{pmatrix} f(s, s) & f(s, 1) & \dots & f(s, n+e) \\ f(1, s) & f(1, 1) & \dots & f(1, n+e) \\ \vdots & \vdots & \vdots & \vdots \\ f(n+e, s) & f(n+e, s) & \dots & f(n+e, n+e) \end{pmatrix} \tag{2.32}$$

The transition probability, $f(j, p)$, expresses the probability for a particle to leave a state j and immediately enter another state p. In other words, it indicates the fraction of air flow at state j tending to leave and to be transferred, by one step, to state p ($j, p \in \boldsymbol{S}$). The $\boldsymbol{F}$ matrix can be partitioned into four submatrices, i.e.,

$$\boldsymbol{F} = \begin{pmatrix} \boldsymbol{D} & \boldsymbol{H} \\ \boldsymbol{O} & \boldsymbol{E} \end{pmatrix} \tag{2.33}$$

Submatrix $\boldsymbol{D}$ is a block with $(n + 1) \times (n + 1)$ elements that represent the transition probabilities between interior states (including the inlet). Submatrix $\boldsymbol{H}$ is a block with $(n + 1) \times e$ elements that represent the transition probabilities from interior states to outlet states. Submatrix $\boldsymbol{O}$ is a zero block with $e \times (n + 1)$ elements that represent the transition probabilities from outlet states to interior states. $\boldsymbol{E}$ is a unit matrix with $e \times e$ elements that represent the transition probabilities from outlet states to outlet states.

Special attention must be paid to the diagonal entries of $\boldsymbol{F}$. Without exception, $f(p, p) \equiv 1$ ($\forall p \in \boldsymbol{S}_O$) for submatrix $\boldsymbol{E}$; and the probability $f(p, p)$ ($p \in \boldsymbol{S}_I$) is usually 0 for submatrix $\boldsymbol{D}$. If there is any by-passing flow which flows back to the same state without experiencing any other states in $\boldsymbol{S}_I$, then $f(p, p) \neq 0$, and this is the fraction of the by-passing flow. For ventilation flows, this situation seldom occurs. An alternative way to deal with the by-passing flow is to extend the state space by assigning additional states for by-passing regions.

Transfer Probability

A new matrix, $\boldsymbol{A}$, can be derived from matrix $\boldsymbol{D}$, whose entries, $a(j, p)$, are the mean number of visits of the particle to a region p with a last state j ($\forall j, p \in \boldsymbol{S}_I$)

$$\boldsymbol{A} = (\boldsymbol{E}_D - \boldsymbol{D})^{-1} \tag{2.34}$$

where $\boldsymbol{E}_D$ is the unit matrix with the same dimension as the $\boldsymbol{D}$ matrix. Let $\boldsymbol{B}$ be another probability matrix with the same dimension as $\boldsymbol{A}$. Its non-diagonal entries $b(j, p)$ ($\forall j, p \in \boldsymbol{S}_I$ and $j \neq p$) express the probability of the particle to ever reach state p when its last state is j. This probability is thus the transfer probability from state j to state p, i.e. $b(j, p) = P_{jp}$ ($\forall j, p \in \boldsymbol{S}_I$ and $j \neq p$). The diagonal elements, $b(p, p)$ for all $p \in \boldsymbol{S}_I$, represent the probability that the particle ever returns to p after it leaves. Assuming that no upstream diffusion occurs at the inlet (i.e. $b(s,s) \equiv 0$), then, for any states j and p, $j, p \in \boldsymbol{S}_I$, we have

$$b(p, p) = 1 - \frac{1}{a(p, p)} \tag{2.35}$$

$$b(j,\ p) = \frac{a(j,\ p)}{a(p,\ p)} \quad (j \neq p) \tag{2.36}$$

For a ventilation flow, $b(p, p)$ ($\forall p \in \boldsymbol{S_I}$) is the fraction of air ever returning to region p after first leaving this region and before being exhausted through the outlet. It is thus the back-mixing probability, β_p, defined in Equation (2.26), i.e. $\beta_p \equiv b(p, p)$. A large $b(p, p)$ means a high degree of recirculation and back-mixing for region p.

It is interesting to point out that it can be shown that the result derived from the deterministic method (Sandberg, 1984) is a special case of the present model, when the particle is initially released from an interior region, see Peng and Davidson (1997b). The present Markov chain model is thus a generalized one.

The contribution of an outlet to the interior regions is represented by the transfer probability from an interior region j ($j \in \boldsymbol{S_I}$) to an outlet k ($k \in \boldsymbol{S_O}$), that is, the probability $b(j, k)$. This can be calculated with matrices $\boldsymbol{H}$ and $\boldsymbol{A}$, i.e.,

$$\boldsymbol{B_O} = \begin{pmatrix} b(s,\ n+1) & b(s,\ n+2) & \dots & b(s,\ n+e) \\ b(1,\ n+1) & b(1,\ n+2) & \dots & b(1,\ n+e) \\ \vdots & \vdots & \vdots & \vdots \\ b(n,\ n+1) & b(n,\ n+2) & \dots & b(n,\ n+e) \end{pmatrix} = \boldsymbol{A} \cdot \boldsymbol{H} \tag{2.37}$$

The elements of each row in the $\boldsymbol{B_O}$ matrix indicate the fractions of the air in a region exhausted by various outlets. The sum of these elements should therefore be unity.

Equations (2.34)-(2.37) provide a method to compute the desired transfer probabilities: from the inlet to the interior regions; from one interior region to another; and from the interior regions to an outlet. These transfer probabilities can be used to calculate the regional purging flow rate, to analyze the effects of the inlet and outlet on the interior region considered, and to explore the connection between various interior regions. The back-mixing probability furthermore provides a new index to explore the flow behaviour in the interior regions.

Flow Systems with Multiple Inlets

When air is supplied into a space through multiple inlets, the Markov chain model can be used to calculate the transfer probabilities from each inlet to any interior regions. With all the inlet states included in the state space $\boldsymbol{S}$, the initial state for the particle tracking needs to be changed from one inlet to another in order to account for the individual effect of each inlet. However, the transition probability between any two interior regions remains unchanged for a set-up flow pattern. By changing only the transition probabilities from the inlet to the interior regions in the $\boldsymbol{F}$ matrix, the calculation can be carried out in the same way as for a system with only one inlet. With Equations (2.34)-(2.37), the transfer probabilities between any two states (the inlet, the outlet and the interior region) can be obtained. Note that the transition probability between any two inlets is always zero.

With multiple inlets, all the inlets contribute to the purging flow rate for the region considered. Using (2.22), the regional purging flow rate for a region p can be determined by

$$U_p = b(s1,\ p)Q_{s1} + b(s2,\ p)Q_{s2} + \ \dots \ + b(sm,\ p)Q_{sm} \tag{2.38}$$

where $s1$, $s2$, ..., sm denote the inlets, and Q_{s1}, Q_{s2}, ..., Q_{sm} are their corresponding supply air

flow rates. Each term in Equation (2.38) represents the individual contribution of each inlet. A similar evaluation can be made for the outlets. In addition, it should be pointed out that Equation (2.25) can directly be used to calculate the regional purging flow rate for systems with multiple inlets, since no transfer probabilities related to inlets are involved in this equation.

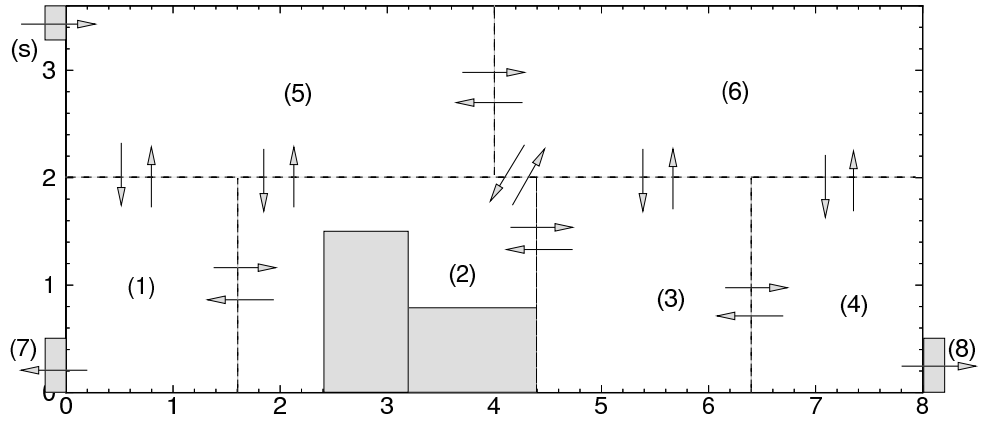

a) Configuration of the room and divided sub-regions

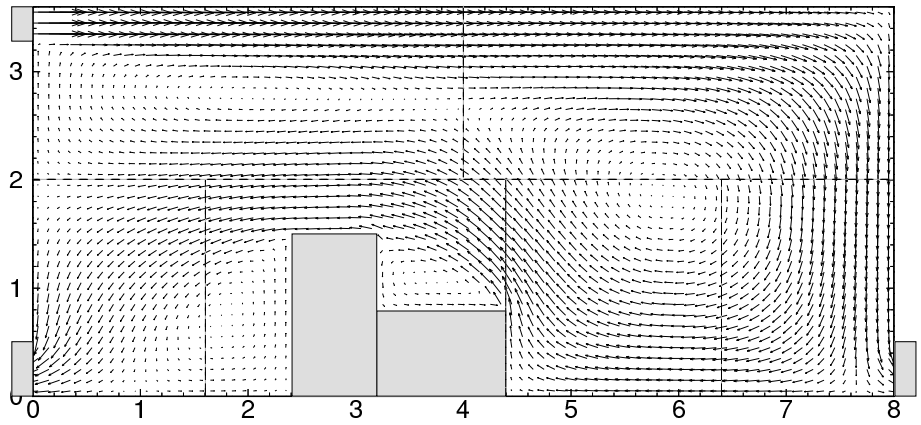

b) Air flow pattern obtained from numerical simulation

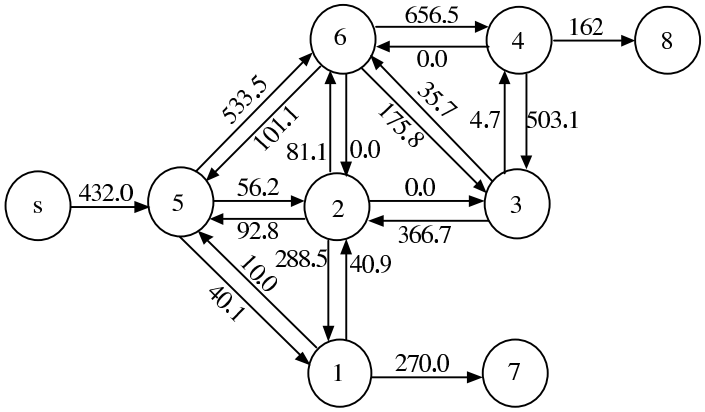

c) Numerically calculated interchanging flow rates between regions (m^3/h)

Figure 2.1 An example used for demonstrating the use of the Markov chain model.

Figures 2.1 a), b) and c) show a two-dimensional configuration for a room with mixing ventilation, where the air is supplied through one inlet under the ceiling and exhausted from two openings above the floor. The room is divided into six interior sub-regions. This flow system is used to demonstrate the calculation of the regional purging flow rate using the Markov chain model.

The interchanging flow rates between different sub-regions given in Figure 2.1 c) were calculated from a numerical simulation which gave the flow field as shown in Figure 2.1 b). The interchanging flow rates are then used to obtain the transition probabilities, which in turn form the $\boldsymbol{F}$ matrix as follows

$$\boldsymbol{F} = \begin{pmatrix} \boldsymbol{D} & \boldsymbol{H} \\ \boldsymbol{O} & \boldsymbol{E} \end{pmatrix}$$

$$= \left(\begin{array}{ccccccc|cc} 0 & 0 & 0 & 0 & 0 & 1.0 & 0 & 0 & 0 \\ 0 & 0 & 0.128 & 0 & 0 & 0.031 & 0 & 0.841 & 0 \\ 0 & 0.624 & 0 & 0 & 0 & 0.201 & 0.175 & 0 & 0 \\ 0 & 0 & 0.670 & 0 & 0.009 & 0 & 0.321 & 0 & 0 \\ 0 & 0 & 0 & 0.756 & 0 & 0 & 0 & 0 & 0.244 \\ 0 & 0.064 & 0.089 & 0 & 0 & 0 & 0.847 & 0 & 0 \\ 0 & 0 & 0 & 0.045 & 0.828 & 0.127 & 0 & 0 & 0 \\ - & - & - & - & - & - & - & - & - \\ 0 & 0 & 0 & 0 & 0 & 0 & 0 & 1 & 0 \\ 0 & 0 & 0 & 0 & 0 & 0 & 0 & 0 & 1 \end{array}\right) \quad (2.39)$$

By using (2.34) and (2.36), the transfer probabilities from the supply opening to an interior region p, P_{sp}, can be determined, and the regional purging flow rate is consequently computed from (2.22). The back-mixing index, β_p, i.e. $b(p, p)$, can be calculated with Equation (2.35). Some regional ventilation scales computed with the Markov chain model are shown in Table 2.1 for the present case, see also Peng and Davidson (1997b). The purging flow rate for region 5 is the same as the supply flow rate since the entire supply air is first delivered to this region.

Table 1 Calculated regional ventilation scales for the case in Figure 2.1.

Scales	Region 1	Region 2	Region 3	Region 4	Region 5	Region 6
P_{sp}	0.65	0.68	0.67	0.86	1.00	0.89
U_p (m^3/h)	281	294	289	372	432	385
β_p	0.13	0.35	0.45	0.44	0.32	0.51
Pe_p	14.4	9.8	7.1	9.3	5.7	4.1

Chapter 3

Modelling of Turbulent Flow and Heat Transfer

As a fluid motion is said to be of a turbulent type, the flow is regarded as being highly random, unsteady, diffusive, dissipative and three-dimensional (Tennekes and Lumley, 1978). In essence, turbulence is not a property of fluids, but of continuum fluid flows. It is thus governed by the equations of fluid mechanics. Since these equations are non-linear, and different flow problems possess individual features caused by various initial and boundary conditions, no general, well-behaved solution to these governing equations is known. For flow problems of engineering interest, the solution to these non-linear differential equations has often been obtained with the use of numerical methods.

In numerical simulation, only motions of scales larger than the mesh size can be resolved. Turbulent flows are associated with a multitude of scales in time and space. The dynamics of eddies in turbulence is characterized by an energy cascade from large to small eddies and, finally, through the action of viscosity, into heat. This suggests that the lower bound to the length scale in turbulence is set by the influence of viscosity, i.e., the dissipative scales. The upper bound is determined by the geometric size of the flow domain. In turbulent ventilation flows, for example, the smallest length scale may be of an order of 0.1 mm, while the largest scale is the dimension of the ventilated room which is usually several meters.

Direct numerical solution (i.e. DNS) to the non-linear differential governing equations appears to be an available approach, which allows full resolution down to the smallest scales and is free of modelling approximations. Note that the span of length scales grows with the macroscale Reynolds number, Re, to a power of 3/4. This means that the number of grid points required for a DNS in three dimensions is of the order of $Re^{9/4}$. With an increasing Reynolds number in the range of engineering applications, direct computation for turbulent flow thus requires a prohibitively increasing computer power. Although this approach is able to provide details on turbulent structure at low Reynolds numbers for validating and improving turbulence models, it is not yet ready as a tool for solving practical flow problems. Comprehensive discussion on DNS can be found in several review articles by, e.g., Rogallo and Moin (1984), Reynolds (1989) and Schumann (1991).

Attempts made to avoid full resolutions of the span of length scales as in DNS bring in another approach, that is, large eddy simulation (LES). The basic philosophy in LES is then naturally to filter out the small scales so as to make a relatively coarse mesh usable for the numerical resolution of the large scales. The small-scale motion, on the other hand, is presumed to be more homogeneous and universal in nature and thus more amenable and requiring of fewer adjustments for successful modelling. To distinguish small-scale and large-scale eddies, a filtering process is carried out on the governing equations. The consequence of the filtering operation is that the small-scale eddies are removed and the equations become governing equations only for the evolution of large-scale motions. Nonetheless, the effect of unresolved small scales on resolved large scales remains, which needs to be accounted for by a model.

LES is similar to DNS in that it provides three-dimensional, time-dependent solutions of the Navier-Stokes equations. The large scales are, in principle, required to contain kinetic energy as much as possible in order for the small scales to obey inertial subrange dynamics. Thus, LES still requires fairly fine meshes. In many engineering applications, it is of interest to detect mean flow properties rather than detailed fluctuating motions. Even with DNS and

LES, the most meaningful and practical result usually lies in the mean field and is obtained by time-averaging the instantaneous quantities. Use of statistical approaches is thus another desirable alternative in which the Reynolds-averaged Navier-Stokes (RANS) equations, which describe the evolution of the mean quantities, are solved. In RANS approaches, all stochastic turbulent fluctuations are averaged out through a time-averaging process. This averaging process, however, introduces unknown correlations. To close the equation system, these unknowns, as in LES, must be modelled.

To shed light on the unknown correlations resulting from the Reynolds-averaging approach, we start with a brief description of the basic governing equations.

3.1 Basic Equations

The equations of motion for a continuum fluid express the conservation of mass, of momentum and of energy. For incompressible flows, these equations can be written as, respectively,

$$\frac{\partial u_i}{\partial x_i} = 0 \tag{3.1}$$

$$\frac{\partial u_i}{\partial t} + \frac{\partial (u_i u_j)}{\partial x_j} = -\frac{1}{\rho}\frac{\partial P}{\partial x_i} + \frac{\partial}{\partial x_j}(2\nu S_{ij}) + f_i \tag{3.2}$$

$$\frac{\partial T}{\partial t} + \frac{\partial (u_j T)}{\partial x_j} = \frac{\partial}{\partial x_j}\left(\alpha \frac{\partial T}{\partial x_j}\right) + S_\phi \tag{3.3}$$

where f_i is the external force, e.g., the buoyancy force, S_ϕ is a source term in the energy equation, and the strain rate tensor, S_{ij}, is expressed as

$$S_{ij} = \frac{1}{2}\left(\frac{\partial u_i}{\partial x_j} + \frac{\partial u_j}{\partial x_i}\right) \tag{3.4}$$

These equations serve as a basis for attacking mean flow problems as well as for analyzing turbulence into harmonic components. In the LES approach, these equations are viewed as governing the fluid motions from the smallest to the largest eddies to enable a space-smoothing or filtering process applicable to rule out the subgrid scales. This will be further addressed in Section 3.6. In RANS approaches, the turbulent motion is regarded as consisting of the sum of a mean part and a fluctuating part. Reynolds decomposition is introduced into the time-averaging process, and the instantaneous variables are then separated as

$$\psi = \overline{\psi} + \psi' \tag{3.5}$$

where ψ' is the fluctuating part of a quantity and $\overline{\psi}$ is the mean part. The time-averaged quantity is defined as

$$\overline{\psi} = \frac{1}{(t_1 - t_0)}\int_{t_0}^{t_1} \psi dt \tag{3.6}$$

where $(t_1 - t_0)$ is the averaging time. Using Reynolds decomposition and time-averaging for Equations (3.1)-(3.3), the continuity equation (3.1) takes the same form, but instead for the mean velocities. Hereafter, the overbar indicating time-averaging is dropped, unless otherwise stated. The Reynolds-averaged Navier-Stokes equations become

$$\frac{\partial u_i}{\partial t} + \frac{\partial (u_i u_j)}{\partial x_j} = -\frac{1}{\rho}\frac{\partial p}{\partial x_i} + \frac{\partial}{\partial x_j}(2\nu S_{ij} - \overline{u_i' u_j'}) + f_i \tag{3.7}$$

and, similarly, the thermal energy equation reads

$$\frac{\partial T}{\partial t} + \frac{\partial (u_j T)}{\partial x_j} = \frac{\partial}{\partial x_j}\left(\alpha \frac{\partial T}{\partial x_j} - \overline{u_j' T'}\right) + S_\phi \tag{3.8}$$

The resultant turbulent Reynolds stresses and heat fluxes, $-\overline{u_i' u_j'}$ and $-\overline{u_j' T'}$, represent the transport of momentum and heat due to fluctuating motions. Consequently, nine unknown correlations in total are introduced into the equation system. The exact equations for these correlations can be derived from the dynamic equations for the fluctuating quantities. The exact equations for $-\overline{u_i' u_j'}$ read

$$\begin{aligned} &\frac{\partial \overline{u_i' u_j'}}{\partial t} + u_k \frac{\partial \overline{u_i' u_j'}}{\partial x_k} = -\left(\overline{u_i' u_k'}\frac{\partial u_j}{\partial x_k} + \overline{u_j' u_k'}\frac{\partial u_i}{\partial x_k}\right) + \beta(g_i \overline{u_j' T'} + g_j \overline{u_i' T'}) \\ &+ \overline{\frac{p'}{\rho}\left(\frac{\partial u_i'}{\partial x_j} + \frac{\partial u_j'}{\partial x_i}\right)} - 2\nu \overline{\frac{\partial u_i'}{\partial x_k}\frac{\partial u_j'}{\partial x_k}} + \frac{\partial}{\partial x_k}\left[-\overline{u_i' u_j' u_k'} - \overline{\frac{p'}{\rho}\left(u_i' \delta_{jk} + u_j' \delta_{ik}\right)} + \nu \frac{\partial \overline{u_i' u_j'}}{\partial x_k}\right] \end{aligned} \tag{3.9}$$

The different terms on the right-hand side in Equation (3.9) successively express production due to mean shear, production due to buoyancy, pressure-strain redistribution, viscous dissipation and turbulent and viscous diffusion.

The exact transport equations for the turbulent heat fluxes, $-\overline{u_j' T'}$, take the form of

$$\begin{aligned} &\frac{\partial \overline{u_i' T'}}{\partial t} + u_k \frac{\partial \overline{u_i' T'}}{\partial x_k} = -\left(\overline{u_i' u_j'}\frac{\partial T}{\partial x_j} + \overline{u_j' T'}\frac{\partial u_i}{\partial x_j}\right) + \beta g_i \overline{T'^2} + \overline{\frac{p'}{\rho}\frac{\partial T'}{\partial x_i}} - \\ &(\alpha + \nu)\left(\overline{\frac{\partial u_i'}{\partial x_k}\frac{\partial T'}{\partial x_k}}\right) + \frac{\partial}{\partial x_k}\left[-\overline{u_i' u_k' T'} - \frac{\delta_{ik}}{\rho}\overline{p' T'} + \nu \frac{\partial \overline{u_i' T'}}{\partial x_k}\right] \end{aligned} \tag{3.10}$$

In analogy to Equation (3.9), the right-hand side in this equation includes, respectively, mean-field production term, buoyancy production term, pressure-temperature gradient correlation term, viscous destruction term and diffusive transport term.

New unknown correlations of various kinds arise in (3.9) and (3.10). A further derivation of transport equations for all these unknowns is possible and would include additional, higher-order correlations and so on in an expanding hierarchy, see e.g. Chou (1940). This consequently leads to a closure problem. To obtain a closed set of equations, it is necessary to ter-

minate the hierarchy at some particular level by modelling the unknown correlations. Models at the second-order level using Equations (3.9) and (3.10) are often termed second-moment closures or Reynolds stress models, on which work has been carried out by, e.g., Rotta (1951), Lumley (1970), Hanjalic and Launder (1972, 1976), Rodi (1976), Launder and Shima (1989), Hallbäck *et al.* (1990), Shih *et al.* (1994) and Wallin and Johanson (1996). Comprehensive reviews can be referred to the work by, e.g., Launder and Spalding (1972), Launder *et al.* (1975), Rodi (1980), Launder (1989), Speziale (1991), Groth (1991), Hanjalic (1994) and Launder (1995).

3.2 Eddy Viscosity/Diffusivity Concept

The task of turbulence modelling is, in short, to make a mathematically well-behaved and physically well-posed equation system for solving turbulent flow problems. Comprehensive discussion on some general aspects for a closure to fulfil, for example, coordinate invariance, material frame indifference, realizability and near-wall asymptotic behaviour can be found in, e.g., Schumann (1977), Lumley (1978), Speziale (1989) and Hallbäck *et al.* (1995).

As the modelling directly formulates the turbulent Reynolds stresses and heat fluxes in terms of known mean flow properties, the eddy viscosity/diffusivity concept has been used for a wide class of turbulence models in practical use. In analogy to the viscous stresses in laminar flows, Boussinesq (1877) suggested that the turbulent stresses are proportional to the mean velocity gradients. This approximation reads

$$\tau_{ij} = -\overline{u_i' u_j'} = \nu_t \left(\frac{\partial u_i}{\partial x_j} + \frac{\partial u_j}{\partial x_i} \right) - \frac{2}{3} k \delta_{ij} \tag{3.11}$$

where ν_t is the eddy viscosity, and k is the turbulent kinetic energy, defined as $k = \frac{1}{2}\overline{u_i' u_i'}$, which is nestled in an additional term to give the model a correct trace. This term is often absorbed in the pressure-gradient term in numerical computations. In a similar way, the turbulent heat fluxes can be formulated through the eddy diffusivity concept, i.e.,

$$h_j = -\overline{u_j' T'} = \alpha_t \frac{\partial T}{\partial x_j} = \frac{\nu_t}{\sigma_t} \frac{\partial T}{\partial x_j} \tag{3.12}$$

where α_t is the eddy diffusivity. In writing Equations (3.11) and (3.12), the ratio of the eddy viscosity and diffusivity has been used to define the turbulent Prandtl number, $\sigma_t = Pr_t = \nu_t/\alpha_t$, whose value is often assumed to be a constant in eddy-viscosity-based models.

Based on the eddy viscosity/diffusivity concept, the modelling now turns out to be a task of finding ν_t or α_t. Unlike the molecular viscosity, the turbulent eddy viscosity is a property of the flow, but not of the fluid. It is thus a function of time and space. Moreover, one may note that the eddy viscosity is essentially an isotropic quantity, that is, it is equal in all directions. Argued with dimensional analyses, the eddy viscosity can be constructed to be a product of turbulent velocity scale (V_t) and length scale (L_t), i.e., $\nu_t \propto V_t L_t$. Depending on how these scales are prescribed, several types of eddy-viscosity-based turbulence closures have been developed and used in engineering practice.

The simplest type is the zero-equation models, where the eddy viscosity is either assumed to be a constant (Prandtl, 1942) or is directly related to the local mean velocity gradient and the flow geometry. For example, using the famous mixing length hypothesis (Prandtl, 1925),

one may write the eddy viscosity in a generalized form as

$$\nu_t = l_m \left[\left(\frac{\partial u_i}{\partial x_j} + \frac{\partial u_j}{\partial x_i} \right) \frac{\partial u_i}{\partial x_j} \right]^{1/2} \tag{3.13}$$

where l_m is the mixing length whose distribution over the flow field is prescribed by means of empirical formulations, see e.g. Rodi (1980).

In one-equation models, the turbulent velocity scale is described by $V_t \propto \sqrt{k}$. This yields

$$\nu_t = c_\mu \sqrt{k} L_t \tag{3.14}$$

where c_μ is a model constant. A transport equation for the turbulent kinetic energy, k, is then required. This can be derived by contracting indices in Equation (3.9) and dividing the result by two, giving

$$\frac{\partial k}{\partial t} + u_j \frac{\partial k}{\partial x_j} = \underbrace{-\overline{u_i' u_j'} \frac{\partial u_i}{\partial x_j}}_{\wp} + \underbrace{\beta g_j \overline{u_j' T'}}_{G} - \underbrace{\nu \overline{\frac{\partial u_i'}{\partial x_j} \frac{\partial u_i'}{\partial x_j}}}_{\varepsilon} - \underbrace{\frac{\partial}{\partial x_j} \left[\overline{u_j' \left(\frac{u_i' u_i'}{2} + \frac{p'}{\rho} \right)} \right]}_{D_t} + \underbrace{\nu \frac{\partial^2 k}{\partial x_j \partial x_j}}_{D_\nu} \tag{3.15}$$

On the right-hand side of (3.15), the terms are, respectively, shear production ($\wp$), buoyancy production (G), viscous dissipation (ε), turbulent diffusion (D_t) and viscous diffusion (D_ν). The unknown correlations in this equation are further modelled in terms of ν_t and L_t so that the remaining work to close the equation system is left only to formulating the turbulent length scale. In most one-equation models, L_t is determined by trial-and-error, empirical relations. As in zero-equation models using Prandtl's mixing length hypothesis, the prescription of the length scale has proven to be a difficult matter in both physics and numerics, particularly for complex flows with complex geometries. Reviews on these models can be found in, e.g., Rodi (1980), Markatos (1987) and Nallasamy (1987). In addition, a three-equation model (the k-ε-v^2 model) should be mentioned, which has recently been proposed by Durbin (1995) and applied to jet-impingement heat transfer (Behnia *et al.*, 1996) with reasonable predictions reported.

3.3 Two-Equation Model

Among the eddy-viscosity-based models, the two-equation models have had the most applications in engineering. The eddy viscosity/diffusivity in two-equation models is prescribed with two turbulent scales having their respective transport equations. After using the eddy viscosity/diffusivity approximations, (3.11) and (3.12), in Equation (3.15), two more terms (D_t and ε) in the exact k-equation must be further modelled. Keeping the k-equation appears a natural choice to formulate ν_t or α_t, since the square root of k is proportional to the turbulent velocity scale. The turbulent diffusion is usually modelled in analogy to its viscous counterpart. The modelled k-equation then takes the form

$$\frac{\partial k}{\partial t} + u_j \frac{\partial k}{\partial x_j} = \tau_{ij} \frac{\partial u_i}{\partial x_j} - \beta g_j h_j - \varepsilon + \frac{\partial}{\partial x_j} \left[(\nu + \frac{\nu_t}{\sigma_k}) \frac{\partial k}{\partial x_j} \right] \tag{3.16}$$

In view of the eddy viscosity formulation in Equation (3.14), a straightforward approach to close the equation system is to derive an additional transport equation for the length scale itself, L_t. The viscous dissipation rate, ε, in Equation (3.16) can be further expressed in terms of k and L_t through a dimensional analysis which gives $\varepsilon \propto k^{3/2}/L_t$. This in turn yields the k-L_t model (cf. Mellor and Herring, 1973).

In other two-equation models, it is often not an equation for L_t itself, but rather an equation for the combination of k and L_t. If such a combination that complements k is denoted as Z, the modelled Z-equation can be written in a general form, in analogy to (3.16), as

$$\frac{\partial Z}{\partial t}+u_j\frac{\partial Z}{\partial x_j}=\frac{Z}{k}\left(c_{Z1}\tau_{ij}\frac{\partial u_i}{\partial x_j}-c_{Zg}\beta g_j h_j\right)-c_{Z2}\frac{Z}{k}\varepsilon+\frac{\partial}{\partial x_j}\left[(\nu+\frac{\nu_t}{\sigma_Z})\frac{\partial Z}{\partial x_j}\right]+S_Z \qquad (3.17)$$

where the source term, S_Z, depends on the specific choice of Z. There have been various combinations in forming the Z-equation. Among others, we mention here the k-ε model (cf. Launder and Spalding, 1972), the k-ω model (cf. Wilcox, 1988) and the k-τ model (cf. Speziale *et al.*, 1992). These three types of models have been used and compared in numerical simulations for turbulent ventilation flows (Peng *et al.*, 1996b). It was found that the k-τ model and the k-ω model in high-*Re* forms, in conjunction with wall functions, gave relatively poor performance for the flows considered.

Of all the existing two-equation models, the k-ε model remains the most used in engineering applications. By its definition in homogeneous turbulence, $\varepsilon=\nu\overline{\partial u_i'/\partial x_j\,\partial u_i'/\partial x_j}$, the exact equation for ε can be derived as

$$\frac{\partial \varepsilon}{\partial t}+u_k\frac{\partial \varepsilon}{\partial x_k}=\underbrace{-2\nu\left(\overline{\frac{\partial u_i'}{\partial x_k}\frac{\partial u_j'}{\partial x_k}}+\overline{\frac{\partial u_k'}{\partial x_i}\frac{\partial u_k'}{\partial x_j}}\right)\frac{\partial u_i}{\partial x_j}-2\nu\overline{u_j'\frac{\partial u_i'}{\partial x_k}}\frac{\partial^2 u_i}{\partial x_j\partial x_k}-2\nu\overline{\frac{\partial u_i'}{\partial x_j}\frac{\partial u_i'}{\partial x_k}\frac{\partial u_j'}{\partial x_k}}}_{\wp_\varepsilon}$$

$$\underbrace{+2\nu\beta g_i\overline{\frac{\partial T'}{\partial x_k}\frac{\partial u_i'}{\partial x_k}}}_{G_\varepsilon}\underbrace{-2\overline{\left(\nu\frac{\partial^2 u_i'}{\partial x_j\partial x_k}\right)^2}}_{\Pi_\varepsilon}\underbrace{-\nu\frac{\partial}{\partial x_k}\left(\overline{u_k'\varepsilon}+\frac{2}{\rho}\overline{\frac{\partial p'}{\partial x_i}\frac{\partial u_k'}{\partial x_i}}\right)}_{D_{t\varepsilon}}+\underbrace{\nu\frac{\partial^2\varepsilon}{\partial x_k\partial x_k}}_{D_{\nu\varepsilon}} \qquad (3.18)$$

On the right-hand side of (3.18), the first three terms are denoted as the production ($\wp_\varepsilon$) due to mean strain field (the first two) and vortex stretching (the last one). The fourth term is a buoyant production (G_ε), the fifth is a viscous destruction term (Π_ε) and the remaining two terms are the turbulent transport ($D_{t\varepsilon}$) and the viscous transport ($D_{\nu\varepsilon}$), respectively. Referring to Equation (3.17), the modelled ε-equation is written as

$$\frac{\partial \varepsilon}{\partial t}+u_j\frac{\partial \varepsilon}{\partial x_j}=\frac{\varepsilon}{k}\left(c_{\varepsilon1}\tau_{ij}\frac{\partial u_i}{\partial x_j}-c_{\varepsilon g}\beta g_j h_j\right)-c_{\varepsilon2}\frac{\varepsilon^2}{k}+\frac{\partial}{\partial x_j}\left[(\nu+\frac{\nu_t}{\sigma_\varepsilon})\frac{\partial \varepsilon}{\partial x_j}\right] \qquad (3.19)$$

The eddy viscosity in the k-ε model reads

$$\nu_t=c_\mu k^2/\varepsilon \qquad (3.20)$$

The model constants in the conventional k-ε model for isothermal flows ($c_{\varepsilon g} = 0$) are specified as (cf. Launder and Spalding, 1972)

$$c_\mu = 0.09,\ \ \sigma_k = 1.0,\ \ \sigma_\varepsilon = 1.3,\ \ \sigma_t = 0.9,\ \ c_{\varepsilon 1} = 1.44,\ \ c_{\varepsilon 2} = 1.92 \tag{3.21}$$

The exact equations for other possible choices of the Z quantity, for example the turbulent time scale τ and its reciprocal ω, can be readily obtained through their respective expressions in terms of k and ε. For the quantity ω, which is termed the *specific dissipation rate* by Wilcox (1988), its exact equation can be derived from the relation of $\omega \propto \varepsilon/k$. This suggests

$$\frac{D\omega}{Dt} = \frac{1}{k}\frac{D\varepsilon}{Dt} - \frac{\omega}{k}\frac{Dk}{Dt} \tag{3.22}$$

where $D/Dt = \partial/\partial t + u_l\,\partial/\partial x_l$. The exact ω-equation is then written as

$$\frac{\partial \omega}{\partial t} + u_j\frac{\partial \omega}{\partial x_j} = \underbrace{\left[\frac{\wp_\varepsilon + G_\varepsilon}{k} - \frac{\omega(\wp + G)}{k}\right]}_{\wp_\omega} + \underbrace{\left(\omega^2 + \frac{\Pi_\varepsilon}{k}\right)}_{\Pi_\omega}$$
$$\underbrace{+\left(\frac{D_{t\varepsilon}}{k} - \frac{\omega D_t}{k}\right)}_{D_{t\omega}} + \underbrace{\left(\nu\frac{\partial^2\omega}{\partial x_j\partial x_j} + \frac{2\nu}{k}\frac{\partial\omega}{\partial x_j}\frac{\partial k}{\partial x_j}\right)}_{D_{\nu\omega}} \tag{3.23}$$

where the terms on the right-hand side are, respectively, the production ($\wp_\omega$), the destruction (Π_ω), the turbulent diffusion ($D_{t\omega}$) and the viscous diffusion ($D_{\nu\omega}$).

Using the relation of $\tau \propto k/\varepsilon$ and the exact equations for k and ε, i.e. (3.15) and (3.18), the exact transport equation for τ can be derived from the following relation

$$\frac{D\tau}{Dt} = \frac{\tau}{k}\frac{Dk}{Dt} - \frac{\tau^2}{k}\frac{D\varepsilon}{Dt} \tag{3.24}$$

Equations (3.22) and (3.24) provide clues for modelling the resultant exact scale-determining equation (e.g., for ω or τ). Referring to the corresponding terms in the k-ε model, various terms in the exact transport equation for ω or τ can be expressed in terms of the primary transport quantities. Rather than using such a transformation in a recently proposed k-ω model, Wilcox (1988, 1993) modelled the ω-equation by directly placing it in the form of the Z-equation. Setting the source term in (3.17) to zero, the modelled ω-equation in Wilcox's k-ω model reads

$$\frac{\partial \omega}{\partial t} + u_j\frac{\partial \omega}{\partial x_j} = \frac{\omega}{k}\left(c_{\omega 1}\tau_{ij}\frac{\partial u_i}{\partial x_j} - c_{\omega g}\beta g_j h_j\right) - c_{\omega 2}\omega^2 + \frac{\partial}{\partial x_j}\left[(\nu + \frac{\nu_t}{\sigma_\omega})\frac{\partial\omega}{\partial x_j}\right] \tag{3.25}$$

The eddy viscosity in the k-ω model is formulated as

$$\nu_t = c_\mu k/\omega \tag{3.26}$$

The dissipation rate, ε, in the modelled k-equation (3.16) can be represented in terms of k and ω. Combining the relations in (3.20) and (3.26) gives $\varepsilon = c_k k\omega$. The model coefficients, for isothermal flows, are parameterized as (cf. Wilcox, 1988)

$$c_\mu = 1.0,\ \sigma_k = 2.0,\ \sigma_\omega = 2.0,\ c_k = 0.09,\ c_{\omega 1} = 5/9,\ c_{\omega 2} = 0.075 \tag{3.27}$$

As noted by Hallbäck *et al.* (1995), the above different types of two-equation models are rather similar in character, since transformations between these models show that the modelling of the production and destruction terms are completely equivalent. Nonetheless, there exist a number of variants for each type of these models. These variants, together with various specifications for the model constants, may lead to considerable differences in predictions. To be distinguished from their variants, the high-*Re* models are often termed the *standard* ones.

Of all the existing models, none can be used with universal validity when dealing with different flow problems. The models described above were originally constructed for fully developed turbulence. In principle, they are thus only applicable for high-Reynolds-number turbulent flows. For low-Reynolds-number turbulent flows, e.g., in near-wall regions where viscous effects play a significant role in turbulent energy dissipation and diffusion, a standard high-*Re* model often fails to correctly simulate the turbulence behaviour. This thus prompts the development of LRN variants of the standard models.

In addition, one may note that the approximation for the Reynolds stresses in Equation (3.11) virtually claims that the normal Reynolds stresses are all equal. This is in substantial contradiction with experiments for flow, e.g., in a non-circular duct. To remedy this and other drawbacks existing in the standard models, other variants of the high-*Re* number models have also been developed, including the non-linear (or anisotropic) variants by, e.g., Speziale (1987), Park and Sung (1995), Craft *et al.* (1995) and Huang and Rajagopal (1996), and the variants derived from the Renormalization group (RNG) analysis by, e.g., Yakhot and Orszag (1986), Yokhot *et al.* (1992) and Karniadakis *et al.* (1993).

3.4 LRN Two-Equation Model

A high-Reynolds-number model can not, in general, be integrated over the whole flow domain for wall-bounded turbulent flows. This is particularly true when applied to flows in ventilated rooms. As described in Section 2.2, a ventilation flow is usually characterized by low-Reynolds-number turbulence not only in near-wall regions but also in regions far away from walls. In near-wall regions, Shih and Lumley (1993) showed that all energetic large eddies reduce to dissipative Kolmogorov eddies and, consequently, all the near-wall flow properties, such as the friction velocity and the mean strain rate, are characterized by Kolmogorov microscales. Viscous modifications to high-*Re* models are thus necessary to make the models have an appropriate response to flows in which the effect of molecular viscosity becomes comparable to that of the eddy viscosity.

Nonetheless, when used in conjunction with wall functions, high-*Re* models have indeed reached remarkable success in solving engineering flow problems. Without integrating the model to the wall surface, the wall-function method helps to patch the core region of the flow to the wall region. The origin of the wall functions is related to the local equilibrium and uniform shear stress assumptions and the so-called *log-law* of the wall. As a consequence, their use for complex flows becomes physically questionable, e.g., for flows with separation. It was

mentioned in Section 2.2 that the near-wall velocity profile measured in a ventilated room with a low supply air flow rate differs from the conventional log-law of the wall. This provides evidence that the use of this approach may be inappropriate in turbulent boundary layers at low Reynolds numbers. Incorporating the wall functions into boundary conditions in numerical simulations, the drawbacks nestled in this approach will give incorrect expressions at near-wall grid points where wall functions are used. Consequently, the prediction for the whole flow domain may be contaminated. Various aspects of the invalidity of the wall-function approach have been addressed briefly or in detail in previous work by, e.g., Patel *et al.* (1984), Chen and Patel (1988) and So *et al.* (1991).

To find alternatives by which the drawbacks of using the wall-function method can be eliminated, different modelling approaches have been developed to account for near-wall turbulence behaviour. Such models can be directly integrated towards the wall surface and are able to simulate near-wall viscous effects. Near-wall modelling methods include, for example, using an anisotropic eddy viscosity formulation (Speziale and Abid, 1995); introducing an additional transport equation into the two-equation closure (i.e. the three-equation model) and using this transport quantity to re-formulate the eddy viscosity (Durbin, 1991); or implementing a two-layer model (Launder, 1986; Chen and Patel, 1988). The most popular approach at present is to modify the model coefficients in high-*Re*- models through LRN formulation, i.e. the damping functions, so that viscous effects can be appropriately reflected in the turbulent transport equations as being integrated towards a wall.

3.4.1 General Considerations for LRN Formulation

The main objective in LRN formulation for a high-*Re* model is to devise proper damping functions to re-model various terms in the turbulent transport equations so that they are able to respond reasonably in physics to near-wall turbulence properties. The basic principle in LRN formulation is to reduce near-wall eddy viscosity in a proper way so as to make viscous effects increasingly dominant over, or comparable to, the eddy viscosity as the model is integrated towards the wall surface. This can be achieved through adjustments in the near-wall turbulent kinetic energy and the dissipation rate by, e.g., damping or reinforcing their respective production and dissipation or destruction. The amenable terms are often the production and destruction terms in turbulent transport equations. Damping functions, however, should not be used for those un-modelled exact terms in the modelled transport equations, e.g., the dissipation term in the k-equation for the k-ε model.

To reduce the near-wall eddy viscosity, ν_t, it is usually re-formulated by multiplying a function f_μ whose limit is unity as the flow becomes fully developed turbulence. In the k-ε and the k-ω models, it reads, respectively,

$$\nu_t = c_\mu f_\mu k^2 / \varepsilon \tag{3.28}$$

and

$$\nu_t = c_\mu f_\mu k / \omega \tag{3.29}$$

Theoretically, it is possible to use only one function f_μ to render the model reasonable near-wall performance. For example, a sophisticated f_μ can be devised to ensure that the eddy viscosity would behave in near-wall regions as it does in a non-linear two-equation model that

has well-behaved near-wall performance. Instead of using only f_μ, however, complementary damping functions are often employed to maintain overall reasonable model behaviour. These functions, in general, should be able to manage a near-wall reduction in k and/or an increment in ε or ω in order to eventually reduce ν_t and give appropriate model behaviour. To better represent the near-wall turbulence characteristics, some models employ extra terms or wall-reflection terms in the turbulent transport equations. For example, an extra term, $D = -2\nu(\partial\sqrt{k}/\partial y)^2$, is added on the right-hand side of the k-equation in some k-ε models and, correspondingly, an additional term, E_ε, is employed in the ε-equation (cf. Patel *et al.*, 1984). Here, the ε-equation in the LRN k-ε models is put in a general form, as follows

$$\frac{\partial \varepsilon}{\partial t} + u_j \frac{\partial \varepsilon}{\partial x_j} = \frac{\varepsilon}{k}\left(c_{\varepsilon 1} f_1 \tau_{ij} \frac{\partial u_i}{\partial x_j} - c_{\varepsilon g} \beta g_j h_j \right) - c_{\varepsilon 2} f_2 \frac{\varepsilon^2}{k} + \frac{\partial}{\partial x_j}\left[(\nu + \frac{\nu_t}{\sigma_\varepsilon}) \frac{\partial \varepsilon}{\partial x_j} \right] + E_\varepsilon \qquad (3.30)$$

Referring to its exact form, i.e. Equation (3.23), the LRN ω-equation can also be written in a general form as

$$\frac{\partial \omega}{\partial t} + u_j \frac{\partial \omega}{\partial x_j} = \frac{\omega}{k}\left(c_{\omega 1} f_1 \tau_{ij} \frac{\partial u_i}{\partial x_j} - c_{\omega g} \beta g_j h_j \right) - (c_{\omega 2} f_2 - 1)\omega^2 + \frac{\partial}{\partial x_j}\left[(\nu + \frac{\nu_t}{\sigma_\omega}) \frac{\partial \omega}{\partial x_j} \right] + E_\omega \qquad (3.31)$$

In the k-ω model, since the dissipation term in the k-equation is transformed from the dissipation term, ε, through an empirical model constant c_k as $\varepsilon = c_k k\omega$, it is thus amenable in LRN formulation by using a damping function, f_k. In addition, the buoyancy production term has been modelled in line with the eddy diffusivity concept, a damping function can also be used to adjust the near-wall behaviour of this term in the k-equation. The same can be done in the equations for ε and ω through model coefficients $c_{\varepsilon g}$ and $c_{\omega g}$. The k-equation in an LRN k-ω model is written as

$$\frac{\partial k}{\partial t} + u_j \frac{\partial k}{\partial x_j} = \tau_{ij} \frac{\partial u_i}{\partial x_j} - f_g \beta g_j h_j - c_k f_k k\omega + \frac{\partial}{\partial x_j}\left[(\nu + \frac{\nu_t}{\sigma_k}) \frac{\partial k}{\partial x_j} \right] \qquad (3.32)$$

In some models, damping functions are also used to re-model the turbulent diffusion terms through the model coefficients σ_k and σ_ε or σ_ω, see e.g. Kawamura and Kawashiba (1997).

The formulation for f_μ, f_g, f_k, f_1 and f_2 is usually devised as continuous functions of some dimensionless variables that are proportional to $(1/\nu)$ to represent increasing viscous effects as a wall approaches. These variables include, e.g., $y^+ = u_\tau y/\nu$, $R_y = \sqrt{k}y/\nu$, $R_\varepsilon = (\nu\varepsilon)^{1/4}/\nu$ and the turbulent Reynolds number, R_t, defined by

$$R_t = \frac{k^2}{\varepsilon\nu} \quad \text{or} \quad R_t = \frac{k}{\omega\nu} \qquad (3.33)$$

The methodology used to determine damping functions is somewhat *ad hoc*. Theoretically, the

division between the exact and the modelled terms is the damping function for the corresponding modelled term. One way is then to use existing DNS data for, e.g., channel flows (Kim *et al.*, 1987) and boundary layer flows (Spalart, 1988) to make term-by-term comparisons, see e.g. Mansour *et al.* (1988), Rodi and Mansour (1993) and Nagano and Shimada (1995). The resultant LRN model as a whole must be carefully calibrated and validated using available experimental and DNS data to ensure reasonable model performance not only in near-wall regions but also in regions where turbulence is fully developed.

There are several basic *laws* to regulate the determination of damping functions. First, a damping function should not break the general requirements in turbulence modelling, as mentioned in the beginning of Section 3.2. Second, for fully developed turbulent flows, the parent model on which LRN formulation is based should have reasonable behaviour and be able to produce acceptable predictions. Third, the effect of a damping function should usually be monotonically disappeared (return to unity) when approaching regions away from a wall where turbulence is fully developed. The LRN model should then, in this case, return to its high-*Re* parent version. It is thus important to estimate the range of the influence of the viscous damping. This is often evaluated by following van Driest (1956), who suggested that near-wall turbulence is damped by a factor of $\left[1-\exp(-y^+/A)\right]$. Moreover, the LRN formulated model should be able to reasonably reproduce the log-law in the wall-layer for equilibrium boundary layers where $\wp \cong \varepsilon$. This is the basic requirement for an LRN model when it is used as an alternative to the wall-function method in near-wall regions. Finally, but being frequently addressed, the damping function should ensure correct near-wall asymptotic behaviour for each damped term and for the model as a whole.

3.4.2 Near-Wall Asymptotic Analyses

A correct near-wall asymptotic behaviour includes two aspects: the primary turbulent quantities, such as the turbulent kinetic energy, the dissipation rate, Reynolds stresses and heat fluxes, behave correctly in the vicinity of walls; the modelled terms in the turbulent transport equations have asymptotic properties identical with their exact counterparts. To make near-wall asymptotic analyses, a Taylor series expansion for the turbulent fluctuations is used

$$u' = a_1 y + a_2 y^2 + \cdots \tag{3.34a}$$

$$v' = b_2 y^2 + b_3 y^3 + \cdots \tag{3.34b}$$

$$w' = c_1 y + c_2 y^2 + \cdots \tag{3.34c}$$

$$p' = d_0 + d_1 y + d_2 y^2 + \cdots \tag{3.34d}$$

$$T' = e_1 y + e_2 y^2 + \cdots \tag{3.34e}$$

where y is the normal distance to a wall. Using these in the definitions of k and ε gives $k \propto y^2$ and $\varepsilon \propto y^0$. Similarly, the asymptotic behaviour, as $y \to 0$, for ω and R_t can be expressed as, respectively,

$$\omega \propto \frac{1}{y^2}, \text{ and } R_t \propto y^4 \tag{3.35}$$

Inserting Equations (3.34a)-(3.34e) into the near-wall simplification of each term in the exact transport equations for k, ε and ω and taking the leading part in the expansion, the following asymptotic relations (as $y \to 0$) are obtained

$$\begin{aligned}
&\wp \propto y^3,\ G \propto y^3,\ D_t \propto y^3,\ D_v = y^0;\\
&\wp_\varepsilon \propto y,\ G_\varepsilon \propto y,\ \Pi_\varepsilon \propto y^0,\ D_{t\varepsilon} \propto y^0,\ D_{v\varepsilon} \propto y^0;\\
&\wp_\omega \propto y^{-1},\ \Pi_\omega \propto y^{-4},\ D_{t\omega} \propto y^{-2},\ D_{v\omega} \propto y^{-4};\\
&\overline{u'v'} \propto y^3,\ \overline{u'T'} \propto y^2,\ \overline{v'T'} \propto y^3,\ \overline{w'T'} \propto y^2.
\end{aligned} \tag{3.36}$$

In deriving the asymptotic expression for the turbulent diffusion term (D_t) for k, the pressure diffusion part has been neglected, since the DNS result indicates that this part is much less than the triple-velocity diffusion part near a wall, see Mansour *et al.* (1988) and Speziale *et al.* (1992). In addition, it is noted that both the buoyancy production terms in the k and ε equations, G and G_ε, have different respective asymptotic behaviours in cases of near a vertical wall and near a horizontal wall, because these terms are conducted by gravity only in the vertical direction. The relation given in Equation (3.36) is for the horizontal wall case. Near vertical walls, one should have $G \propto x^2$ and $G_\varepsilon \propto x^0$, where x represents the normal distance to a vertical wall, see also Peng and Davidson (1997d).

In the vicinity of a wall, the modelled turbulent quantity is required to have asymptotic behaviour consistent with its exact counterpart. To ensure this for the Reynolds stresses, the eddy viscosity must be $\nu_t \propto y^3$ (cf. Equations (3.11) and (3.36)). The damping function, f_μ, should then behave as $f_\mu \propto 1/y$ in both Equations (3.28) and (3.29). Comparing the near-wall behaviours between the exact and its modelled term, the near-wall asymptotic requirement on each damping function can readily be figured out. For LRN k-ε models, one should have $f_1 \propto y^0$, $f_2 \propto y^2$; and for LRN k-ω models, $f_k \propto y^0$, $f_1 \propto y^0$ and $f_2 \propto y^2$. Note that f_2 in the LRN k-ω model is used to model the (Π_ε/k)-part of Π_ω in (3.23) (cf. Equation (3.31)). Damping function f_g in the k-equation should be $f_g \propto y^0$ near a horizontal wall and $f_g \propto y^{-1}$ near a vertical wall.

Although asymptotic behaviour has been emphasized in some previous work on LRN model development, many existing models do not exploit these properties (cf. Patel *et al.*, 1984). Savill (1995) recently reported that the correct wall-limiting behaviour for $-\overline{u'v'}$ can be credited in predicting low-Reynolds-number transitional regions of boundary layer flows. Satisfying $f_\mu \propto 1/y$ in an LRN model appears to be a favoured aspect.

3.4.3 Wilcox's LRN k-ω Model

There have been a number of LRN variants for different types of two-equation models. Representative examples include the LRN k-ε model by Jones and Launder (1972, 1973), the LRN k-ω model by Wilcox (1994) and the LRN k-τ model by Speziale *et al.* (1992). It would entail a great deal of work to get a full picture for all the existing LRN models: there might be some dozens of different LRN variants constructed since 1970s. Some other LRN models often referred to in studies include the Launder-Sharma model (1974), the Lam-Bremhorst model (1981), the Chien model (1982), the Myong-Kasagi model (1988), the Nagano-Tagawa model (1990), the Lai-So model (1990), the Yang-Shih model (1993), the Rodi-Mansour model (1993) and the Abe-Kondoh-Nagano model (1994). Patel *et al.* (1984) reviewed eight different models by scrutinising them with experimental data for flat-plate boundary layer and pipe

flows. More recently, Hrenya *et al.* (1995) extended this comparison to some later LRN models after Patel *et al.*'s review work and evaluated ten different versions in predicting turbulent pipe flow.

For later use, Wilcox's LRN k-ω model (Wilcox, 1994) is briefly described here. Based on its high-Re version (Wilcox, 1988), this model was originally developed for simulating transition for forced convection boundary layer flows, and thus $c_{\omega g} = f_g = 0$ in Equations (3.31) and (3.32). Setting $f_2 = 1$ and $E_\omega = 0$, Wilcox proposed the following damping functions

$$f_\mu = \frac{0.025 + R_t/6}{1 + R_t/6} \tag{3.37}$$

$$f_k = \frac{5/18 + (R_t/8)^4}{1 + (R_t/8)^4} \tag{3.38}$$

$$f_1 = \frac{0.1 + R_t/2.7}{1 + R_t/2.7} f_\mu^{-1} \tag{3.39}$$

Similar to those in the high-Reynolds-number version, the model constants are given by

$$c_\mu = 1.0,\ \ \sigma_k = 2.0,\ \ \sigma_\omega = 2.0,\ c_k = 0.09,\ \ c_{\omega 1} = 5/9,\ \ c_{\omega 2} = 1.075 \tag{3.40}$$

One of the positive features of this model is that the damping functions are related only to R_t, without using other wall proximity dependent quantities (e.g. y^+, R_y and R_ε etc.). Savill (1995) found that such an R_t-dependence feature is desired for LRN models in predicting transitional boundary layer flows. In addition, the wall-distance free damping functions make it numerically convenient for simulating flows with complex geometries.

The mechanism of simulating transitional flows with this model was analyzed using a Blasius transformation (Wilcox, 1994). It was argued that, starting from the laminar stage, the net production of k per unit dissipation term ($\wp/\varepsilon - 1$) must be amplified earlier than that of ω ($\wp_\omega/\Pi_\omega - 1$) to ensure the onset of transition. Consequently, as $R_t \to 0$, this requires

$$c_{\omega 1} f_1 c_\mu f_\mu < c_{\omega 2} \tag{3.41}$$

Second, the net production of k should initiate its amplification at the minimum critical Reynolds number at which Tollmien-Schlichting waves begin forming in the Blasius boundary layer. This is to ensure a reasonable prediction for the location of the transition onset. To satisfy this condition, as $R_t \to 0$, it must be

$$c_k f_k / (c_\mu f_\mu) \to 1 \tag{3.42}$$

Finally, to have a correct asymptotic behaviour for k, an analysis on the near-wall balance between the dissipation term and the viscous diffusion term in the k-equation indicates that, as $y \to 0$,

$$c_k f_k / c_{\omega 2} \to 1/3 \tag{3.43}$$

The above three conditions have been satisfied in Wilcox's LRN model through adjustments in the model constants and the damping functions. Wilcox used a so-called *numerical roughness strip* to trigger transition at the desired location and reported reasonable simulations for a series of transitional isothermal boundary layer flows. It should be noted that the damping function f_μ in this model does not have correct wall-limiting behaviour, yielding incorrectly $\overline{u'v'} \propto y^4$ as $y \to 0$.

3.5 Modifications to the k-ω Model

Using the high-Reynolds-number (standard) k-ω model and its LRN variant, reasonable predictions have been reported by, e.g., Liu and Zheng (1994) and Patel and Yoon (1995). However, when they are applied to ventilation or other equivalent flows, it was found that the model fails to give reasonable results (Peng *et al.*, 1996c, 1997c). Modifications have thus been made to improve the model performance.

3.5.1 The Modified High-*Re* k-ω Model

As with other high-Reynolds-number two-equation models not using wall functions, the standard k-ω model recovers a lower near-wall peak in the turbulent kinetic energy in boundary layers as compared with experiments data. This drawback remains when the standard k-ω model is applied to complex flows, e.g., backward-facing step flows, which is a flow phenomenon that often occurs in rooms with mixing ventilation. It was found that the near-wall eddy viscosity is considerably under-estimated by this model. As a result, the reattachment location is overpredicted, leading to inaccurate predictions. Modifications to this model thus aim at finding an appropriate way to enhance the eddy viscosity and meanwhile to properly maintain near-wall viscous effects as required in LRN models. This has been achieved by modifying the turbulent transport equation and re-establishing the model constants.

The Modified ω-Equation

In a comparison with the exact ω-equation, (3.23), it may be noted that an exact viscous cross-diffusion term has been neglected in the modelled ω-equation, (3.25), where the exact turbulent diffusion, as a whole, has been modelled in a single second-order diffusive term. It is noted that, close to a wall, the gradients of k and ω are of opposite sign. A cross-diffusion term thus turns out to be negative in the vicinity of a wall. Its inclusion in the ω-equation can then be expected to suppress the near-wall ω level and consequently to enhance the eddy viscosity, as desired. Inspired by this near-wall property of a cross-diffusion term, the turbulent diffusion is then modelled in terms of a second-order diffusion and a cross diffusion, in analogy to its viscous counterparts in the exact ω-equation. Retaining the viscous cross-diffusion term in the modelled ω-equation, however, will introduce an unrealizable problem into the near-wall ω solution, unless a damping function, f_2, is employed as in (3.31). Without using f_2, this unrealizability can be easily shown to be true by the near-wall balance between the viscous diffusion and viscous dissipation terms, i.e.,

$$\nu \frac{\partial^2 \omega}{\partial y^2} + \frac{2\nu}{k} \frac{\partial k}{\partial y} \frac{\partial \omega}{\partial y} - c_{\omega 2} \omega^2 = 0 \qquad (3.44)$$

Note that, in the vicinity of the wall, $k \propto y^{3.23}$ for the high-Reynolds-number k-ω model (Peng *et al.*, 1996c). Introducing this asymptotic relation into (3.44) will lead to a negative ω as the

wall is approached. The viscous cross-diffusion term in the modified model, therefore, must be dropped as in Wilcox's model. In its high-*Re* form, the modified ω-equation for isothermal flows then reads

$$\frac{\partial \omega}{\partial t}+u_j\frac{\partial \omega}{\partial x_j}=c_{\omega 1}\frac{\omega}{k}\left(\tau_{ij}\frac{\partial u_i}{\partial x_j}\right)-c_{\omega 2}\omega^2+\frac{\partial}{\partial x_j}\left[(\nu+\frac{\nu_t}{\sigma_\omega})\frac{\partial \omega}{\partial x_j}\right]+c_\omega\frac{\nu_t}{k}\frac{\partial k}{\partial x_j}\frac{\partial \omega}{\partial x_j} \qquad (3.45)$$

The addition of the turbulent cross-diffusion term can also be derived from a model transformation using the k-ε model. By inserting the modelled k and ε equations into the right-hand side of (3.22), an equivalent turbulent cross-diffusion term can be recovered in the resultant ω-equation.

This turbulent cross-diffusion term was also employed in the k-ω model for solving free shear flows, but was used only in the regions away from the wall to eliminate the model sensitivity to the freestream value of ω (cf. Wilcox, 1993). By contrast, this term in the present modified model is generalized for the whole flow domain. Moreover, it is well known that the k-ε model overpredicts the near-wall turbulent length scale for wall-bounded flows in the presence of an adverse pressure gradient. A so-called *Yap-correction* has often been employed to remedy this problem. With Wilcox's k-ω model, it has been argued that the resultant ε-equation transformed from the k-ω model (by exploiting (3.22)) contains a term that plays a role similar to the Yap-correction. The k-ω model thus performs better than the k-ε model without using any correction in this case. In this modified model, a similar term can be recovered only if the related model constants are established in a relation as (Peng *et al.*, 1997c)

$$c_\omega < \left(\frac{1}{\sigma_k}+\frac{1}{\sigma_\omega}\right) \qquad (3.46)$$

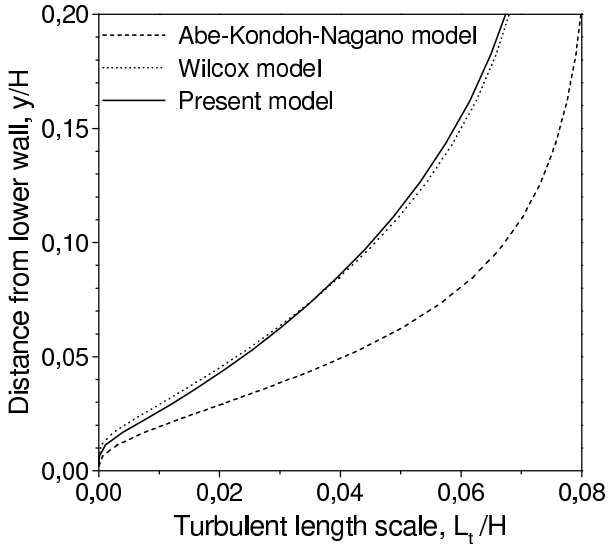

Figure 3.1 Comparison of turbulent length scales predicted by different LRN models.

Figure 3.1 shows a comparison of the turbulent length scales near the reattachment location predicted by different LRN models for a backward-facing step flow with an expansion ratio of

ER = 6. The modified model indeed preserves a Yap-correction-like function as well as in Wilcox's model, giving a smaller turbulent length scale at the reattachment location than the LRN k-ε model does.

The Modified Model Constants

Bearing in mind the under-estimation in the eddy viscosity, one may note that a straightforward remedy is to suppress the specific dissipation rate by reducing its production. This can be achieved by adjusting the model constant, $c_{\omega 1}$, for the production term in the ω-equation. However, the model constant should not be randomly changed in order to retain a reasonable model performance for some fundamental turbulent flows that have been frequently used in model calibration, for which theoretical solutions are known or well-documented experimental data are available.

For a local equilibrium boundary layer, the model should be able to recover the law of the wall (log-law) in the wall-layer, where the Reynolds shear stress is constant and equal to u_τ^2. The balance between the production and dissipation of k requires

$$\sqrt{c_\mu c_k} = \frac{-\overline{u'v'}}{k} = \frac{u_\tau^{\,2}}{k} \tag{3.47}$$

Experiments indicate that $u_\tau^2/k \approx 0.3$. This thus suggests

$$c_\mu c_k = 0.09 \tag{3.48}$$

Further, from the simplified ω-equation in the local equilibrium boundary layer, one gets

$$c_{\omega 1} = \frac{c_{\omega 2}}{c_k} - \frac{\kappa^2}{\sigma_\omega \sqrt{c_\mu c_k}} \tag{3.49}$$

In addition, for a decaying isotropic turbulence, experiments found that turbulence decays with time to a power of about $-(1 \sim 1.25)$. Through the k and ω equations, this can be argued in a relation of

$$\frac{c_k}{c_{\omega 2}} = 1 \sim 1.25 \tag{3.50}$$

As indicated by Wilcox (1988), setting $c_\mu = 1$ possesses the generality of using other values for this model coefficient. It can be shown that varying this constant will alter ω by only a factor of c_μ in the wall-layer; the kinetic energy and the eddy viscosity will remain unchanged only if Equation (3.48) holds.

On the basis of the aforementioned arguments, and having been calibrated and optimized further in numerical experiments for typical ventilation flows, the model constants in the modified model have been re-established. Under the conditions of (3.46), (3.48), (3.49) and (3.50), they are given as

$$c_\mu = 1.0,\ \ \sigma_k = 0.8,\ \ \sigma_\omega = 1.35,\ c_k = 0.09,\ \ c_{\omega 1} = 0.42,\ \ c_{\omega 2} = 0.075,\ c_\omega = 1.35 \tag{3.51}$$

3.5.2 The Modified LRN k-ω Model

There is evidence that the k-ω model is more computationally robust than the standard k-ε model for the integration of turbulent flow to a solid boundary (Speziale *et al.*, 1992). Wilcox (1988) thus proposed integrating this model directly to the wall surface without using wall functions as a bridge. This is termed the *extended-to-wall* method for a high-Reynolds-number model. However, both the Wilcox and the modified models yield solutions for k that are asymptotically inconsistent in the vicinity of a wall. Along with this drawback, the near-wall k peak is considerably underpredicted for, e.g., channel flows. Using Wilcox's LRN model (Wilcox, 1994) as described in Section 3.4.3, this problem is remedied. However, it was found that this LRN model retains poor performance for typical ventilation flows. A new LRN k-ω model has thus been developed, see Peng *et al.* (1997c).

Since the above modified high-*Re* version appears to have reasonable behaviour for simulating recirculating ventilation flows (Peng *et al.*, 1996b, c), it is thus used as the parent model for further LRN modifications. This suggests that the modified LRN model should return to the modified high-*Re* version for fully developed turbulent flows. The turbulent transport equations and the model constants are therefore virtually the same as in the modified high-*Re* model. Instead of using the form as in (3.31), the modified LRN ω-equation for isothermal flows has the following form, similar to its high-*Re* parent version

$$\frac{\partial \omega}{\partial t}+u_j\frac{\partial \omega}{\partial x_j}=c_{\omega 1}f_1\frac{\omega}{k}\left(\tau_{ij}\frac{\partial u_i}{\partial x_j}\right)-c_{\omega 2}f_2\omega^2+\frac{\partial}{\partial x_j}\left[(\nu+\frac{\nu_t}{\sigma_\omega})\frac{\partial \omega}{\partial x_j}\right]+c_\omega\frac{\nu_t}{k}\frac{\partial k}{\partial x_j}\frac{\partial \omega}{\partial x_j} \quad (3.52)$$

Note that the near-wall asymptotic behaviour for f_2 in (3.52) is different from that in Equation (3.31), where the dissipation term was separated into two parts. To retain a correct asymptotic solution for ω, f_2 should be $f_2 \propto y^0$ as $y \to 0$, if the related dissipation term in (3.52) is damped. The k-equation in the modified LRN model takes the same form as Equation (3.32), setting $f_g = 0$ for isothermal flows.

In developing the near-wall viscous modifications, effort has been made to preserve two merits as in Wilcox's LRN model (Wilcox, 1994). First, the mechanism of simulating transition, as described in section 3.4.3 in Wilcox's model, has been retained in the modifications. Second, the damping functions have been devised to be dependent only on the turbulent Reynolds number (R_t) without using any other wall proximity dependence. Furthermore, the inconsistent asymptotic behaviour nestled in Wilcox's LRN model for the near-wall Reynolds shear stress has been corrected.

Referring to the near-wall asymptotic analysis presented in Section 3.4.2 and validated in numerical experiments, the following damping functions have been proposed

$$f_\mu=0.025+\left\{1-\exp\left[-\left(\frac{R_t}{10}\right)^{3/4}\right]\right\}\times\left\{0.975+\frac{0.001}{R_t}\exp\left[-\left(\frac{R_t}{200}\right)\right]^2\right\} \quad (3.53)$$

$$f_k=1-0.722\exp\left[-\left(\frac{R_t}{10}\right)^4\right] \quad (3.54)$$

$$f_1=1+4.3\exp\left[-\left(\frac{R_t}{1.5}\right)^{1/2}\right] \quad (3.55)$$

The dissipation term in Equation (3.52) is kept in its high-*Re* form by setting $f_2 = 1$. As $R_t \to 0$, Equation (3.53) yields $f_\mu \sim (1/R_t^{1/4} + \ldots)$, which complies with the correct asymptotic condition of $f_\mu \sim y^{-1}$. Furthermore, as $R_t \to 0$, it gives

$$\nu_t \sim (k/\omega) R_t^{-1/4} \sim L_t u_k \tag{3.56}$$

where $L_t \sim k^{1/2}/\omega$ is the turbulent length scale, and u_k is the Kolmogorov velocity scale in terms of ν, k and ω, i.e. $u_k \sim (\nu k\omega)^{1/4}$. Equation (3.56) thus suggests that the near-wall eddy viscosity is determined by the small-scale eddies. The turbulent length scale, L_t, is proportional to y^3 in the near-wall region and decreases towards the wall surface. As L_t approaches the Kolmogorov length scale, $\eta_k \sim (\nu^3/k\omega)^{1/4} \sim L_t R_t^{-3/4}$, the eddy viscosity is reduced to the same order as the molecular viscosity. This is consistent with the analysis of Kolmogorov behaviour in near-wall turbulence by Shih and Lumley (1993).

The modified model has been applied to channel flows, backward-facing step flows and typical ventilation flows. In comparison with Wilcox's LRN model, the prediction is generally improved with the present modifications, see Peng *et al.* (1997c). Figure 3.2 shows some results for a channel flow at $Re_\tau = 395$ in comparing with the DNS data by Kim *et al.* (1987).

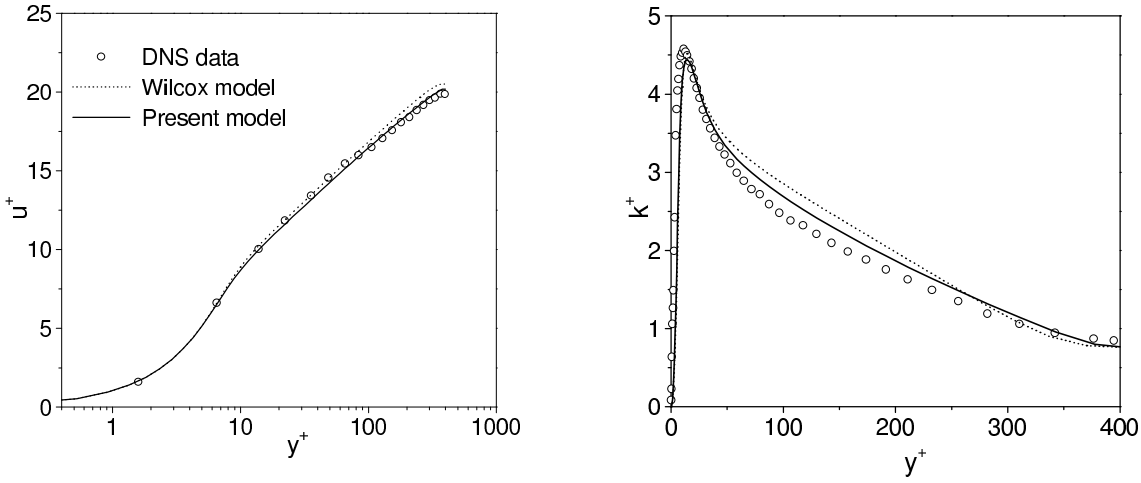

a) Distribution of mean velocity b) Distribution of turbulent kinetic energy

Figure 3.2 Comparison of predictions for a channel flow at $Re_\tau = 395$.

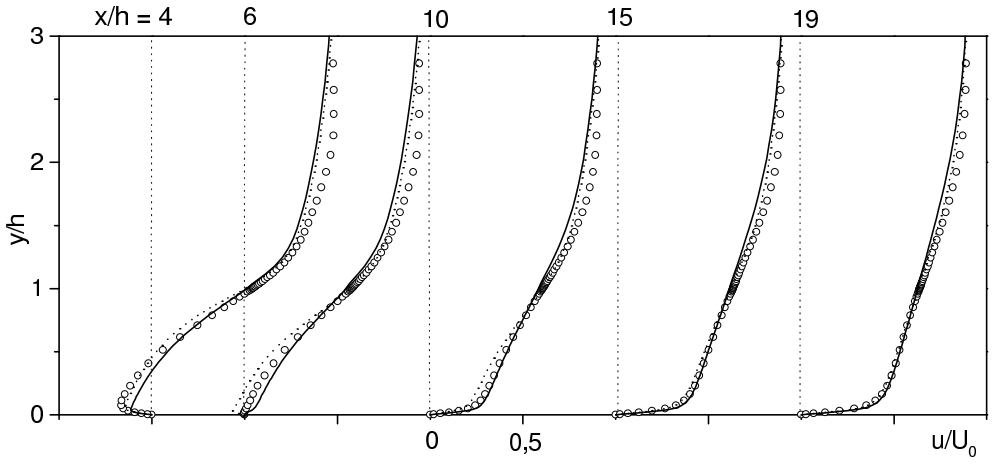

a) Distributions of mean velocity

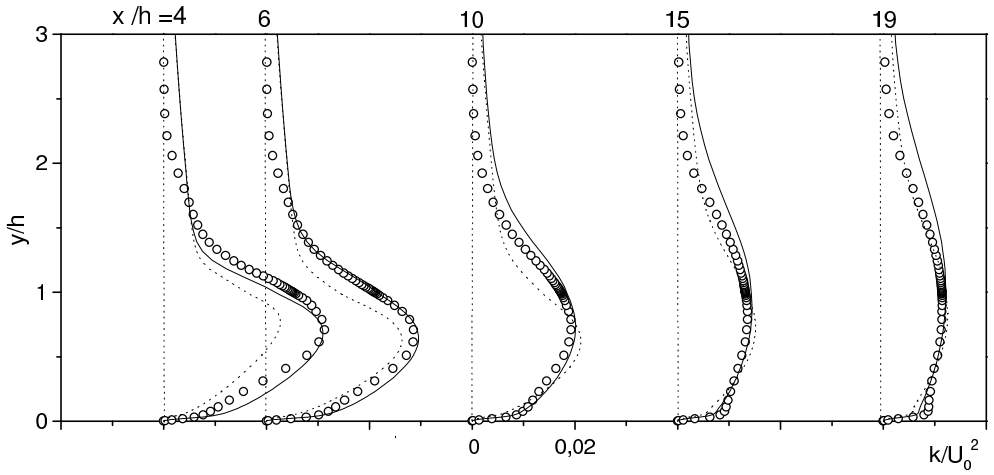

b) Distributions of turbulence kinetic energy

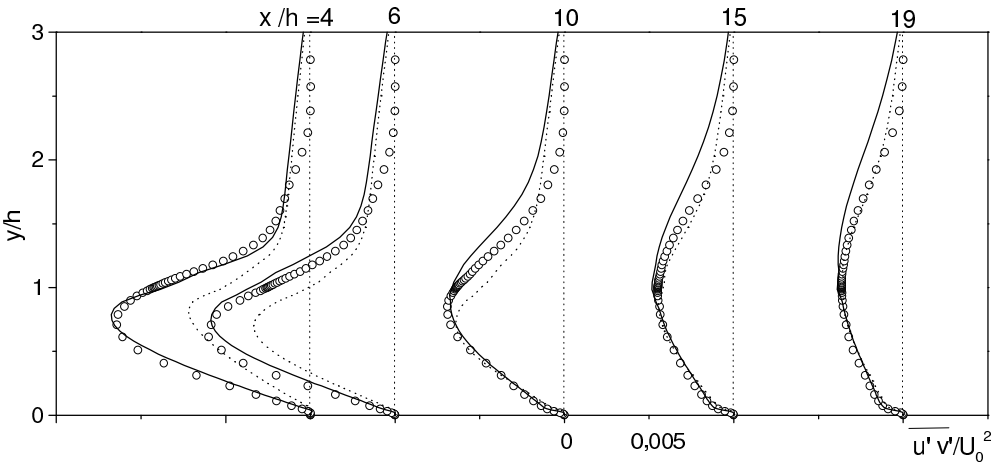

c) Distributions of shear stress

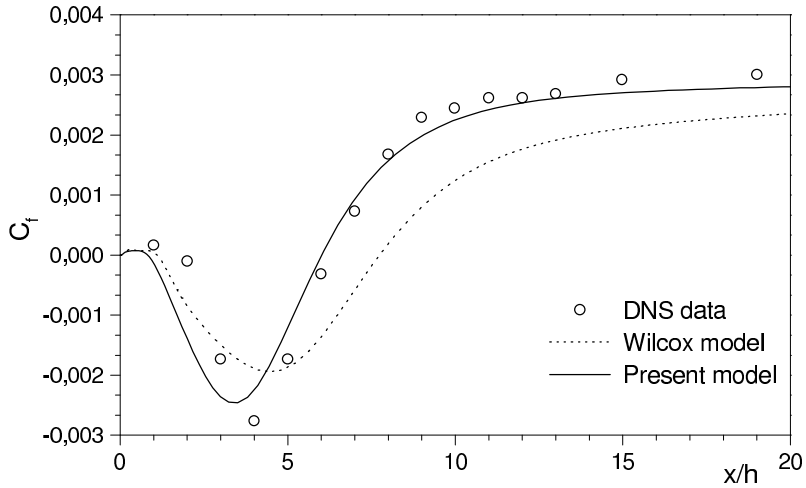

d) Distribution of friction coefficient

Figure 3.3 Comparison of predictions for a backward-facing step flow.

In Figure 3.3, the two models are further compared for predicting a flow over a backward-facing step with a small expansion ratio of $ER = 1.2$ at a Reynolds number of $Re = 5100$ based

on the step height, h. The result is normalized with the maximum inlet velocity, U_0, and is compared with the DNS data by Le and Moin (1994). In general, the prediction was improved with the present modifications as compared with the original model.

3.5.3 Analyses of Model Behaviour for Turbulent Buoyant Flows

Turbulent buoyant flows often occur in building ventilation, where generation and transport of turbulence rely significantly on the thermal stratification. It would be desirable to extend the application of the modified LRN k-ω model to natural convection flows. In many ways, the natural convection flow in an enclosed cavity is similar to the ventilation flow in a room with non-adiabatic outer walls. Moreover, the cavity flow is regarded as a fundamental type for buoyant turbulence research. This type of flow has thus been commonly applied to model validations in which turbulent buoyant influences need to be accounted for.

For buoyant cavity flows at moderate Rayleigh numbers, Ra, turbulence is fully developed only in some regions along the vertical walls (the upper part along the heated wall and the lower part along the cooled wall), and it decays away from the walls. This thus requires the turbulence models used in computations to be able to appropriately capture the turbulence evolution starting from laminar flow in order to obtain reliable predictions for convective heat transfer. The transition from laminar to turbulence causes an increase in air-to-wall convective heat transfer along the vertical wall. The strong interaction between the thermal and hydrodynamic instabilities requires a particular effort to describe the non-linear growth of disturbances that lead the flow from laminar to turbulence.

In general, the inclusion of LRN modifications in the k-ε model improves the prediction of wall heat transfer for buoyant cavity flows, as stated by Heindel *et al.* (1994). However, some problems have also been reported in a comparison using the results from a workshop conducted by Henkes and Hoogendoorn (1995). Among others, the solution was found to be grid-dependent when using the k-ε model: the transition onset along the non-adiabatic vertical walls is delayed with refining grid. Note that both Wilcox's and the modified LRN k-ω models preserve a mechanism for simulating transition in isothermal boundary layer flows. It is thus desired to investigate their performance for flows in which turbulence is promoted from laminar with both the thermal and the hydrodynamic instabilities, e.g., for cavity flows.

As with the LRN k-ε models, however, the predictions given by both LRN k-ω models were disappointing – the transition regime along the vertical wall was delayed as the grid was successively refined (Peng and Davidson, 1997d). When the grid is sufficiently refined, both models return a laminar solution in the whole cavity. Since the transition-simulation mechanism in the LRN k-ω models originally gained its credit with forced convection boundary layer flows, this mechanism needs to be re-examined for natural convection boundary layer flows in which buoyancy plays a significant role.

Analysis of Transition Regime in Natural Convection Boundary Layer

Along a non-adiabatic vertical wall, e.g. the hot wall of an enclosure with two differentially heated side walls, the natural convection boundary layer flow at a moderate Rayleigh number usually undergoes three stages: the laminar flow near the lower left corner and the subsequent transitional and turbulent flows. The transition onset can be observed through the convective heat transfer along the wall surface, in which a sudden jump occurs.

In comparison with an isothermal transitional boundary layer flow, which is dominated by shear or by pressure gradient, a buoyancy-driven boundary layer flow possesses one further turbulence evolution mechanism owing to the thermal stratification. This is reflected by the buoy-

ant production term ($G = g_j \beta \overline{u_j' T'}$) in the transport equation for the turbulent kinetic energy. The transition arising in a natural convection boundary layer flow thus depends on both the flow deformation and the buoyancy.

In essence, the transitional flow is of a low-Reynolds/Rayleigh-number type. It is well known that the physical transition mechanism itself is not tractable with a Reynolds-averaging model, since all the spectra effects are lost in the time-averaging process, and the RANS approach is capable of distinguishing only the magnitude and an average frequency of perturbations that fall in a specific range of frequencies inducing instability. Therefore, the RANS method cannot predict the development of instability and natural transition from a purely laminar flow. Nonetheless, under appropriate conditions, statistical models are able to reproduce the transition to some extent, particularly for the transition onset. One example is the by-pass transition triggered by the diffusion of free-stream turbulence into the flow, for which a moderate degree of success with some LRN two-equation models has been reported (cf. Savill, 1995). For internal flows, e.g. the buoyant flow in a confined cavity at a moderate Rayleigh number, a statistical model usually requires some initial background turbulence in the prediction to represent the turbulence evolution through transition in the boundary layer along the vertical walls. The background turbulence should be sufficiently weak not to influence laminar-like mean flow properties, but not so weak as to be amplified when the flow deformation and buoyancy are imposed, see Hanjalic *et al.* (1993).

With the RANS approach, the model implicitly assumes that the free-stream-turbulence or the background turbulence leads to a build-up of weakly correlated turbulence activity in the initial pseudo-laminar stage, and transition is triggered once the local production of turbulence energy sufficiently exceeds the local dissipation. For natural convection in a cavity, the turbulence is often very weak (or is a kind of *turbulescence* according to Hanjalic *et al.* (1993)). This turbulence tends to be stabilized in the boundary layer along the horizontal wall and in the core region of the cavity with stable thermal stratification. If such a stabilization deters this turbulescence from an appropriate further evolution, the amplification of the local production of turbulence energy represented in a two-equation model will either be slowed down or stopped and, consequently, the predicted transition onset is delayed or no transition can even be produced at all. The buoyant production term in the *k*-equation is often very small, but the role played by this term in the pseudo-laminar stage may be significant in the amplification of turbulence energy, see Peng and Davidson (1997d). This term is often negative with stable thermal stratification and is comparable to or larger than the shear production term in the outer region away from the wall. It thus tends to *absorb* turbulence energy from the boundary layer and destroy the sustaining of turbulence there. In view of the prediction of transition onset, an analysis of the behaviour of the LRN *k*-ω model is given below.

For buoyant flows, the equations for *k* and ω in the LRN model are rewritten in the following forms

$$\frac{\partial k}{\partial t} + u_j \frac{\partial k}{\partial x_j} = \tau_{ij} \frac{\partial u_i}{\partial x_j} + G - c_k f_k k\omega + \frac{\partial}{\partial x_j}\left[(\nu + \frac{\nu_t}{\sigma_k}) \frac{\partial k}{\partial x_j} \right] \tag{3.57}$$

and

$$\frac{\partial \omega}{\partial t} + u_j \frac{\partial \omega}{\partial x_j} = \frac{\omega}{k}\left(c_{\omega 1} f_1 \tau_{ij} \frac{\partial u_i}{\partial x_j} + c_{\omega g} G \right) - c_{\omega 2}\omega^2 + \frac{\partial}{\partial x_j}\left[(\nu + \frac{\nu_t}{\sigma_\omega}) \frac{\partial \omega}{\partial x_j} \right] + E_\omega \tag{3.58}$$

If the G term is modelled with the standard gradient diffusion hypothesis, SGDH (i.e. Equation (3.12)), or the generalize gradient diffusion hypothesis, GGDH (cf. Ince and Launder, 1989), this term can be written in a general form

$$G = g_j \beta \overline{u_j' T'} = \nu_t F\left(\omega, \frac{\partial u_i}{\partial x_j}, \frac{\partial T}{\partial x_j}\right) \tag{3.59}$$

where F is a function of ω, and the gradients of mean velocities and temperature.

For an incompressible, two-dimensional natural convection boundary layer flow along a vertical heated wall, in analogy to Wilcox's analyses (Wilcox, 1994), the net production per unit dissipation term for k and ω, N_k and N_ω, can be written as, respectively,

$$N_k = \frac{c_\mu f_\mu}{c_k f_k}\left[\left(\frac{\partial v/\partial x}{\omega}\right)^2 + \frac{F}{\omega^2}\right] - 1 \tag{3.60}$$

$$N_\omega = \frac{c_\mu f_\mu}{c_{\omega 2}}\left[c_{\omega 1} f_1 \left(\frac{\partial v/\partial x}{\omega}\right)^2 + c_{\omega g}\frac{F}{\omega^2}\right] - 1 \tag{3.61}$$

To ensure transition occurring from laminar to turbulence, k must be amplified earlier than ω. It is necessary to have $N_k > N_\omega \geq 0$. Consequently, as $R_t \to 0$, this requires

$$\left(\frac{1}{c_k f_k} - \frac{c_{\omega 1} f_1}{c_{\omega 2}}\right)\left(\frac{\partial v/\partial x}{\omega}\right)^2 + \left(\frac{1}{c_k f_k} - \frac{c_{\omega g}}{c_{\omega 2}}\right)\frac{F}{\omega^2} > 0 \tag{3.62}$$

For forced convection boundary layer flows, $F = 0$. Equation (3.62) is satisfied as expressed in (3.41) by both LRN k-ω models.

For natural convection boundary layer flows, the condition in (3.41) is no longer sufficient because the heat flux vector contributes to the net productions. It was argued that the model constant $c_{\omega g}$ imposes insignificant effects on predictions, and this constant can be set to zero (Peng and Davidson, 1997d). The amplification of k in the boundary layer, as transition occurs, depends on both the normalized production due to shear, $N_{ks} = C_{Nk}[(\partial v/\partial x)/\omega]^2$ with $C_{Nk} = c_\mu f_\mu / c_k f_k$, and the normalized production due to buoyancy, $N_{kb} = C_{Nk} F/\omega^2$.

Two uncertain points consequently arise. First, the addition of the buoyancy term in the k-equation could not ensure that k is amplified before ω, particularly as $F < 0$ with stable thermal stratification where $\partial T/\partial y > 0$. Second, because the buoyancy term interferes with the net production of turbulence kinetic energy, N_k, it cannot guarantee that k starts to grow at the critical Ra number where the secondary instability occurs, e.g., $Ra_{cr} \approx 2 \times 10^8$ for 2D cavity flows as given by DNS (Paolucci and Chenoweth, 1989). This is essential to accurately predict the location of transition onset.

According to Henkes (1990), the quantities H, $\Delta T = (T_h - T_{ref})$ and $u_T = (g\beta\Delta T H)^{1/2}$ are appropriate scalings for y, T and v, respectively. Here, H is the height of the vertical wall, T_h is the temperature on the wall surface and T_{ref} is a reference temperature (e.g. the surface temperature on the cold wall, T_c, for a cavity flow). Further, a similarity variable, ζ, is defined as

$$\zeta = \left(\frac{u_T^{\,2}}{4\nu^2 Hy} \right)^{1/4} x \tag{3.63}$$

Note that x is the direction normal to the vertical wall, and y is the streamwise direction along the wall. Using this similarity variable and the above scalings, v and T are written in terms of ζ, giving

$$v = u_T V(\zeta) \tag{3.64}$$

$$T = \Delta T \Theta(\zeta) \tag{3.65}$$

By means of the asymptotic solution of ω, $\omega \propto 1/x^2$ as $x \to 0$, ω can be expressed as

$$\omega = \left(\frac{u_T^{\,2}}{4Hy} \right)^{1/2} \Omega(\zeta) \tag{3.66}$$

The SGDH approach expressed in Equation (3.12), which gives $F = -(g\beta/\sigma_t)(\partial T/\partial y)$, is used to model the buoyancy term G. Setting $c_{\omega g} = 0$ and using (3.63)-(3.66) in Equations (3.60) and (3.61) yield, respectively,

$$N_k = \frac{c_\mu f_\mu}{c_k f_k} \left[2 \left(\frac{Ra}{Pr} \right)^{1/2} \left(\frac{y}{H} \right)^{1/2} \left(\frac{\partial V/\partial \zeta}{\Omega} \right)^2 + \left(\frac{\zeta}{\sigma_t} \right) \left(\frac{\partial \Theta/\partial \zeta}{\Omega^2} \right) \right] - 1 \tag{3.67}$$

$$N_\omega = \frac{c_\mu f_\mu c_{\omega 1} f_1}{c_{\omega 2}} \left[2 \left(\frac{Ra}{Pr} \right)^{1/2} \left(\frac{y}{H} \right)^{1/2} \left(\frac{\partial V/\partial \zeta}{\Omega} \right)^2 \right] - 1 \tag{3.68}$$

A dramatic amplification in k (starts as N_k changes its sign to positive) indicates the onset of transition, whereafter the amplification of ω controls the width of transition. Note that the turbulence energy starts to grow as the first term in (3.67) reaches unity. Somewhere after this point, the eddy viscosity sharply increases, and the transition from laminar to turbulence occurs. At the onset position of transition, this suggests

$$\lambda_1 \left(\frac{Ra}{Pr} \right)^{1/2} \left(\frac{y}{H} \right)_{tr}^{1/2} + \lambda_2 = \alpha_0 \quad (\alpha_0 > 1) \tag{3.69}$$

where

$$\lambda_1 = \frac{2 c_\mu f_\mu}{c_k f_k} \left(\frac{\partial V/\partial \zeta}{\Omega} \right)^2, \quad \lambda_2 = \frac{c_\mu f_\mu}{c_k f_k \sigma_t} \left(\frac{\zeta \partial \Theta/\partial \zeta}{\Omega^2} \right) \tag{3.70}$$

In Equations (3.69) and (3.70), λ_1 and λ_2 are functions of the similarity variable, ζ. As the transition occurs at a location (height) y_{tr} in the natural convection boundary layer along a vertical wall, the first part on the right-hand side in Equation (3.67) should reach its maximum value, α_0,

at a certain location of ζ from the wall surface. The location of transition onset can then be estimated by solving Equation (3.69) for $(y/H)_{tr}$. This gives

$$y_{tr} = \left(\frac{Pr}{Ra}\right)\left(\frac{\alpha_0 - \lambda_2}{\lambda_1}\right)^2 H \tag{3.71}$$

Note that $\alpha_0 = (N_{ks} + N_{kb})_{\max}$ is the maximum total production of k per unit dissipation term as transition occurs. Equation (3.71) shows that the height of transition onset along a vertical heated wall decreases with increasing Rayleigh number. This means that the transition onset moves toward the leading edge of the wall with increasing *Ra*. For flows in a square cavity, Henkes (1990) used Chien's LRN k-ε model (Chien, 1982) to numerically reveal the dependence of y_{tr} on *Ra*. It was shown that y_{tr} tends to be zero as the Rayleigh number was up to 10^{17}. Moreover, Equation (3.71) suggests that an appropriate prediction of y_{tr} depends on the model behaviour in simulating λ_1, λ_2 and α_0 as the flow approaches the transitional state from laminar. Usually, λ_1 reaches its maximum value somewhere near the velocity peak across the boundary layer, whereas λ_2 is normally much smaller than unity owing to a large near-wall ω, i.e. $|\lambda_2| << 1 < \alpha_0$. The location of the transition onset then relies mainly on the predicted ratio of (α_0/λ_1), as shown in (3.71).

For a *laminar* natural convection boundary layer flow along a vertical flat plate, λ_1 is a similarity parameter whose streamwise dependence vanishes. Assuming there exists a near-wall streamwise-independent maximum value for λ_1 next to the transition regime in the upstream laminar stage, whereas $|\lambda_2|$ is usually much smaller than α_0, a condition for the total normalized production, α_0, to trigger transition at the desired location (y_{tr}/H) is then

$$\alpha_0 = (N_{ks} + N_{kb})_{\max} \approx \left(\frac{Ra}{Pr}\frac{y_{tr}}{H}\right)^{1/2} \lambda_1 \tag{3.72}$$

At a certain Rayleigh number and Prandtl number, Equation (3.72) appears to be a necessary condition for a two-equation LRN model to correctly predict the onset location of the transition in a natural convection boundary layer flow along a vertical heated/cooled wall.

Extended LRN Modification for Turbulent Buoyant Flows

There is evidence that the aforementioned grid-dependence of the transition onset prediction is related to the thermal production source. This can be verified in numerical simulations by dropping the buoyancy production term, G, in the k-equation. Indeed, it was found that this exclusion can rid the model of the grid-dependent behaviour for predicting the transition regime along the vertical side walls of a cavity, but the convective heat transfer is largely overpredicted in comparison with experiments. Moreover, the turbulence energy in the core region is not sufficiently damped as desired. This implies that a simple exclusion of G is not preferable.

The shear production is an important origin of inducing transition in the boundary layer along the vertical wall. On the other hand, the thermal production in the outer region of the boundary layer (and in the core region of the cavity) may also either enhance or dampen turbulence owing to unstable or stable thermal stratification. With stable thermal stratification, if turbulence in the outer region of the boundary layer and in the core regions is over-dampened (through G), the amplification of the shear production in the near-wall region of the boundary layer becomes slower by diffusion of turbulence energy to compensate for the stabilization in the neighboring

outer region. This in turn will delay the transition onset. If this energy diffusion makes a negative value of ($N_k - 1$) be maintained for a sufficiently long distance along the vertical wall, turbulence will hardly grow because the laminar boundary layer near the horizontal adiabatic wall will reinforce the compensation as the flow approaches the cavity corner. The model will eventually give a laminar solution, returning zero kinetic energy to the whole flow field.

To remove this undesired model behaviour associated with thermal stratification, measures must be taken to control the performance of the buoyancy source term, G. A practical approach is to use a damping function that is able to appropriately deter this term from absorbing too much energy powered by the near-wall shear production. Furthermore, the method of using a damping function for G is supported by an analysis of asymptotic behaviour near the vertical wall: using the SGDH approach, Equation (3.12), gives rise to an incorrect asymptotic behaviour for the modelled G. As discussed previously, the exact buoyancy source term is proportional to x^2 near a vertical wall, whereas the modelled G term has a relation of $G \propto x^3$ for the modified model and of $G \propto x^4$ for Wilcox's model. Note that the GGDH approach renders also incorrect asymptotic behaviour near a vertical wall.

Since the SGDH has the greatest popularity in practical applications for its simplicity, this approach is employed for the modified model, and a damping function, f_g, has been devised, which meets $f_g \propto 1/x$ as $x \to 0$. Note that the use of a damping function will render incorrect asymptotic behaviour for G near a horizontal wall, but this is of no significant consequence since the flow along the vertical walls is dominant in an overall fashion for flow induced by heated/cooled vertical walls. The role played by the damping function is twofold: to render correct near-wall asymptotic behaviour for G in the boundary layer along the vertical wall; and to avoid delayed prediction for the transition onset as analyzed above. This function is devised as

$$f_g = \left\{1 - \exp\left[-\left(\frac{R_t}{12}\right)^3\right]\right\} \times \left(1 + \frac{10}{R_t^{3.25}}\right) \tag{3.73}$$

The buoyancy source term in the k-equation is thus modelled as

$$G = -g\beta f_g \frac{\nu_t}{\sigma_t} \frac{\partial T}{\partial x_j} \delta_{2j} \tag{3.74}$$

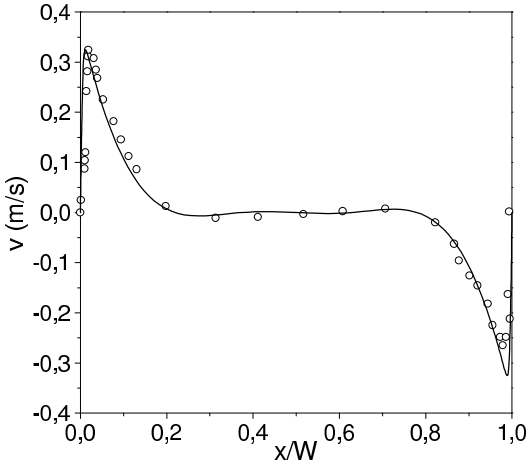

a) Mean velocity

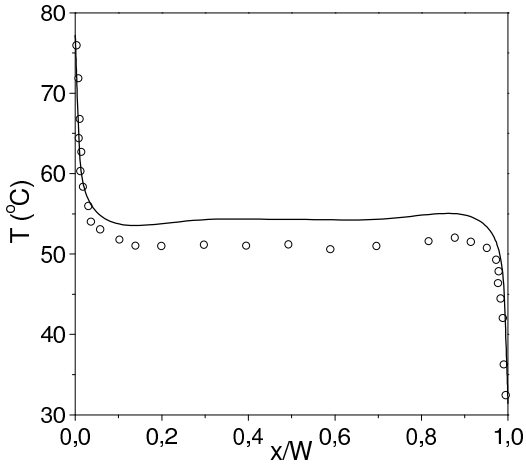

b) Mean temperature

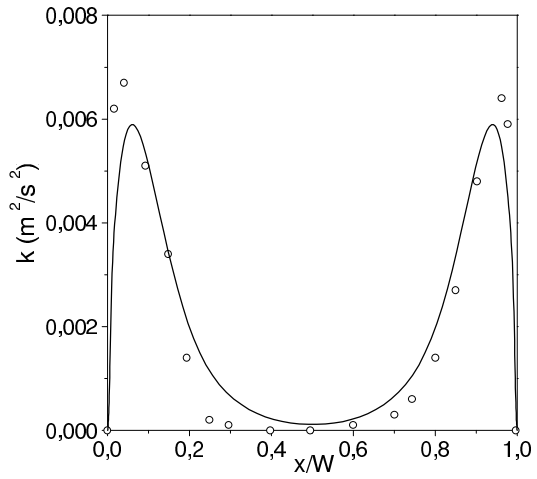

c) Turbulence kinetic energy

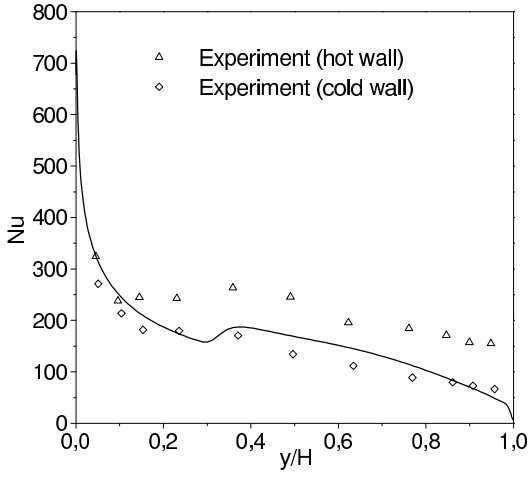

d) Nusselt number along the vertical wall

Figure 3.4 Predictions for a cavity flow, distributions for v, T and k are plotted at the mid-height section ($y = H/2$). The symbol is the experimental data, and the solid line is the prediction.

The modified model was validated by applying it to a turbulent buoyant flow in a confined rectangular cavity with an aspect ratio of 5 at $Ra = 5 \times 10^{10}$. The undesirable grid-dependent performance of the model has been eliminated, and reasonable predictions are obtained, see Peng and Davidson (1997d). Figure 3.4 shows a comparison of some results with the experimental data in this case. These results were computed by the modified model with 160 × 160 meshes, and were validated to be grid-independent.

It should be pointed out that the above analysis is also expected to be applicable for LRN k-ε models, as well as for the LRN k-ω model, by transforming the ε-equation into an ω-equation. Using the relation in (3.22), the general form of the LRN ε-equation in (3.30) (let $E_\varepsilon = 0$ and $\varepsilon = c_k k\omega$) can be transformed into an LRN ω-equation. This gives

$$\frac{\partial \omega}{\partial t} + u_j \frac{\partial \omega}{\partial x_j} = \frac{\omega}{k}\left[(c_{\varepsilon 1} f_1 - 1)\tau_{ij}\frac{\partial u_i}{\partial x_j} - (c_{\varepsilon g} - f_g)\beta g_j h_j\right] - (c_{\varepsilon 2} f_2 - 1)c_k \omega^2$$
$$+ \frac{\partial}{\partial x_j}\left[\left(\nu + \frac{\nu_t}{\sigma_\varepsilon}\right)\frac{\partial \omega}{\partial x_j}\right] + \frac{2}{k}\left(\nu + \frac{\nu_t}{\sigma_\varepsilon}\right)\frac{\partial k}{\partial x_j}\frac{\partial \omega}{\partial x_j} + \left(\frac{1}{\sigma_\varepsilon} - \frac{1}{\sigma_k}\right)\frac{\omega}{k}\frac{\partial}{\partial x_j}\left(\nu_t \frac{\partial k}{\partial x_j}\right) \qquad (3.75)$$

Equation (3.75) is nearly identical with Equation (3.31) except for the additional diffusion term. The damping function, f_g, originates from the k-equation, and the other damping functions and model constants in this equation are the same as those in the general LRN ε-equation (3.30). With respect to the transition regime in a natural convection boundary layer along a vertical wall, a similar analysis can be performed as described above for the LRN k-ω model. For an incompressible boundary layer, the net production per unit dissipation term for ω in (3.75), N_ω^ε, can be written as

$$N_\omega^\varepsilon = \frac{c_\mu f_\mu}{(c_{\varepsilon 2} f_2 - 1)c_k}\left[(c_{\varepsilon 1} f_1 - 1)\left(\frac{\partial v/\partial x}{\omega}\right)^2 + (c_{\varepsilon g} - f_g)\frac{F}{\omega^2}\right] - 1 \qquad (3.76)$$

To ensure that k is amplified earlier than ω so that the laminar-turbulence transition occurs, it can be similarly argued that it must be $N_k > N_\omega^\varepsilon \geq 0$. This thus suggests, as $R_t \to 0$,

$$\left[\frac{1}{f_k}-\left(\frac{c_{\varepsilon 1}f_1-1}{c_{\varepsilon 2}f_2-1}\right)\right]\left(\frac{\partial v/\partial x}{\omega}\right)^2+\left[\frac{1}{f_k}-\left(\frac{c_{\varepsilon g}-f_g}{c_{\varepsilon 2}f_2-1}\right)\right]\frac{F}{\omega^2}>0 \tag{3.77}$$

Equation (3.77) forms, in theory, a necessary condition for enabling an LRN k-ε model to be applicable for transition onset predictions. As stated previously, the dissipation term in the k-equation for a k-ε LRN model concerns the exact definition for ε. It is thus not associated with a damping function, i.e. $f_k = 1$, as is done in most LRN k-ε models. For isothermal flows ($F = 0$), a condition can be derived from Equation (3.77) with which related damping functions should be satisfied when the LRN model is applied to simulating transition. This gives, as $R_t \to 0$,

$$c_{\varepsilon 1}f_1 < c_{\varepsilon 2}f_2 \tag{3.78}$$

For an LRN k-ε model that sets $f_1 = 1$ and uses damping function f_2, referring to the conventional model constants in Equation (3.21) and the asymptotic analysis of $f_2 \propto y^2$, it is difficult to satisfy this condition. As Wilcox (1993) pointed out, such models will then have an undesirable effect on predictions for both the onset of and the width of the transition region.

For natural convection boundary layer flows ($F \neq 0$), performing an analysis similar to that as was carried out with the LRN k-ω model, a relation such as that in (3.71) can be obtained to evaluate the location of the transition onset along a vertical wall. However, the functions, λ_1 and λ_2, are different from those in (3.70).

3.6 Large Eddy Simulation

Since the 1970s, large eddy simulation has been extensively studied and increasingly applied. LES is a technique intermediate between DNS and RANS approaches. Unlike in DNS, which aims at full resolution of various scales in turbulence, only the contribution of the large, energy-bearing structures to momentum and energy transfer is resolved in LES, and the motion of the smallest scales is modelled. Since the small scales tend to be more isotropic and universal in nature, their modelling is expected to be more amenable to success and to require fewer adjustments when applied to different flows than models in the RANS approach. LES is often viewed as more conceptually suitable for complex flows, while the RANS approach may fail to handle, e.g., the flow in which large-scale eddy structures dominate the turbulent transport and when unsteady processes such as vortex shedding and bistable behaviour prevail and dynamic loading is of importance (Rodi, 1996).

3.6.1 Subgrid-Scale Modelling

Different from the RANS approach, where the turbulent fluctuations are ruled out by a time-averaging process during which all the spectra effects are lost, LES simulates turbulent flows by accounting for the motion of eddies in sizes down to the inertial subrange (Leonard, 1974), i.e. for the scales with wavelengths of, typically, about the grid mesh size. In order to define the large-scale variables that are separated out from the subgrid-scale (SGS) components, the instantaneous fluid motion is regarded as a superimposed outcome of the large-scale and small-scale motions. It is thus written as

$$f = \bar{f} + f' \tag{3.79}$$

where $\bar{f}$ is the filtered, resolvable variable, and f' is its SGS component. The filtered variable is defined as

$$\bar{f}(\vec{x}) = \int_D f(\vec{x}')G(\vec{x},\vec{x}')d\vec{x}' \tag{3.80}$$

where D is the entire domain and G is a filter function.

Applying the filtering process to Equations (3.1)-(3.3), the resultant equations turn out to be the governing equations for the evolution of the energy-bearing, large-scale fluid motions, and they are written as, respectively,

$$\frac{\partial \bar{u}_i}{\partial x_i} = 0 \tag{3.81}$$

$$\frac{\partial \bar{u}_i}{\partial t} + \frac{\partial(\bar{u}_i\bar{u}_j)}{\partial x_j} = -\frac{1}{\rho}\frac{\partial \bar{p}}{\partial x_i} + \frac{\partial}{\partial x_j}(2\nu\bar{S}_{ij}) - \frac{\partial \tau_{ij}}{\partial x_j} + g_i\beta(\bar{T} - T_{ref})\delta_{2i} \tag{3.82}$$

$$\frac{\partial \bar{T}}{\partial t} + \frac{\partial(\bar{u}_j\bar{T})}{\partial x_j} = \frac{\partial}{\partial x_j}\left(\alpha\frac{\partial \bar{T}}{\partial x_j}\right) - \frac{\partial h_j}{\partial x_j} + \bar{S}_\phi \tag{3.83}$$

The local deformation tensor of the filtered field, $\bar{S}_{ij}$, is expressed as

$$\bar{S}_{ij} = \frac{1}{2}\left(\frac{\partial \bar{u}_i}{\partial x_j} + \frac{\partial \bar{u}_j}{\partial x_i}\right) \tag{3.84}$$

Owing to the non-linear terms, the filtered out small-scale eddies feed back their effects on the large-scale motion through subgrid-scale stresses and heat fluxes in the filtered governing equations, i.e. τ_{ij} and h_j. These SGS terms are unknowns that must be modelled, and read, respectively,

$$\tau_{ij} = \overline{u_iu_j} - \bar{u}_i\bar{u}_j \tag{3.85}$$

and

$$h_j = \overline{u_jT} - \bar{u}_j\bar{T} \tag{3.86}$$

In adopting the filtering operation, the following important properties have been used (cf. Germano, 1992)

$$\overline{\frac{\partial f}{\partial x_i}} = \frac{\partial \bar{f}}{\partial x_i},\ \bar{\bar{f}} \neq 0 \text{ and } \overline{\bar{f}f'} \neq 0 \tag{3.87}$$

These properties decompose the resultant SGS terms in a manner different from the time-averaging turbulent stresses/heat fluxes using the Reynolds decomposition in the RANS approach. As a result, the SGS stresses can be expanded as (Leonard, 1974)

$$\tau_{ij} = \underbrace{\overline{\overline{u}_i\overline{u}_j} - \overline{u}_i\overline{u}_j}_{\lambda_{ij}} + \underbrace{\overline{\overline{u}_i u_j}' + \overline{\overline{u}_j u_i}'}_{C_{ij}} + \underbrace{\overline{u_i' u_j'}}_{R_{ij}} \tag{3.88}$$

where the first term is the Leonard stresses, which are resolvable, the second is the cross term and the third is the SGS Reynolds stresses. Similarly, the SGS heat fluxes can be decomposed as

$$h_j = \underbrace{\overline{\overline{u}_j\overline{T}} - \overline{u}_j\overline{T}}_{\lambda_j^t} + \underbrace{\overline{\overline{u}_j T}' + \overline{\overline{T} u_j}'}_{C_j^t} + \underbrace{\overline{u_j' T'}}_{R_j^t} \tag{3.89}$$

In an analogous way, we denote here the three terms in (3.89), respectively, as the Leonard heat fluxes, SGS cross heat fluxes and SGS Reynolds heat fluxes. In some earlier SGS modelling work, the Leonard term and the cross term were neglected, see e.g. Lilly (1967) and Deardorff (1970). The SGS modelling is then simply subjected to the Reynolds terms in Equations (3.88) and (3.89). Similar to the second-moment closures in the RANS approach, the transport equations for the Reynolds SGS stresses and heat fluxes can be derived. Models on this level are the *second-moment SGS closures*, see Deardorff (1973) and Horiuti (1987).

Some SGS Models

Leonard (1974) showed that the Leonard term in (3.88) is not generally negligible and actually plays an important role in producing the correct spectral distribution. Moreover, in some *a priori* tests of LES models using the DNS data base, it was revealed that the cross term also makes significant contributions, see e.g. Clark *et al.* (1979), Bardina *et al.* (1980) and Piomelli *et al.* (1988). Based on the assumption that the interaction between resolved and SGS eddies takes place between the smallest resolved eddies and the largest SGS ones, i.e., the scale similarity hypothesis, Bardina *et al.* (1980) proposed the *scale-similarity model*. The SGS component is approximated by the difference between the filtered and twice-filtered corresponding components. The terms in (3.88), C_{ij} and R_{ij}, are thus modelled as follows

$$C_{ij} \sim \overline{\overline{u}}_i(\overline{u}_j - \overline{\overline{u}}_j) + (\overline{u}_i - \overline{\overline{u}}_i)\overline{\overline{u}}_j, \text{ and } R_{ij} \sim (\overline{u}_i - \overline{\overline{u}}_i)(\overline{u}_j - \overline{\overline{u}}_j) \tag{3.90}$$

With the scale-similarity model, the SGS stresses are then computed as

$$\tau_{ij} = \lambda_{ij} + C_B\left(\overline{u}_i\overline{u}_j - \overline{\overline{u}}_i\overline{\overline{u}}_j\right) \tag{3.91}$$

where C_B is a model constant. When applied in LES, it was found that this model does not dissipate sufficient energy; rather, it possesses a desirable performance of describing energy backscatter from subgrid scales to large scales. To improve the behaviour with insufficient energy dissipation for this model, the dissipative Smagorinsky model is linearly combined into the above scale-similarity model. This leads to the so-called *mixed model* (Bardina *et al.*, 1980), giving

$$\tau_{ij} - \frac{1}{3}\tau_{kk}\delta_{ij} = -2\nu_t \bar{S}_{ij} + L_{ij}^m - \frac{1}{3}L_{kk}^m \delta_{ij} \tag{3.92}$$

where

$$L_{ij}^m = \lambda_{ij} + C_B\left(\bar{u}_i\bar{u}_j - \bar{\bar{u}}_i\bar{\bar{u}}_j\right) \tag{3.93}$$

In the mixed model, the Leonard stresses can be explicitly computed in terms of the filtered field. The scale-similarity component in (3.92) functions mainly for energy backscatter. Further improvement to this model was made by Speziale (1985), who showed that the model constant C_B must be unity to ensure Galilean invariance, i.e., $C_B = 1$.

Instead of using the above decomposition, it seems preferable to model τ_{ij} as a whole without splitting it into parts. As in the RANS approach, most SGS models employ an eddy viscosity assumption to model the SGS stress tensor. An alignment is assumed between the anisotropic part, τ_{ij}^a, of this tensor and the local resolved large-scale strain rate tensor, i.e.,

$$\tau_{ij}^{\ a} = \tau_{ij} - \frac{1}{3}\tau_{kk}\delta_{ij} = -2\nu_t \bar{S}_{ij} \tag{3.94}$$

Once again, the SGS modelling becomes a task of formulating the SGS eddy viscosity in this case. By means of dimensional analyses, it is argued that $\nu_t \propto V_{sgs} L_{sgs}$, where V_{sgs} and L_{sgs} are, respectively, the SGS turbulent velocity and length scales. The length scale can usually be related to the filter width, Δ, since the most active of the unresolved scales are those closest to the filtering cutoff. Different SGS eddy viscosity based models therefore have their variations mainly in the prescription of V_{sgs}. One of the approaches to determine V_{sgs} is to bridge this scale to the SGS turbulent kinetic energy, k_{sgs}, as $V_{sgs} \propto (k_{sgs})^{1/2}$. An additional transport equation for k_{sgs} is then used to close the equation system. This type of model is the *one-equation SGS model* or the *SGS kinetic energy model*, see e.g. Schumann (1975), Yoshizawa and Horiuti (1985), Wong (1992), Ghosal *et al.* (1995) and Davidson (1997b). On the basis of the eddy viscosity/diffusivity concept, other SGS models have also been developed. Detailed reviews can be found in articles by, e.g., Yoshizawa (1987), Piomelli (1993), and Lesieur and Métais (1996).

The most widely used eddy viscosity model is the *Smagorinsky model* (1963). The origin of this model is based on a production-dissipation equilibrium hypothesis for the small scales. The small eddies have shorter time scales than the large, energy-bearing eddies. It is thus assumed that they adjust more rapidly than the large scales to perturbations, and recover to equilibrium nearly instantaneously (Piomelli and Chasnov, 1995). With this equilibrium assumption, the SGS eddy viscosity in the Smagorinsky model is derived as

$$\nu_t = C\Delta^2 |\bar{S}| \tag{3.95}$$

where the magnitude of the local strain rate tensor is defined by $|\bar{S}| = \sqrt{2\bar{S}_{ij}\bar{S}_{ij}}$, and C is a model constant or, alternatively, $C_s = \sqrt{C}$ is the Smagorinsky constant.

It has been argued that the Smagorinsky constant is an *ad hoc* one, which varies with different flow problems. Lilly (1967) derived $C_s \approx 0.17$ from homogeneous isotropic turbulence

with cutoff in the inertial subrange. Deardorff (1970) used $C_s \approx 0.094$ in his LES for channel flows. Mason and Callen (1986) found that too large a C_s would cause the resolved-scale motions to be damped out, and its critical value depends on the mesh resolution. This constant is thus regarded as a measure of numerical resolution, and values of C_s less than about 0.2 correspond to inadequate resolution. Some historical reviews of this model can be found in Smagorinsky (1993).

Ferziger (1977) proposed a *vorticity model* based on the eddy viscosity concept. In this model, the magnitude of the strain rate tensor in the Smagorinsky model, i.e. (3.95), is replaced by that of the rotation tensor,

$$\bar{r}_{ij} = \frac{1}{2}\left(\frac{\partial \bar{u}_i}{\partial x_j} - \frac{\partial \bar{u}_j}{\partial x_i}\right) \tag{3.96}$$

No significant difference in LES has been detected between the vorticity model and the Smagorinsky model, however.

SGS Modelling for Turbulent Buoyant Flows

In nearly all the modelling work on turbulent flows with heat transfer, the turbulent heat-flux model has often been constructed in analogy to that for the turbulent stresses. As the velocity correlations find their ways to be approximated in terms of the resolved flow field, the velocity-temperature correlations are then cast into analogous approximations. Based on this consideration, several SGS models for handling turbulent thermal flows can thus be derived.

If the scale-similarity hypothesis is applied to the SGS heat fluxes in the decomposition (3.89), one should have

$$C_j^t \sim \bar{\bar{u}}_j(\bar{T} - \bar{\bar{T}}) + (\bar{u}_j - \bar{\bar{u}}_j)\bar{\bar{T}}, \text{ and } R_j^t \sim (\bar{u}_j - \bar{\bar{u}}_j)(\bar{T} - \bar{\bar{T}}) \tag{3.97}$$

A scale-similarity model for the SGS heat fluxes may then be written as

$$h_j = \lambda^t{}_j + C_B^t\left(\bar{u}_j\bar{T} - \bar{\bar{u}}_j\bar{\bar{T}}\right) \tag{3.98}$$

where the Leonard heat fluxes can be explicitly computed from the resolved field, and C_B^t is a model constant. Furthermore, combined with an SGS eddy diffusivity model, a mixed model can be constructed in a way similar to Equation (3.92), giving

$$h_j = -\alpha_t \frac{\partial \bar{T}}{\partial x_j} + \lambda^t{}_j + C_B^t\left(\bar{u}_j\bar{T} - \bar{\bar{u}}_j\bar{\bar{T}}\right) \tag{3.99}$$

where α_t is the SGS eddy diffusivity. Using the Galilean group of transformations, as was done by Speziale (1985), it can be shown that the model constant, C_B^t, must be unity to ensure Galilean invariance for the model, i.e., $C_B^t = 1$.

Without making any decomposition on the SGS heat fluxes, h_j, the eddy diffusivity concept is often employed to model this quantity as a whole. Similar to the SGS stresses in the Smagorinsky model, the SGS heat fluxes are modelled in alignment with the local resolved tem-

perature gradients (cf. Moin *et al.*, 1991; Cabot and Moin, 1993)

$$h_j = -\alpha_t \frac{\partial \overline{T}}{\partial x_j} = -\frac{\nu_t}{Pr_t}\frac{\partial \overline{T}}{\partial x_j} \tag{3.100}$$

where Pr_t is the SGS turbulent Prandtl number. A broad range of values has been proposed in the literature for the SGS Prandtl number, Pr_t, ranging from 0.25 to 0.85 (cf. Ciofalo, 1993). The SGS eddy diffusivity is written as

$$\alpha_t = C_t \Delta^2 |\overline{S}| = \frac{C}{Pr_t}\Delta^2 |\overline{S}| \tag{3.101}$$

This formulation, together with the Smagorinsky model for the SGS eddy viscosity in (3.95), has been widely used in LES for turbulent flows with heat transfer. In this case, the influence of the buoyancy has been implicitly imposed on the SGS eddy viscosity/diffusivity. For turbulent buoyant flows, one may note that the SGS turbulent production, P_{sgs}, includes two parts: the SGS shear production, P_{sgs}^S, and the SGS buoyancy production, P_{sgs}^T. SGS models directly accounting for buoyancy effects on the eddy viscosity can be derived from the assumption of production-dissipation equilibrium for subgrid scales, i.e.,

$$P_{sgs} = \left(P_{sgs}^S + P_{sgs}^T\right) \cong \varepsilon_{sgs} \tag{3.102}$$

The total SGS turbulent production caused by shear and buoyancy reads

$$P_{sgs} = -\tau_{ij}\overline{S}_{ij} + g_j \beta h_j \tag{3.103}$$

The SGS dissipation is the viscous dissipation rate for the SGS kinetic energy. With a dimensional argument, one has

$$\nu_t = C^{2/3}\Delta^{4/3}\varepsilon_{sgs}{}^{1/3} \tag{3.104}$$

Depending on how the SGS stresses and heat fluxes in (3.103) are represented in an eddy viscosity/diffusivity based model, one can derive different formulations for the SGS eddy viscosity from the equilibrium assumption in (3.102). In general, this can be written as

$$\nu_t = C^{2/3}\Delta^{4/3}\left(-\tau_{ij}\overline{S}_{ij} + g_j \beta h_j\right)^{1/3} \tag{3.105}$$

Eidson (1985) proposed an SGS buoyancy model where the approximations in (3.94) and (3.100) were used. Inserting (3.94) and (3.100) into Equation (3.105) and solving the equation for ν_t, one then readily gets

$$\nu_t = C\Delta^2\left(|\overline{S}|^2 - \frac{g\beta}{Pr_t}\frac{\partial \overline{T}}{\partial x_j}\delta_{2j}\right)^{1/2} \tag{3.106}$$

The SGS eddy diffusivity in the Eidson model is given by

$$\alpha_t = C_t \Delta^2 \left(|\bar{S}|^2 - \frac{g\beta}{Pr_t} \frac{\partial \bar{T}}{\partial x_j} \delta_{2j} \right)^{1/2} = \frac{C}{Pr_t} \Delta^2 \left(|\bar{S}|^2 - \frac{g\beta}{Pr_t} \frac{\partial \bar{T}}{\partial x_j} \delta_{2j} \right)^{1/2} \tag{3.107}$$

This SGS buoyancy model makes the eddy viscosity/diffusivity enhanced for flows with unstable thermal stratification. In large eddy simulations for Rayleigh-Bénard convection flows, Eidson proposed using $C = 0.0441$ and $Pr_t = 0.4$. Further, ν_t and α_t have to be constrained to be zero when $|\bar{S}|^2 < \left(\frac{g\beta}{Pr_t} \frac{\partial \bar{T}}{\partial x_j} \delta_{2j} \right)$ to avoid giving rise to no-real solutions. Other SGS models for handling turbulent buoyant flows were also developed by, e.g., Schumann (1991), Wong and Lilly (1994) and Canuto *et al.* (1997).

Note that in both the Smagorinsky model and the Eidson buoyancy model the SGS eddy viscosity and diffusivity are constrained to hold non-negative values. The behaviour of energy transfer inherent in the model is thus always directed from resolved large scales to subgrid scales, without any backscatter. These models are therefore regarded as being absolutely dissipative.

Cabot (1992) used the Smagorinsky model and the Eidson buoyancy model as base models in constructing corresponding dynamic SGS models and applied them to buoyancy-driven channel flows. The simulation showed that the dynamic Eidson model generally gave better results than the dynamic Smagorinsky model, but may entail locally no-real solutions. To preserve the buoyancy-related term in the SGS eddy viscosity/diffusivity formulation and to overcome the problem associated with no-real solutions occurring when $|\bar{S}|^2 < \left(\frac{g\beta}{Pr_t} \frac{\partial \bar{T}}{\partial x_j} \delta_{2j} \right)$, a modified SGS model has been proposed (Peng and Davidson, 1997e, 1998a).

The modified model is essentially a combination of the Smagorinsky model and the Eidson model. The eddy viscosity is rewritten in a general form as

$$\nu_t = C \Delta^2 \bar{N} \tag{3.108}$$

where $\bar{N}$ denotes the reciprocal of SGS time scaling, $1/\tau_{sgs}$, and takes different forms for the Smagorinsky model and the Eidson buoyancy model, represented here by $\bar{N}_s$ and $\bar{N}_b$, respectively, see (3.95) and (3.106). The proposed combined model is then constructed as

$$\nu_t = C \Delta^2 \bar{N}_c = C \Delta^2 \frac{\bar{N}_b^2}{\bar{N}_s} = C \Delta^2 \frac{1}{|\bar{S}|} \left(|\bar{S}|^2 - \frac{g\beta}{Pr_t} \frac{\partial \bar{T}}{\partial x_j} \delta_{2j} \right) \tag{3.109}$$

and, similarly, the SGS eddy diffusivity is expressed as

$$\alpha_t = C_t \Delta^2 \bar{N}_c = \frac{C_t}{Pr_t} \Delta^2 \frac{1}{|\bar{S}|} \left(|\bar{S}|^2 - \frac{g\beta}{Pr_t} \frac{\partial \bar{T}}{\partial x_j} \delta_{2j} \right) \tag{3.110}$$

It is interesting to note that the modified model allows negative values for ν_t (and α_t) as $|\bar{S}|^2 < \left(\frac{g\beta}{Pr_t} \frac{\partial \bar{T}}{\partial x_j} \delta_{2j} \right)$, only if the total viscosity ($\nu_t + \nu$) is positive, to avoid causing numerical in-

stability in computations. This modified model is thus capable of accounting for some energy backscatter for buoyant flows with positive and significant thermal stratification. For isothermal turbulent flows, this model becomes identical to the conventional Smagorinsky model. The modified model thus works for both isothermal and non-isothermal turbulent flows.

3.6.2 Dynamic SGS Approach

In deriving the above models from the SGS eddy viscosity/diffusivity hypothesis, it may be noted that several drawbacks exist in these models. These include: *a*) the model constant is *ad hoc* for different flows; *b*) the SGS viscosity/diffusivity does not vanish for laminar flows; *c*) the model does not have correct near-wall asymptotic behaviour; *d*) the Smagorinsky model and the Eidson buoyancy model are absolutely dissipative: they cannot represent any energy backscatter that is important in LES for, e.g., transitional flows. To remedy these and other problems (cf. Moin *et al.*, 1991), Germano *et al.* (1991) developed a dynamic procedure by which the model coefficient is dynamically computed as a function of time and space, eliminating the above problems.

The basic principle of the dynamic procedure is to use flow properties at the smallest resolved scales to formulate the model coefficients on the subgrid-scale level by assuming scale similarity. The dynamic procedure relies on a large eddy simulation of an SGS base model, such as the Smagorinsky model, on the grid filtering level. The computed result is then filtered again by a test filter that has a width, $\tilde{\Delta}$, larger than the width of the grid filter, Δ, e.g. $\tilde{\Delta} = 2\Delta$. The test filtering operation is performed to obtain the flow characteristics of the smallest resolved scales. If such a double filtering process is applied to the Navier-Stokes equations, the resultant stress tensor on the test filtering level is

$$Y_{ij} = \widetilde{\overline{u_i u_j}} - \tilde{\bar{u}}_i \tilde{\bar{u}}_j \tag{3.111}$$

Similarly, for the energy equation, the heat fluxes on the test filtering level are written as

$$H_j = \widetilde{\overline{u_j T}} - \tilde{\bar{u}}_j \tilde{\bar{T}} \tag{3.112}$$

The stress tensor and the heat fluxes on the test filtering level are modelled in analogy to their counterparts on the grid filtering level. Using the SGS eddy viscosity based models, similar to Equations (3.94) and (3.100), one can write

$$Y_{ij} = -2\tilde{\nu}_t \tilde{\bar{S}}_{ij} + \frac{1}{3} Y_{kk} \delta_{ij}, \quad \tilde{\nu}_t = C \tilde{\Delta}^2 \tilde{\bar{N}} \tag{3.113}$$

and

$$H_j = -\tilde{\alpha}_t \frac{\partial \tilde{\bar{T}}}{\partial x_j}, \quad \tilde{\alpha}_t = C_t \tilde{\Delta}^2 \tilde{\bar{N}} \tag{3.114}$$

In Equations (3.113) and (3.114), it should be noted that the model coefficients, C and C_t, have been regarded as being independent of, and thus extracted from, the filtering operation on the assumption that these coefficients are very slowly varying functions of space (cf. Moin and Jimenéz, 1993). The Germano identities (Germano *et al.*, 1991) suggest

$$L_{ij} = Y_{ij} - \tilde{\tau}_{ij} = \widetilde{\bar{u}_i \bar{u}_j} - \tilde{\bar{u}}_i \tilde{\bar{u}}_j \tag{3.115}$$

and

$$E_j = H_j - \tilde{h}_j = \widetilde{\bar{u}_j \bar{T}} - \tilde{\bar{u}}_j \tilde{\bar{T}} \tag{3.116}$$

Note that $L_{ij} = \widetilde{\bar{u}_i \bar{u}_j} - \tilde{\bar{u}}_i \tilde{\bar{u}}_j$ and $E_j = \widetilde{\bar{u}_j \bar{T}} - \tilde{\bar{u}}_j \tilde{\bar{T}}$ can be explicitly computed form the resolved large-scale variables. Substituting (3.94) and (3.113) into (3.115) yields

$$L_{ij} - \frac{1}{3}\delta_{ij} L_{kk} = -2CM_{ij}, \quad M_{ij} = \tilde{\Delta}^2 \gamma_{ij} - \Delta^2 \tilde{\eta}_{ij} \tag{3.117}$$

where

$$\gamma_{ij} = \tilde{\bar{N}}\, \tilde{\bar{S}}_{ij}, \quad \eta_{ij} = \bar{N}\, \bar{S}_{ij} \tag{3.118}$$

Similarly, inserting (3.100) and (3.114) into Equation (3.116) gives

$$E_j = -C_t Q_j, \quad Q_j = \tilde{\Delta}^2 \varphi_j - \Delta^2 \tilde{\xi}_j \tag{3.119}$$

where

$$\varphi_j = \tilde{\bar{N}}\, \frac{\partial \tilde{\bar{T}}}{\partial x_j}, \quad \xi_j = \bar{N}\, \frac{\partial \bar{T}}{\partial x_j} \tag{3.120}$$

It may be noted that (3.117) represents an equation system with five independent entries for one unknown C; (3.119) gives three independent equations for the coefficient C_t. They are thus overdetermined. Germano *et al.* (1991) proposed contracting (3.117) with $\bar{S}_{ij}$ to obtain C. Moin *et al.* (1991) used an analogous contraction with $\frac{\partial \bar{T}}{\partial x_j}$ for (3.119) to determine C_t. The resultant coefficient, however, is found to be ill-conditioned because the denominator in the expression for the coefficient could vanish or become small enough to induce numerical instability. Instead, Lilly (1992) suggested applying least-squares analyses to minimize the difference between the modelled and exact stresses. This approach is equivalent to contracting (3.117) and (3.119) with M_{ij} and Q_j, respectively, giving

$$C = -\frac{1}{2}\frac{L_{ij} M_{ij}}{M_{ij} M_{ij}} \tag{3.121}$$

and

$$C_t = -\frac{E_j Q_j}{Q_j Q_j} \tag{3.122}$$

This approach, in contrast to Germano *et al.*'s contraction, has the merit of having the denominators in (3.121) and (3.122) be positive definitely, and thus holds the possibility of returning locally well-behaved model coefficients. The dynamic approach can in the same manner be applied to other SGS models, e.g., the mixed model, see Zang *et al.* (1993).

Incorporated into the dynamic procedure, the SGS model renders correct asymptotic behaviour near solid boundaries and returns zero SGS eddy viscosity/diffusivity for laminar flows, as it should. Moreover, the model coefficients can be positive or negative. A negative coefficient entails a locally negative SGS eddy viscosity/diffusivity, which implies an energy backscatter from subgrid scales to resolved large scales. This is a desirable feature for an SGS model.

Nonetheless, significant problems also arise when using the above dynamic model. First, the model in (3.121) and (3.122) may still be ill-conditioned with a frequently small enough denominator (compared with the numerator), e.g. for channel flows, to make locally determined model coefficient ill-behaved (Cabot and Moin, 1993). It was found that, once the model coefficient becomes locally negative, its auto-correlation time becomes so large that it remains negative for an excessively long period during which a divergence of the total energy can be triggered (Ghosal *et al.*, 1995). Moreover, the scale-invariance assumption for the model coefficient is not mathematically self-consistent since this assumption wipes out the time and spatially dependent features from a filtering operation. *A priori* tests revealed that the model coefficient actually varies strongly in space and contains a significant fraction of negative values (cf. Piomelli and Liu, 1995).

Several remedies have been developed to treat these deficiencies. Germano *et al.* (1991) proposed using the assumption in which coefficient C is a function only of time and the inhomogeneous direction. The numerator and the denominator are then averaged over the homogeneous direction. This suggests

$$C = -\frac{1}{2}\frac{< L_{ij} M_{ij} >}{< M_{ij} M_{ij} >} \tag{3.123}$$

and

$$C_t = -\frac{< E_j Q_j >}{< Q_j Q_j >} \tag{3.124}$$

where $< \cdot >$ denotes a spatial averaging over the homogeneous direction. Temporal averaging (Akselvoll and Moin, 1993) and local space-averaging over the test filter cell (Zang *et al.*, 1993) were also used in computations. Moreover, a so-called *clipping* method has often been used to avoid numerical instability attributed to negative eddy viscosity. This method constrains the total viscosity to be non-negative and thus allows a small amount of energy backscatter.

Other alternative dynamic formulations for C and C_t have also been developed. Moin and Jimenéz (1993) proposed using two coefficients for τ_{ij} and Y_{ij}, respectively, and determining them by means of the least-square formulation, as proposed by Lilly (1992). To remove the mathematical inconsistency associated with the scale-invariance assumption for the model coefficient, Ghosal *et al.* (1995) used a global variational approach to account for the spatial variation of C in the filtering process. This consequently leads to an integral equation for C that can be iteratively solved at a relatively high computational cost. Piomelli and Liu (1995)

proposed a localized dynamic model in which C is retained within the test filtering operation and is approximated by its value from the previous time step. Meneveau *et al.* (1996) developed an approach in which the error associated with the Germano identity is minimized along particle trajectories rather than over directions of statistically homogeneity. Meneveau and Lund (1996) examined several approaches to account for scale-dependent coefficients associated with the dynamic procedure through *a priori* tests for isotropic turbulence. No entirely satisfactory option was suggested in their studies. Other versions of dynamic models have also been developed to allow a self-consistent determination of the model coefficient, see e.g. Liu *et al.* (1994) and Davidson (1997b).

SGS Turbulent Prandtl Number, Pr_t

When using the Eidson buoyancy model or the modified buoyancy model in the dynamic procedure, the SGS turbulent Prandtl number, $Pr_t = C/C_t$, needs to be determined in computations. Moin *et al.* (1991) estimated Pr_t in a homogeneous shear flow using the DNS data. Equations (3.123) and (3.124) were used with spatial average over the entire domain, and Pr_t depends solely on time. They found that Pr_t tends to reach relatively constant values after a long period of time, which approximately fall in a range of $Pr_t = 0.4 - 0.6$. In LES for Rayleigh-Bénard convection flows conducted by Eidson (1985) where the dynamic procedure was not used, the SGS turbulent Prandtl number was optimized as $Pr_t = 0.4$. Cabot (1992) used this *standard* constant value in the dynamic Eidson buoyancy model for simulating buoyancy-driven channel flows. It was found that the resultant prediction is better than those given by the dynamic Smagorinsky model and by the dynamic buoyancy model in which Pr_t is locally computed with an iterative Newton's method. Furthermore, it was found that an iterative determination of Pr_t doubles the computational cost in the SGS model and occasionally entails non-real or multiple solutions when using the Eidson buoyancy model (Cabot, 1992; Wong and Lilly, 1994).

To avoid using a computationally costly iterative scheme for determining Pr_t, Peng and Davidson (1997e) proposed using an approximated approach. It has been argued that the model coefficients are fairly slowly varying functions of time because of the temporal filtering introduced implicitly by the spatial filtering (Piomelli and Liu, 1995). The SGS Prandtl number, Pr_t, at the present time step can then be approximately estimated with the ratio between C and C_t at the previous time step. This suggests

$$Pr_t^n \approx \left(\frac{C}{C_t} \right)^{(n-1)} \tag{3.125}$$

Using both a constant Pr_t (= 0.4), and the approximation in (3.125), Peng and Davidson (1997e, 1998a) compared several SGS models for a Rayleigh-Bénard thermal convection flow at $Ra = 3.8 \times 10^5$ with $Pr = 1.0$. Figure 3.5 shows some results from this prediction using the dynamic modified buoyancy model. The results have been normalized using the temperature difference of ΔT between the top and the bottom wall surfaces and the velocity scale $U_0 = \sqrt{g\beta\Delta TH}$, where H is the height of the fluid layer. The symbol $< \cdot >$ in Figure 3.5 denotes the averaging over time and the homogeneous directions, i.e., the longitudinal (x) and the spanwise (z) directions. The two specifications for Pr_t entail little difference in the result. The dynamic Smagorinsky model and buoyancy model were also used in the comparison, see Peng and Davidson (1998a). The predictions given by all these models were very similar for this thermal convection flow.

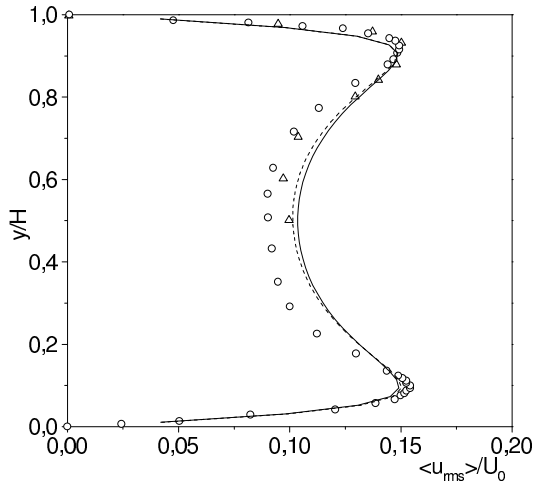

a) Distribution of r.m.s. of $\overline{u}$

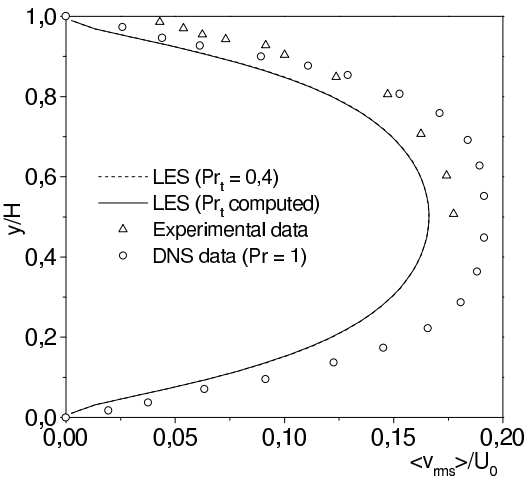

b) Distribution of r.m.s. of $\overline{v}$

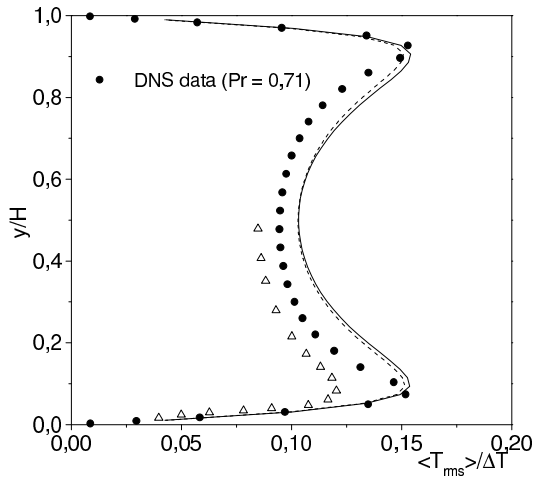

c) Distribution of r.m.s. of $\overline{T}$

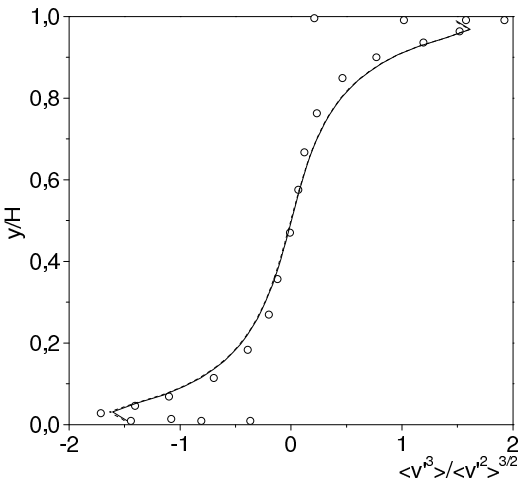

d) Distribution of the skewness of $\overline{v}$

Figure 3.5 Predictions with the dynamic modified buoyancy model for the Rayleigh-Bénard thermal convection at $Ra = 3.8 \times 10^5$ ($Pr = 1.0$).

Note that model coefficients C and C_t may vary with different grid resolutions for the same flow, since they contain information extrapolated from the smallest resolved scales whose cutoff depends on the test filter and is thus related to the mesh size. On the other hand, in LES for several different buoyant flows considered in this work, it was noticed that the value of the statistically averaged SGS Prandtl number, $Pr_t = C/C_t$, appears to be relatively stable, although C and C_t vary with different grid resolutions and flows. Usually, Pr_t has a value between 0.3-0.6, except in near-wall regions where Pr_t may rise to 0.8-1.0.

Other buoyancy-induced flows considered in this work include the flow in a confined rectangular cavity with an aspect ratio of 5 and the flow created between two differentially heated, infinite vertical walls. For the buoyant cavity flow at a moderate Rayleigh number, e.g. $Ra = 5 \times 10^{10}$, as described in Section 3.5.3, boundary layers are triggered along the heated and cooled vertical side walls, undergoing subsequently laminar, transitional and fully developed turbulent stages. It was found that the dynamic model, based on either the Smagorinsky model or the modified buoyancy model, fails to reasonably capture the flow structure (Peng and Davidson, 1998b). It has been argued that the prediction for the transition onset in the boundary layer relies strongly on the account of energy backscatter taken by the SGS model

used. The Smagorinsky model is absolutely dissipative. It thus cannot represent any energy backscatter. When applied to buoyant cavity flows characterized by weak turbulence and transitional phenomenon, the Smagorinsky model dampens the turbulence in the large scales and tends to give the solution some laminar-like features, see Peng and Davidson (1998b). Unlike the two-equation models in the RANS approach, the Smagorinsky model will never produce a pure laminar solution for the flow, since, as stated previously, this model returns unrealistic SGS eddy viscosities for laminar flows.

With a dynamic model, the representation of energy backscatter is associated with the grid resolution used in LES, since the filter width is specified with the mesh size. A coarse grid resolution will increase the amount of energy backscatter simulated by the model. A correct estimation of energy backscatter (its magnitude and its active location) is an essential ingredient for a dynamic model to predict low-Reynolds/Rayleigh-number transitional flows. For the buoyant cavity flow mentioned above, there exists a certain difficulty in appropriately accounting at the same time for both the thin boundary layer flow along the vertical walls and the remainder of this flow. Because of the difficulty in the grid resolution required for an appropriate representation of energy backscatter as well as the limitation inherent in the dynamic model itself, the magnitude of energy backscatter may be incorrectly simulated in the boundary layer along the vertical walls. For example, the clipping approach employed to constrain the total viscosity for numerical stability may lead to an under-estimated prediction of energy backscatter. An insufficient grid resolution, on the other hand, will result in an over-estimation, which will consequently reinforce the large-scale turbulent diffusion, giving an over-predicted thickness of the boundary layer, whereas the streamwise velocities are under-estimated overall, see Peng and Davidson (1998b).

Since the grid resolution substantially affects the representation of energy occurrence between large scales and subgrid scales by an SGS model, a refined grid is desired in LES for flows with a low turbulence level and physical energy backscatter features. Using a fine grid with the Smagorinsky model may decrease the inaccuracy in energy forward scatter represented by the model. On the other hand, a fine grid will decrease the load of energy backscatter carried by a dynamic model. In this case, most energy backscatter can be left to occur in resolved-scale motions.

For handling buoyant cavity flows at moderate Rayleigh numbers, further studies to investigate the flow structure and dynamic behaviour of the SGS model are desirable to improve the prediction.

For the flow created between two differentially heated, infinite vertical walls, i.e. an infinite cavity, at $Ra = 5.4 \times 10^5$ with $Pr = 0.71$, a comparison was also made between different SGS models (Peng and Davidson, 1998b). Owing to the flow configuration, the fully developed mean flow is essentially of a one-dimensional type along the vertical direction without thermal stratification. The dynamic model, based on either the Smagorinsky model or the modified buoyancy model, produces improved or similar predictions as compared with the Smagorinsky model. Slight improvements can be found in the predictions for, e.g., the mean streamwise velocity and some turbulent quantities including the spanwise fluctuations and the vertical heat fluxes, see Peng and Davidson (1998b). Owing to the statistically non-stratified flow feature, the variation between the statistically averaged forms of the dynamic Smagorinsky model and the dynamic modified buoyancy model lies only in the correlation of non-linear terms with respect to time averaging. This variation was verified to be of no significant consequence in the prediction for this flow. The results given by both dynamic models are thus very similar, and only a slight improvement was observed when using the dynamic modified buoyancy model, see Peng and Davidson (1998b).

Chapter 4

Simulation Methodology

To realize a numerical simulation for turbulent flow and heat transfer, three aspects must generally be well accounted for. These include a well-behaved turbulence model, mathematically well-posed numerical methods and physically well-consistent boundary conditions. Chapter 3 presented and discussed the modelling of turbulent flow and heat transfer. All the models are constructed with a set of non-linear differential equations, which must be solved by using numerical methods together with specific boundary conditions for different flow problems.

Solution efficiency and accuracy are closely related to numerical methods. Boundary specification, in addition, is a necessary auxiliary condition to solve the governing equations for a flow problem, which ensures that the solution exists and is unique. It should neither be overprescribed nor underprescribed, see Fletcher (1991). Moreover, solution accuracy can also be significantly influenced by boundary specifications. Inappropriately specified boundary conditions may lead to a solution deviating largely from reality. In principle, boundary conditions should be specified to be identical with those in practice. In this chapter, numerical methods and boundary conditions used in this work are summarized.

4.1 Numerical Methods

When using two-equation turbulence models, all the computations in this work were performed on the basis of a computer code, CALC-BFC. This code uses collocated grid and Cartesian velocity components and is applicable for three-dimensional complex geometries. Details on various numerical aspects employed in this code have been documented by Davidson and Farhanieh (1992). In large eddy simulations, collocated grid has also been employed, but the solution procedure is somewhat different, which is described in Section 4.1.2.

4.1.1 Numerical Procedure in RANS Approach

The computation is based on the solution of the partial differential equations governing the flow and convective heat transfer. The finite volume method is used to transform these non-linear differential equations into algebraic relations which link the values of the independent variables at the nodes of the computational grid. For convenience, the governing equations are re-cast in a general form

$$\frac{\partial \rho\phi}{\partial t}+\frac{\partial(\rho u_i\phi)}{\partial x_i}=\frac{\partial}{\partial x_i}\left(\Gamma_\phi \frac{\partial \phi}{\partial x_i}\right)+S^\phi \qquad (4.1)$$

where ϕ is the independent variable to be solved, Γ_ϕ is its corresponding effective viscosity/diffusivity and S^ϕ is a source term, which may include the buoyancy term, the production and dissipation terms, the cross diffusion term and so on.

Discrete Representation

The discretization of Equation (4.1) is made over a collocated grid, as shown in Figure 4.1. All the variables are stored in the centre of the control volume. Integrating Equation (4.1) over the control volume, δV, and a time interval Δt, one gets

$$\left(\phi-\phi^{0}\right)\frac{\rho\delta V}{\Delta t}+\sum_{m}\left[\rho\mathbf{U}\phi\cdot\mathbf{A}\right]=\sum_{m}\left(\Gamma_{\phi}\nabla\phi\cdot\mathbf{A}\right)+S^{\phi}\delta V \tag{4.2}$$

where ϕ^{0} is the value at the previous time step, **U** is the convecting velocity vector, **A** is the face-area vector and m is the number of the faces of the hexahedron control volume. To compute the convective and diffusive fluxes through the volume faces, some formulations must be used to estimate the face values of independent variables from those at the neighbouring grid points.

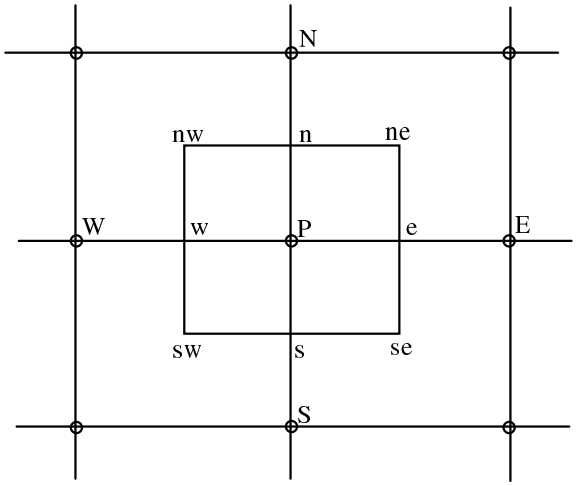

Figure 4.1 A control volume in a collocated grid.

Several numerical schemes for discretizing the convective term have been incorporated into the code. These include a hybrid upwind/central differencing scheme, a second-order bounded van Leer scheme (van Leer, 1974) and a third-order QUICK scheme (Leonard, 1979) that has been employed in this work. The diffusion term and source terms are discretized using the second-order central differencing scheme (Patankar, 1980). By means of these numerical schemes, the non-linear differential equations are then cast into a set of algebraic relations for all the grid nodes. At an arbitrary node P in the numerical domain, the discrete algebraic equation can be written as

$$a_{P}\phi_{P}=\sum a_{nb}\phi_{nb}+b \tag{4.3}$$

where *nb* denotes neighbouring nodes of P, and

$$a_{P}=\sum a_{nb}+\frac{\rho\delta V}{\Delta t}-S_{P}{}^{\phi}\delta V \tag{4.4}$$

$$b=S_{c}{}^{\phi}\delta V+\frac{\rho\delta V}{\Delta t}\phi_{P}{}^{0} \tag{4.5}$$

Note that the source term, S^{ϕ}, has been linearlized as $S^{\phi}=S_{c}{}^{\phi}+S_{P}{}^{\phi}\phi_{P}$, and $S_{P}{}^{\phi}\le 0$ to increase the diagonal dominance for the resultant coefficient matrix (Patankar, 1980). For the momentum equations, the pressure gradient term is combined in the source term, b.

There is no obvious equation for obtaining pressure. Instead, the pressure field is indirectly specified through the continuity equation. When a correct pressure field is used for the momentum equations, the resulting velocity field then satisfies the continuity equation. As all the independent variables are stored at the centre of the control volumes, using the second-order central differencing scheme, the pressure gradient term is then discretized with the pressure difference between two alternate nodes, instead of between two adjacent ones. The same discretized form also arises for the velocity gradient in the continuity equation. Consequently, such numerical representations may lead to an unrealistic, so-called *checkerboard pattern*, see Patankar (1980). One remedy is to use a staggered grid where the velocity components are located on the faces of the control volume, and the scalar quantities, such as the pressure and temperature, are arranged at the centre.

Nonetheless, with a collocated grid, the above problem can be overcome by using a Rhie-Chow interpolation approach (Rhie and Chow, 1984). Since, in the discretized momentum equations, this causes problems in representing the pressure gradient by the pressure difference between two alternate nodes, this representation should then be smoothed out to avoid un-physical oscillations in the pressure and velocity fields. This can be achieved by reformulating the linear interpolation for the velocities on the volume faces. The face velocity is first interpolated linearly using its two neighbouring *node velocities* from which the troublesome, pressure-related term is subtracted. Referring to Figure 4.1, to obtain, e.g., the face velocity, u_w, in the x-direction, the node velocities used in the linear interpolation are written as

$$u_P' = u_P - \Pi_P(\delta p), \quad u_W' = u_W - \Pi_W(\delta p) \tag{4.6}$$

where $\Pi(\delta p) = -(\partial p/\partial x)(\delta V/a_p)$ denotes the subtracted, pressure gradient-related term at nodes P and W. Let f_x be the interpolation factor, $f_x = |Ww|/|WP|$ (see Figure 4.1). The subtraction in these node velocities is then compensated for by adding a similar term to the *face velocity*. This suggests

$$u_w = f_x u_P + (1 - f_x)u_W - \left[f_x \Pi_P(\delta p) + (1 - f_x)\Pi_W(\delta p)\right] + \Pi_w(\delta p) \tag{4.7}$$

where $\Pi_w(\delta p)$ is the compensated pressure-related term for the volume face w. In this term, the pressure gradient can be represented by the pressure difference between two adjacent nodes on each side of the face considered, i.e., P and W. The possible non-physical oscillation can thus be ruled out.

Solution Algorithms

The velocity-pressure coupling is handled by the SIMPLEC algorithm (van Doormaal and Raithby, 1984), which is a variant of the SIMPLE method (Patankar, 1980). The standing point in the SIMPLE type algorithms is to use an equation for pressure correction that originates from the continuity equation. A pressure field is first guessed to solve the momentum equations. The pressure correction and velocity correction are then calculated and used to improve the solutions of the pressure and velocity fields, respectively. This procedure is iteratively implemented until a converged solution is obtained.

In general, the number of the nodes defined over the computational domain is the same as the number of the discrete algebraic equations to be solved. These equations are cast into a nominally linear form, although the original differential equations are non-linear and interlinked. The non-linear terms call for an iterative solution procedure and preserve the real in-

trinsic coupling existing between the governing equations. The solver used for the transport equations is the Tri-diagonal Matrix Algorithm (TDMA) (Patankar, 1980), and the pressure correction equation is solved with the Strongly Implicit Procedure (SIP) (Stone, 1968).

Under-relaxation is employed to promote solution stability and convergent rate. Using a factor, γ, which is less than unity, the under-relaxation is then carried out as

$$\frac{a_P}{\gamma}\phi_P = \sum a_{nb}\phi_{nb} + b + (1-\gamma)\frac{a_P}{\gamma}\phi_P^* \tag{4.8}$$

where ϕ_P^* is the value from the previous iteration.

For steady-state flow problems in this work, a false time step, Δt_{false}, has also sometimes been used for under-relaxation. The under-relaxation in this case is expressed as

$$\left(a_P + \frac{\rho\delta V}{\Delta t_{false}}\right)\phi_P = \sum a_{nb}\phi_{nb} + b + \left(\frac{\rho\delta V}{\Delta t_{false}}\right)\phi_P^* \tag{4.9}$$

The smaller the false time step taken, the stronger is the resulting under-relaxation.

Estimation of Grid-Independent Solution

Numerical accuracy in computations is an important aspect, particularly for validations of turbulence modelling. The assessment of numerical accuracy is closely related to the numerical methods used. These include the order of accuracy of the truncation error introduced by individual terms in the governing equations, the grid resolution and the terminating criteria for iterative calculations. Furthermore, eventually, the solution must be validated by using reliable experimental and/or DNS data. It is well known that higher order numerical schemes are more accurate than lower order schemes, e.g. than the first-order upwind scheme that introduces inherent artificial viscosity (diffusivity). The turbulent transport is typically switched off above a component turbulent grid Reynolds (Péclet) number of 2 when using the hybrid scheme, or about 6 for the exponential scheme, because the physical diffusion is replaced by the inherent artificial numerical diffusion (cf. Leonard and Drummond, 1995). The simulation thus becomes insensitive to the turbulence model. High order schemes are preferable to enhance numerical accuracy. By its nature, the artificial numerical diffusion is grid-dependent. The grid therefore needs to be refined until the artificial diffusion is negligible with respect to physical diffusion.

To validate the performance of a turbulence model, grid-independent (or grid-convergent) solutions are required to ensure that the result is not contaminated by numerical diffusion. This is often done through successively refining the grid. If the result is successively converged to a solution with respect to refining grids, the solution is regarded as being grid-independent. The assessment of grid-independence can be analyzed with error estimations based on methods such as the Richardson extrapolation (namely, the h^2 extrapolation). The discrete solution, F, is assumed to have a series representation, in the grid spacing h, as

$$F = F_e + a_1 h + a_2 h^2 + a_3 h^3 + \cdots \tag{4.10}$$

where F_e is the exact solution to the problem considered. If F_1 and F_2 are two separate discrete solutions on two grids with spacing h_1 (fine grid) and h_2 (coarse grid), for a second-order ap-

proximation ($a_1 = 0$), one has

$$F_e \approx F_1 + \frac{F_1 - F_2}{r^2 - 1} \tag{4.11}$$

where higher order terms have been dropped, and r is the grid refinement ratio, $r = h_2/h_1$. Equation (4.11) can be generalized to pth-order approximations (Roache, 1994) as

$$F_e \approx F_1 + \frac{F_1 - F_2}{r^p - 1} \tag{4.12}$$

The correction part (the last term) in (4.11) or (4.12) appears to be an error estimator of the fine grid solution, F_1. Expressing this estimator as a relative factor for F_1 gives

$$E \approx \frac{e}{r^p - 1}, \text{ and } e = \frac{F_2 - F_1}{F_1} \tag{4.13}$$

Instead of using E, e has been commonly employed as an error estimator in grid refinement studies, which is also used in this work, see e.g. Peng *et al.* (1997c). This error estimator should be assessed together with some indication that shows that the calculations are asymptotically reaching a unique solution with refining grids. On the basis of the Richardson extrapolation, Roache (1994) proposed the use of a Grid Convergence Index (GCI) for uniform reporting of grid-convergent solutions.

4.1.2 Numerical Procedure in LES

In large eddy simulations of this work, the finite volume method was used to discretize the governing equations on a collocated grid. A detailed description of the numerical methods used in the LES code has been given by Davidson (1996, 1997a). The main features of the solution procedure are briefly summarized here.

The central differencing scheme is used to discretize the convection, diffusion, stresses and buoyancy source terms, and the second-order Crank-Nicholson scheme is employed for temporal discretization. An implicit, fractional-step method (cf. Kim and Moin, 1985) is implemented to solve the equation system. The filtered Navier-Stokes equations (3.82) are discretized as

$$\bar{u}_i^{n+1} = \bar{u}_i^n + \Delta t L_u\left(D_{u,c}{}^n,\ D_{u,c}{}^{n+1}\right) - \frac{1}{\rho}\alpha\Delta t\frac{\partial \bar{p}^{n+1}}{\partial x_i} - \frac{1}{\rho}(1-\alpha)\Delta t\frac{\partial \bar{p}^n}{\partial x_i} \tag{4.14}$$

where $L_u\left(D_{u,c}{}^n,\ D_{u,c}{}^{n+1}\right)$ represents the discrete terms on the right-hand side in (3.82) except for the pressure gradient term, $D_{u,c}$ denotes the central differencing approximation applied to these terms, and $\alpha = 0.5$ for the second-order Crank-Nicholson scheme. In a similar way, the filtered energy equation (3.83) is represented in its discrete form by

$$\bar{T}_i^{n+1} = \bar{T}_i^n + \Delta t L_T\left(D_{T,c}{}^n,\ D_{T,c}{}^{n+1}\right) \tag{4.15}$$

First, Equation (4.14) is solved with a symmetric Gauss-Seidel method. To reinforce the ve-

locity-pressure coupling, an approach similar to the Rhie-Chow interpolation in the RANS computation is employed. An intermediate velocity field, $\bar{u}_i^*$, is computed by subtracting the implicit part of the pressure gradient from Equation (4.14), giving

$$\bar{u}_i^* = \bar{u}_i^{n+1} + \frac{1}{\rho}\alpha\Delta t\frac{\partial \bar{p}^{n+1}}{\partial x_i} \tag{4.16}$$

Note that the intermediate velocities do not satisfy the continuity equation. A divergence is made for (4.16), where the velocity field at the volume faces, $\bar{u}_{if}^{n+1}$, is required to satisfy continuity, i.e., $\partial \bar{u}_{if}^{n+1}/\partial x_i = 0$. This divergence leads to a Poisson equation for the pressure, giving

$$\frac{\partial^2 \bar{p}^{n+1}}{\partial x_i \partial x_i} = \frac{\rho}{\alpha\Delta t}\frac{\partial \bar{u}_{if}^*}{\partial x_i} \tag{4.17}$$

In equation (4.17), the velocity divergence is calculated using the intermediate velocities at the control volume faces obtained through linear interpolation from neighbouring intermediate nodal velocities. This equation is solved with a multigrid method (Emvin, 1997). The resultant pressure field, together with the intermediate velocities, is then employed to obtain the velocity field which satisfies the continuity. This is done by using

$$\bar{u}_{if}^{n+1} = \bar{u}_{if}^* - \frac{1}{\rho}\alpha\Delta t\left(\frac{\partial \bar{p}^{n+1}}{\partial x_i}\right)_f \tag{4.18}$$

The resulting face velocities, $\bar{u}_{if}^{n+1}$, are then used to compute the mass fluxes at cell faces. The energy equation (4.15) is then solved. The SGS eddy viscosity and diffusivity are subsequently computed.

Starting with an initial field, which in this work is either computed by two-equation turbulence models or generated with small, random perturbations in near-wall regions, the above solution procedure is iteratively carried out within one time step until convergence is reached, and then runs to the next time step. Both the pointwise and linewise symmetric Gauss-Seidel relaxation methods have been applied for solving the momentum equations and the energy equation. For the cavity flow problem (Peng and Davidson, 1998b), it was found that the *CFL* number usually needs to be restricted below 0.5 to retain numerical stability. Parallelization computations were carried out for this flow in a 64-processor ORIGIN 2000 Sillicon Graphics machine. The LES code was paralleled by Zacharov (Zacharov, European Supercomputer Team, Sillicon Graphics Inc., private communication, 1997). Four processors were used. It was assessed that the computation is faster than using a single processor by a factor of about 3 for simulating the confined cavity flow considered.

The box filter is used to distinguish the small scales from the turbulent motions. The width of the grid filter, Δ, is the same as the mesh size, and the width of the test filter is twice Δ, i.e., $\tilde{\Delta} = 2\Delta$, which is the optimal choice proposed by Germano *et al.* (1991) in LES for turbulent channel flows. The filtering operation at the test level is carried out by integrating the variables over the test cell with the linear variation assumption and the trapezoidal rule (Zang *et*

al., 1993). Referring to Figure 4.2, the test filtering for $\overline{\phi}$ at node (i, j, k) is then a volume-averaging process, yielding

$$\tilde{\overline{\phi}}_{i,j,k} = \frac{1}{8}\left(\overline{\phi}_{i+1/2,j+1/2,k+1/2} + \overline{\phi}_{i-1/2,j+1/2,k+1/2} + \overline{\phi}_{i+1/2,j-1/2,k+1/2} + \overline{\phi}_{i-1/2,j-1/2,k+1/2} + \overline{\phi}_{i+1/2,j+1/2,k-1/2} + \overline{\phi}_{i-1/2,j+1/2,k-1/2} + \overline{\phi}_{i+1/2,j-1/2,k-1/2} + \overline{\phi}_{i-1/2,j-1/2,k-1/2}\right) \tag{4.19}$$

The value at the location at which it is not defined is computed by using linear interpolation.

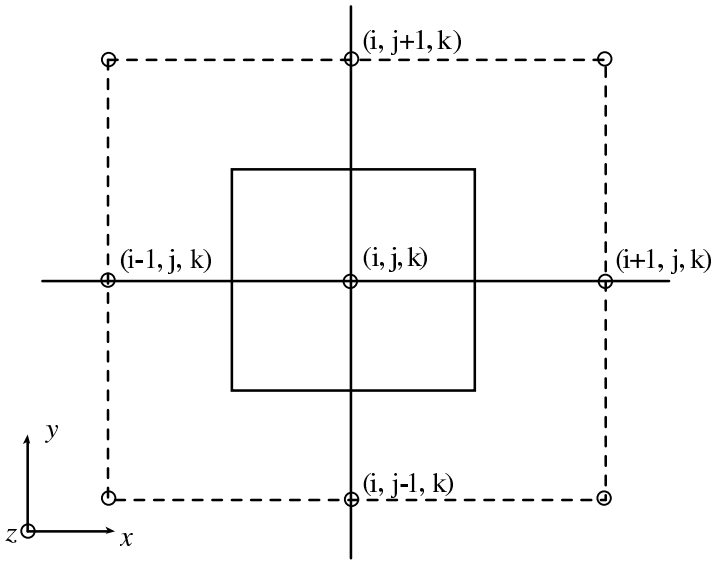

Figure 4.2 Sketch for the filtering volumes at grid (volume enclosed by solid line) and test (enclosed by dashed line) levels.

4.2 Boundary Conditions

Several different boundaries were encountered in this work, including inflow, outflow, solid wall and homogeneous boundaries. Each has its own specifications, which are summarized in this section.

Inflow Conditions. These have been used in the computation of ventilation flows with two-equation turbulence models. The velocities, temperature and turbulent transport quantities over the inlet boundary are usually prescribed, either from the experimental data or from pre-calculated distributions for, e.g., channel flows. In cases of lack of information on the turbulent quantities, they have been specified as

$$k_{in} = \frac{3}{2}\left(Tu_{in}u_{in}\right)^2, \quad \varepsilon_{in} = {k_{in}}^{3/2} \Big/ L_{in}, \quad \omega_{in} = C_w \frac{\sqrt{k_{in}}}{L_{in}} \tag{4.20}$$

where Tu_{in} is the turbulent intensity at inlet, C_w is a constant (C_w = 1/0.09) and L_{in} is specified as a fraction of the inlet size.

Outflow Conditions. Neumann conditions have often been set for the flow variables at outlet

boundaries, giving

$$\frac{\partial \phi}{\partial n} = 0 \tag{4.21}$$

where n is the direction normal to the outflow boundary. Moreover, to ensure a global mass conservation and enhance the convergence procedure, the velocity is required to satisfy the following condition along the boundaries of the computation domain Ω,

$$\oint_{\Omega} \rho \mathbf{U} \cdot \mathbf{n} d\Omega = 0 \tag{4.22}$$

Wall Conditions. In the computation with high-Reynolds-number two-equation turbulence models, wall functions have been employed. The wall function for the velocity is obtained from the log-law of the wall. It reads

$$u = \frac{u_\tau}{\kappa} ln\left(Ey^+\right) \tag{4.23}$$

The wall functions for the turbulent transport quantities can be derived by assuming a local equilibrium for turbulence in the logarithmic layer of boundary layer flows. For the k-ε model, these are

$$k = \frac{{u_\tau}^2}{\sqrt{c_\mu}}, \quad \varepsilon = \frac{{u_\tau}^3}{\kappa y} \tag{4.24}$$

and, for the k-ω model,

$$k = \frac{{u_\tau}^2}{\sqrt{c_\mu c_k}}, \quad \omega = \sqrt{\frac{c_\mu}{c_k}} \frac{u_\tau}{\kappa y} \tag{4.25}$$

The wall function for the temperature is an empirical expression, giving

$$T^+ = \frac{\rho u_\tau c_p (T_w - T)}{q_w} = Pr_t \left(\frac{u}{u_\tau} + \hat{P} \right) \tag{4.26}$$

where

$$\hat{P} = 9.24 \left[\left(\frac{Pr}{Pr_t} \right)^{3/4} - 1 \right] \left\{ 1 + 0.28 \exp\left[-0.007 \left(\frac{Pr}{Pr_t} \right) \right] \right\} \tag{4.27}$$

These wall functions are applicable for a range of $y^+ \in (30, 100)$ near the wall. For adiabatic walls, Equation (4.21) is employed for the temperature. Constant temperatures are set for isothermal walls according to experiments.

When using the LRN two-equation models, as well as in large eddy simulations, no-slip condition is used for the velocities on the wall boundaries, where the turbulent kinetic energy is set to zero. With the LRN k-ε model, several alternatives have been used to specify the dissipation rate, ε, at the wall. For example, its first derivative can be assumed to be zero in the direction normal to the wall (Lam and Bremhorst, 1981). A relation can also be derived from the balance of k in the viscous sublayer, where the viscous diffusion is equal to the dissipation of k. At the closest near-wall node, ε is then given by (cf. Patel *et al.*, 1984)

$$\varepsilon = \nu \frac{\partial^2 k}{\partial y^2} \tag{4.28}$$

Using a Taylor series expansion for $k^{1/2}$ with respect to y, Equation (4.28) can be alternatively approximated for ε at the wall as (cf. To and Humphrey, 1986)

$$\varepsilon_w = \nu \left(\frac{\partial k^{1/2}}{\partial y} \right)_w^2 \tag{4.29}$$

With the k-ω model, the balance between the viscous diffusion and the dissipation terms in the turbulent transport equations holds true in the viscous sublayer (cf. Wilcox, 1988). This yields an exact asymptotic solution for ω, as $y \to 0$, giving

$$\omega = \frac{6\nu}{c_{\omega 2} y^2} \tag{4.30}$$

When using the LRN k-ω model or its high-Re version with the so-called *extended-to-wall* method, (4.29) has been used at the nodes closest to the wall boundaries.

The boundary condition for the pressure in LES was specified with the Neumann condition at the wall. This gives $\partial \overline{p} / \partial y = 0$.

Homogeneous Conditions. Flows that are statistically homogeneous in one or more directions are often encountered in large eddy simulations. This has been handled with periodic boundary conditions in the homogeneous direction by specifying

$$\phi_0 = \phi_{N-1}, \quad \phi_N = \phi_1 \tag{4.31}$$

where 0 and N denote the computational boundary nodes in the homogeneous direction, with nodes 1 and (N–1) as their interior neighbouring nodes, respectively. Special attention should be paid to the computational domain, which must be large enough to contain all unstable modes when using homogeneous conditions.

Besides the above boundaries, symmetric boundaries were also employed when solving flow problems that are symmetric around one or more boundaries. In this case, only a half or one-fourth of the computational domain is used in order to save computational resources. The no-flux condition, which has the same mathematical description as (4.21), was used for such boundaries.

Chapter 5

Summary

Numerical simulation of indoor air flow and heat transfer has been increasingly used in research and development of building technology. CFD techniques are able, and have been widely used, to investigate various aspects of the indoor environment and building energy consumption. Along with experimental measurements, numerical simulation has proven to be an efficient tool in diagnosing system problems, optimizing system designs and improving system efficiency. To promote and widen its applications in building ventilation, numerical simulation must be further developed and improved towards a higher degree of reliability and accuracy. On the one hand, the development should follow the general, mainstream research in fluid mechanics and numerical methods; on the other hand, extensive studies are required to improve various aspects of CFD specifically adapted to building ventilation. The work in this thesis has contributed to combined research concerned with the assessment of ventilation flow systems and modelling of turbulent flow and heat transfer.

Carrying out numerical simulations for a flow system is always based on some specific purposes, such as revealing flow and heat transfer characteristics, diagnosing system problems, optimizing system designs and so on. Such specific purposes must be founded on a series of assessments for the system considered. Consequently, some measures are required to serve as scales or indices to evaluate system performance. In building ventilation, various scales have been invented to assess ventilation efficiency and effectiveness, to quantify indoor air quality and energy consumption and to indicate the indoor thermal environment. The first part of this work is devoted to the development of new scales and methods for assessing the performance of ventilation flow systems. In developing these scales and methods, numerical simulation has been considered as an applicable and efficient tool for exploring them in ventilation practice.

The analysis of ventilation scales depends on the transport phenomena created by a ventilation system. When CFD is used to quantify these scales, characteristics of indoor air motion and heat transfer must be appropriately incorporated, which involves a number of different disciplines. Main aspects include the modelling of turbulent flow and heat transfer, numerical methods and boundary conditions.

Ventilation flow has, locally or globally, its own specific flow features, such as being characterized by low-Reynolds-number turbulence, by mixing and recirculating air motions, by thermal stratification and so on. These must be well accounted for in a turbulence model. The second part of this work was directed toward the modelling of turbulent flow and heat transfer, which was considered mainly on the basis of two-equation models and on SGS models in large eddy simulation.

Some fundamental turbulent flows were used to calibrate and improve the models. These fundamental flows were carefully chosen such that they, alone or together, form the main flow features in a typical ventilated space. In other words, they have been taken from complex flow phenomena that may co-exist in one typical ventilation flow to form relatively simple flow configurations for which the influence of various physical processes can be isolated and studied in detail. Fundamental flow configurations used in this work include three types.

- *Channel flow*. This type is one of the most fundamental flows in calibrating turbulence models. It has been used to validate the model performance in predicting near-wall tur-

bulence features.

- *Backward-facing step flow*. This type of flow is characterized by recirculation, separation and reattachment. With a large expansion ratio, it is equivalent to the flow created in rooms by a mixing ventilation system.
- *Buoyancy-driven flows in a cavity and a channel*. Such flows are often characterized by coherent structures and heat transfer. The buoyant flow in a confined cavity at a moderate Rayleigh number is thermally stratified, with transitional boundary layers along the vertical walls. These flows are typical flow phenomena arising in many non-isothermal ventilation applications, e.g., when the building enclosures adjacent to the outdoors are not adiabatic, when heat sources exist and when cooled or warmed air is supplied. A typical example is the flow triggered in rooms by a displacement ventilation system.

Since the modelling background is set up with some fundamental turbulent flows that commonly exist in engineering applications, it by no means constrains the potential relevance of the model to other engineering flows. On the other hand, it would be an exaggeration to claim that one study could improve all aspects of modelling complex ventilation flows. The path toward achieving reliable modelling of indoor air flows has no end. One of the highest expectations for this work is that it will draw more attention from ventilation researchers and engineers to studies of ventilation flow mechanisms, about which our understanding at present is far less than what is needed to model flow behaviours in a ventilated room.

5.1 Conclusions

This work includes two main aspects: performance assessment of ventilation flow systems and modelling and simulation of turbulent flow and heat transfer. In the first part, both compartmental and numerical methods were used in combination with imaginary tracer experiments to develop some new scales and to analyze ventilation flow systems. Stochastic theory was used to quantify some ventilation scales. In the second part, both two-equation turbulence modelling and subgrid-scale modelling were presented and discussed. From this work, the following conclusions are derived.

- Local/zonal scales should be used to achieve a reliable assessment of ventilation performance rather than placing reliance only on global indices. Several new local ventilation scales have been proposed. These include the local purging effectiveness and the expected contaminant dispersion index, which are derived from analyses of air age variation, as well as the local specific contaminant-accumulating index based on a new concept termed the local age-integrated exposure to contaminants. These local scales can be explored with numerical simulation coupled with the equation for local mean air age and/or with their own transport equations as derived in this work. Some of these scales can also be measured in experiments. Their use has been demonstrated. These scales are expected to be useful in practice for diagnosing system problems and improving systems designs.
- One of the important concepts for quantifying ventilation efficiency, i.e., the purging flow rate, was comprehensively discussed and re-formulated. This concept has been embodied in several different mathematical expressions that are more accessible and have a better-posed physical basis than in the original definition. Some ventilation indices related to this concept were defined and reviewed.
- On the basis of stochastic analyses for a flow system divided into multiple compartments, a Markov chain model was proposed for determining transfer probabilities that

are needed to calculate the purging flow rate. This model is the general and extended formulation of a previous deterministic method and is able to give additional information that the deterministic method does not include.

- A comparison of different types of two-equation turbulence models was made, which showed that the k-τ model and k-ω model used in their high-Re forms exhibit relatively poor performance for simulating typical ventilation flows. Modifications were made on the basis of Wilcox's high-Re k-ω model. These modifications were shown to be reasonable and able to improve predictions over the original model for ventilation flows.
- An LRN variant of the k-ω model was developed and extended to buoyancy-driven turbulent flows where thermal stratification and the transitional boundary layer regime exist. The proposed LRN k-ω model produces reasonable simulations for both isothermal and buoyancy-driven turbulent flows.
- For buoyant flows at moderate Rayleigh numbers, the transition regime in the boundary layer along a vertical wall was analyzed using the modified LRN k-ω model. It was found that the buoyant production for the turbulent kinetic energy plays a significant role in the prediction of transition onset. For cavity flow with stable thermal stratification, this term is a destruction term for turbulence, which tends to absorb energy from the near-wall boundary layer and consequently delay the transition onset. The model behaviour required for handling such flows was discussed and analyzed. The grid-dependence of the model can be eliminated as desired by damping the buoyant source term for k. The result can be used to adjust LRN formulation for two-equation turbulence models.
- Large eddy simulation was performed for turbulent convection flows with heat transfer. A modified buoyancy SGS model was proposed to explicitly accommodate the effect of buoyancy on the SGS eddy viscosity/diffusivity and to avoid giving rise to no-real solutions entailed by the original buoyancy model. The proposed SGS model is able to account for some energy backscatter for flows with thermal stratification. For isothermal flows, this modified model returns to the Smagorinsky model. The dynamic modified buoyancy model has shown reasonable performance.
- In general, the dynamic SGS model performs better than the Smagorinsky model in which the dynamic procedure is not incorporated. Nonetheless, it was found that the dynamic SGS model gives unreasonable performance for predicting the buoyant cavity flow at a moderate Rayleigh number. The failure and success of using SGS models are discussed in dealing with such type of flows. The main problem is argued to lie in the difficulties of the grid resolution, as well as in the constraint inherent in the SGS model itself, for which the energy backscatter cannot be correctly represented. Further studies are desired to improve the dynamic behaviour of SGS models in LES for the thermally stratified buoyant flows in which transitional boundary layers exist.

5.2 Summary of Papers

This work was initiated as a program combining studies on computational fluid dynamics and its applications and development in building ventilation. It was originally considered that numerical simulation would be efficient to explore the effect of local, detailed air/contaminant convection and diffusion on ventilation efficiency. Such an exploration, however, appeared to be purely a task of applying CFD to ventilation flow simulations. On the other hand, it was noticed that the concept of ventilation efficiency used until now has been too general when employed to quantify various aspects of ventilation performance. The study then became in-

stead an attempt to re-examine and develop some new concepts and approaches for the assessment of ventilation flow systems. This led to the work included in Paper 1 and Paper 2.

With respect to turbulence modelling, this was aimed at developing turbulence models that should be applicable on an intermediate level for predicting ventilation flows and should be acceptable in practice for ventilation engineers and researchers. More advanced models were previously used in ventilation engineering, such as second-moment closures and LES, but their applications have seemingly not yet found wide acceptance for various reasons. The study thus started with two-equation models of different types that have been used frequently in recent studies. A comparison was first made in Paper 3 of the k-ε model, the k-ω model and the k-τ model. No significant dismerits against the conventional k-ε model were found in the comparison. However, the preference was to develop an LRN model for predicting ventilation flows characterized by low-Reynolds-number turbulence and local laminar and transitional flow phenomena.

It was noticed that an LRN k-ε model usually fails to retain turbulent transport in numerical simulations for flows created by a displacement ventilation system, returning an unrealistic laminar solution. Wilcox's LRN k-ω model was originally developed for simulating transitional boundary layer flows. This model as a whole gave relatively poor performance for typical recirculating ventilation flows, but its model feature was expected to be exploitable. Modifications were thus first made on the high-Re k-ω model (report not included here). On the basis of this modified form, an LRN k-ω model was developed in Paper 4, where the establishment of the modified high-Re version can be traced. In Paper 5, the behaviour of the modified LRN model was further analyzed for natural convection flows with heat transfer.

Motivated by the sophisticated flow structure and the undesirable performance of some LRN two-equation models for turbulent buoyant cavity flows at moderate Rayleigh numbers, the development of more advanced modelling approach was considered. LES was thus implemented, where an SGS buoyancy model was proposed. The performance of several SGS models was investigated for handling turbulent thermal convection flows. These were reported in Paper 6 and Paper 7.

To close this summary, a short review is given of each paper in the sections below.

Paper 1

The assessment of ventilation performance is discussed in view of room air distribution and passive contaminant dispersion. Different concepts and methods for analyzing and assessing ventilation flow systems are addressed and re-examined. Several new ventilation scales are developed. The local purging effectiveness is able to distinguish the individual contribution of each supply opening to an arbitrary region in a ventilated space with multiple inlets. The expected contaminant dispersion index can be used to forecast passive contaminant transport emitted from specific locations with unknown source strengths. These two scales can be derived from air age variation analysis that obeys a transport equation. The local specific contaminant-accumulating index is proposed to evaluate the tolerance of a set-up ventilation flow to specific contaminant sources. This index is based on a new concept termed the local age-integrated exposure whose governing equation can be derived from the mass transport equation. These new scales are expected to be applicable for diagnosing problems and improving designs of ventilation systems.

Paper 2

This paper deals with the description and determination of the purging flow rate, U_p, for venti-

lation systems or equivalent flow systems. The regional purging flow rate and its use are discussed and proposed. By using the mass conservation principle in conjunction with the compartmental method, U_p is embodied in various mathematical expressions in terms of the transfer probability. Some U_p-related parameters are described. Using stochastic analyses, a Markov chain model is proposed for determining the transfer probability and exploring several useful ventilation indices that are not included in the previous deterministic method. Numerical simulation is used to calculate the interchanging flow rates between various regions. The application of these proposals is demonstrated, and they appear to be promising for analyzing and assessing ventilation performance.

Paper 3

To investigate the performance of turbulence models in numerical simulations of recirculating ventilation flows, comparisons are made of three types of two-equation models, including the k-ε, the k-ω and the k-τ models. A modified high-Re k-ω model is introduced and implemented. All the models are applied with the wall-function method. When using the k-ω models, an extended-to-wall method is also employed without using wall functions as a bridge. Two typical recirculating flows are calculated: the separated flow behind a backward-facing step with a large expansion ratio relevant to room ventilation and the wall-jet-induced flow in a two-dimensional ventilation enclosure. The predictions are compared with experimental data. The performance of the models is discussed. It is found that the original k-ω model and the k-τ model give relatively poor predictions for the flows considered. The modified k-ω model is shown to be an attractive alternative to the k-ε model.

Paper 4

A modified form of Wilcox's low-Reynolds-number (LRN) k-ω model (Wilcox, 1994) is proposed for predicting turbulent recirculating flows. The turbulent diffusion for the specific dissipation rate, ω, is modelled with two parts: a second-order diffusion term and a first-order cross-diffusion term. The model constants are re-evaluated. The damping functions are redevised, which reproduces correct near-wall asymptotic behaviours and retains the mechanism of describing transition as in the original model. The new model is applied to channel flow, backward-facing step flow with a large expansion ratio (H/h = 6) and recirculating flow in a ventilation enclosure. The predictions are considerably improved. The effects of the modification are discussed.

Paper 5

The computation of turbulent buoyant convection flows with thermal stratification was considered using the low-Reynolds-number (LRN) k-ω model. When applying the k-ε model to buoyancy-driven cavity flows induced by differentially heated side walls, a commonly encountered problem at moderate Rayleigh numbers (Ra = 10^{10} ~ 10^{12}) is that the model is not able to give grid-independent predictions for the transition regime along the vertical walls. It was found that the buoyant source term for the turbulence energy, G_k, exhibits strong grid sensitivity, as this term is modelled with the Standard Gradient Diffusion Hypothesis (SGDH). In the pseudo-laminar stage, this term tends to absorb energy from the near-wall boundary layer and delays the transition onset. By introducing a damping function into this term, the grid dependence of the model is eliminated, and the modelled G_k renders correct asymptotic behaviour near the vertical walls. The mechanism held in the k-ω model for predicting natural transition onset is analyzed. The present approach is simple for practical use and able to give reasonable predictions.

Paper 6

Dynamic subgrid-scale (SGS) modelling in LES for engineering flows usually uses Smagorinsky's eddy viscosity model as a basis, where the subgrid scaling is constructed by assuming a local equilibrium between the subgrid turbulent shear production and dissipation rate. For turbulent thermal convection flows, an additional buoyancy production term can also be included in this argument. The buoyancy effect on the SGS eddy viscosity is then explicitly accommodated in the base model. This in turn forms the so-called *buoyancy model*. A problem usually encountered with this model is that it may entail non-real solutions for thermal convection flows. To remedy this problem, a new SGS time scaling is proposed to re-formulate the eddy viscosity. In the modified model, the magnitude of the local strain rate tensor is employed to weight the SGS time scaling in the original buoyancy model. This approach makes the base model capable of accounting for energy backscatter from subgrid scales to resolved large scales for thermally stratified flows. The modified model was applied to the Rayleigh-Bénard convection flow and compared with the scalar model and the buoyancy model. The results are found to be in good agreement with both DNS and experimental data.

Paper 7

Large eddy simulation was performed for turbulent natural convection flows induced by two differentially heated vertical walls. These include the flow in a confined cavity with an aspect ratio of 5 at a Rayleigh number, Ra, of about 5×10^{10} and the flow between two differentially heated, infinite vertical walls at $Ra = 5.4 \times 10^{5}$ (an infinite cavity). The SGS models employed were the conventional Smagorinsky model and the dynamic model. A recently proposed SGS buoyancy model was also used in comparison. The performance of SGS models in handling these flows was investigated. It was found that the dynamic model fails to reasonably capture the flow structure and gives poor predictions when solving the buoyant cavity flow where the boundary layer subsequently exhibits laminar, transitional and fully developed turbulent characteristics along the vertical side walls. The dynamic model over-estimated the thickness of the boundary layer with under-predicted streamwise velocities. The unreasonable model behaviour was analyzed. Arguments were imposed on the prediction of energy backscatter from subgrid to resolved large scales, which is regarded as being an essential ingredient in accounting for transitional and low-Reynolds/Rayleigh-number turbulent flows. For the flow created in the infinite cavity, the SGS models generally showed acceptable performance. Variations can, however, also be observed between the LES prediction and DNS data for some turbulent quantities. The success and failure of applying LES to these flows were discussed.

References

Abe, K., Kondoh, T., and Nagano, Y., A new turbulence model for predicting fluid flow and heat transfer in separating and reattaching flows - I: Flow field calculations. *Int. J. Heat and Mass Transfer*, **37**, 139-151 (1994).

Akselvoll, K. and Moin, P., Large eddy simulation of a backward facing step flow. In *Engineering Turbulence Modelling and Experiments*, **2** (eds W. Rodi and F. Martelli), 303-314, Florence, Italy (1993).

Bardina, J., Ferziger, J. H. and Reynolds, W. C., Improved subgrid models for large eddy simulation. *AIAA Paper* 80-1357 (1980).

Bauman, F., Gadgil, A., Kammerud, R., Altmayer, E. and Nansteel, M., Convective heat transfer in buildings: Recent research results. *ASHRAE Trans.*, **89** (1), 215-232 (1983).

Bergstrom, D. J. and Huang, X., LES of buoyant cavity flow: challenge for subgrid scale models. In *Proc. of 2nd Int. Symp. on Turbulence, Heat and Mass Transfer* (ed. K. Hanjalic and T. W. J. Peeters), 421-430, Delft University Press (1997).

Behnia, M., Parneix, S. and Durbin, P., Simulation of jet impingement heat transfer with the k-ε-v^2 model. *Annual Research Briefs 1996*, 3-16, Centre for Turbulence Research, Stanford University (1996).

Boris, J. P., New directions in computational fluid dynamics. *Ann. Rev. Fluid Mech.*, **21**, 345-385 (1989).

Boussinesq, J., Théorie de l'écoulement tourbillant. *Mem. Pre. par. div. Sav.*, **23** (1877).

Cabot, W., Large eddy simulations of time-dependent and buoyant-driven channel flows. *Annual Research Briefs 1992*, 45-60 , Centre for Turbulence Research, Stanford University (1992).

Cabot, W. and Moin, P., Large eddy simulation of scalar transport with the dynamic subgrid-scale model. In *Large Eddy Simulation of Complex Engineering and Geophysical Flows* (eds B. Galperin and S. A. Orszag), Cambridge University Press, 142-158 (1993).

Canuto, V. M., Dubovikov, M. S. and Dienstfrey, A., A dynamic model for turbulence. IV. Buoyancy-driven flows. *Phys. Fluids*, **9** (7), 2118-2131 (1997).

Chen, H. C. and Patel, V. C., Near-wall turbulence models for complex flows including separation. *AIAA J.*, **26**, 641-648 (1988).

Chen, Q., *Indoor Air Flow, Air Quality and Energy Consumption of Buildings*. Ph. D. Thesis, Delft University of Technology, the Netherlands (1988).

Chiang, C. L., *Introduction to Stochastic Processes and Their Applications*, Robert E. Krieger, New York (1980).

Chien, K-Y., Predictions of channel and boundary-layer flows with a low-Reynolds-number turbulence model. *AIAA J.*, **20**, 33-38 (1982).

Chou, P. Y., On an extension of Reynolds method of finding apparent stress and the nature of turbulence, *China J. of Phys.*, 1-53 (1940).

Chou, P. Y., On velocity correlations and the solutions of the equations of turbulent fluctuations. *Q. Appl. Math.*, **111**(1), 38-54 (1945).

Chow, W. K., Application of computational fluid dynamics in building service engineering. *Building and Environment*, **24**, 363-372 (1996).

Cinlar, E., *Introduction to Stochastic Processes*. Prentice-Hall Inc. (1975).

Ciofalo M., Large eddy simulation of turbulent flow and heat transfer: A state of the art review. *QUADERNI*, Dipartimento di Ingegneria Nucleare, Dell'Universita di Palermo, Italy (1993).

Clark, R. A., Ferziger, J. H. and Reynolds, W. C., Evaluation of subgrid-scale models using an accurately simulated turbulent flow. *J. Fluid Mech.*, **91**, 1-16 (1979).

Craft, T. J., Launder, B. E. and Suga, K., A non-linear eddy-viscosity model including sensitivity to stress anisotropy. In *Proc. of 10th Symposium on Turbulent Shear Flows*, Pennsylvania State University, State College, PA. (1995).

Danckwerts, P. V., Continuous flow systems: distribution of residence time. *Chem. Engng Sci.*, **2**, 1-13 (1952).

Davidson, L. and Olsson, E., Calculation of age and local purging flow rate in rooms. *Building and Environment*, **22**, 111-127 (1987).

Davidson, L., Ventilation by displacement in a three-dimensional room - A numerical study. *Building and Environment*, **24**, 363-372 (1989).

Davidson, L., Second-order corrections account for non-isotropic turbulence due to buoyancy. *Int. J. Heat and Mass Transfer*, **33**, 2599-2608 (1990).

Davidson, L., and Farhanieh, B., CALC-BFC: A finite-volume code employing collocated variable arrangement and Cartesian velocity components for computation of fluid flow and heat transfer in complex three-dimensional geometries. *Report* **92/4**, Department of Thermo and Fluid Dynamics, Chalmers University of Technology, Gothenburg (1992).

Davidson, L., LES of recirculating flow without any homogeneous direction: A dynamic one-equation subgrid model. In *Proc. 2nd Int. Symp. on Turbulence Heat and Mass Transfer* (Delfta, 1997), 481-490 (1997a).

Davidson, L., Large eddy simulation: A dynamic one-equation subgrid model for three-dimensional recirculating flows. In *Proc. 11th Int. Symp. on Turbulent Shear Flow*, **3**, 26.1-26.6, Genoble (1997b).

Deardorff, J. W., A numerical study of three-dimensional turbulent channel flow at large Reynolds numbers. *J. Fluid Mech.*, **41**, 453-480 (1970).

Deardorff, J. W., The use of subgrid transport equations in a three-dimensional model of atmospheric turbulence. *ASME J. Fluid Engineering*, 429-438, September (1973).

Durbin, P. A., Near-wall turbulence closure modeling without 'damping functions'. *Theoret. Comput. Fluid Dynamics*, **3**, 1-13 (1991).

Durbin, P.A., Separated flow computations with the k-ε-v^2 model. *AIAA J.*, **33**, 659-664 (1995).

Eidson, T. M., Numerical simulation of the turbulent Rayleigh-Bénard problem using subgrid modelling. *J. Fluid. Mech.*, **158**, 245-268 (1985).

Emvin, P., *The Full Multigrid Method Applied to Turbulent Flow in Ventilated Enclosures Using Structured and Unstructured Grids*, Ph. D. Thesis, Department of Thermo and Fluid Dynamics, Chalmers University of Technology, Gothenburg, Sweden (1997).

Etheridge, D. and Sandberg, M., *Building Ventilation: Theory and Measurement*. John Wiley & Sons Ltd., England (1996).

Fanger, P. O., *Thermal Comfort: Analysis and Applications in Environmental Engineering*. Florida, Robert E. Krieger Publishing Company (1982).

Fanger, P. O., Melikov, A. K. Hanzawa, H. and Ring, J., Air turbulence and sensation of draught. *Energy and Buildings*, **12**, 21-39 (1988).

Feller, W., *An Introduction to Probability Theory and Its Applications*, II (2nd Ed.). John Wiley & Sons, Inc.(1971).

Ferziger, J. H., Large eddy numerical simulations of turbulent flows. *AIAA J.*, **15**, 1261-1267 (1977).

Ferziger, J. H., Subgrid-scale modeling. In *Large Eddy Simulation of Complex Engineering and Geophysical Flows* (eds B. Galperin and S. A. Orszag), Cambridge University Press, 38-54 (1993).

Fletcher, C. A. J., *Computational Techniques for Fluid Dynamics*, Vol. **I** & **II**, 2nd Ed. Springer-Verlag, Berlin Heidelberg (1991).

Gan, G., Croome, D. J, and Awbi, H. B., Numerical prediction of contaminant distribution in ventilated rooms. In *Proceedings of Ventilation '91*, 359-366, Cincinnati, Ohio, USA (1991).

Gan, G., Numerical method for a full assessment of indoor thermal comfort. *Indoor Air*, **4**, 154-168 (1994).

Germano, M., A proposal for a redefinition of the turbulent stresses in the filtered Navier-Stokes equations. *Phys. Fluids*, **29** (7), 2323-2324 (1986).

Germano, M., Piomelli, U., Moin, P. and Cabot, W. H., A dynamic subgrid scale eddy viscosity model. *Phys. Fluids A*, **3**, 1760-1765 (1991).

Germano, M., Turbulence: the filtering approach. *J. Fluid Mech.*, **238**, 325-336 (1992).

Ghosal, S., Lund, T., Moin, P. and Akselvoll, K., A dynamic localization model for large-eddy simulation of turbulent flows. *J. Fluid Mech.*, **286**, 229-255 (1995).

Groth, J., *On the Modelling of Homogeneous Turbulence*. Ph. D. Thesis, Department of Fluid Mechanics, Royal Institute of Technology, Stockholm, Sweden (1991).
Hallbäck, M., Groth, J. and Johansson, A. V., An algebraic model for nonisotropic turbulence dissipation rate in Reynolds stress closures. *Phys. Fluids A*, **2**, 1859-1866 (1990).
Hallbäck, M., Henningson, D. S., Johansson, A. and Alfredsson, P. H., The Basics of turbulence modelling. In ERCOFTAC Series, **2**, *Turbulence and Transition Modelling* (eds M. Hallbäck, D. S. Henningson, A. Johansson and P. H. Alfredsson), 81-154, Kluwer Academic Publishers (1995).
Hanjalic, K. and Launder, B. E., A Reynolds stress model of turbulence and its application to thin shear flows. *J. Fluid Mech*., **53**, 609-638 (1972).
Hanjalic, K. and Launder, B. E., Contribution towards a Reynolds-stress closure for low-Reynolds-number turbulence. *J. Fluid Mech*., **74**, 593-610 (1976).
Hanjalic,K., Jakirlic, S. and Hadzic, I., Computation of oscillating turbulent flows at transitional Re-numbers. In *Proc. 9th Symp. Turbulent Shear Flow*, 1-4, Kyoto, Japan (1993).
Hanjalic, K. and Vasic, S., Computation of turbulent natural convection in rectangular enclosures with an algebraic flux model. *Int. J. Heat and Mass Transfer*, **36**, 3603-3624 (1993).
Hanjalic, K., Advanced turbulence closure models: A view of current status and future prospects. *Int. J. Heat and Fluid Flow*, **15**, 178-203 (1994).
Heindel, T. J., Ramadhyani, S. and Incropera, F. P., Assessment of turbulence models for natural convection in an enclosure. *Numerical Heat Transfer*, **26** (Part B), 147-172 (1994).
Heinsohn, R. J., *Industrial Ventilation*. John Wiley & Sons, Inc. New York (1991).
Henkes, R. A. W. M., *Natural-Convection Boundary Layers*. Ph. D. Thesis, Delft University, Netherlands (1990).
Henkes, R. A. W. M., van Der Vlugt, F. F. and Hoogendoorn, C. J., Natural-convection flow in a square cavity calculated with low-Reynolds-number turbulence models. *Int. J. Heat and Mass Transfer*, **34**, 377-388 (1991).
Henkes, R. A. W. M. and Hoogendoorn, C. J., Comparison exercise for computations of turbulent natural convection in enclosures. *Numerical Heat Transfer*, **28** (Part B), 59-78 (1995).
Henkes, R. A. W. M. and Le Quéré, P., Three-dimensional transition of natural-convection flows. *J. Fluid Mech.*, **319**, 281-303 (1996).
Horiuti, K., Comparison of conservative and rotational forms in large eddy simulation of turbulent channel flow. *J. Comp. Physics*, **71**, 343-370 (1987).
Hossain, M. S. and Rodi, W., A turbulence model for buoyant flows and its application to vertical buoyant jets. In *Turbulent Buoyant Jets and Plumes* (ed. W. Rodi), Pergamon, New York (1982).
Hrenya, C. M., Bolio, E. J., Chakrabarti, D. and Sinclair, J. L., Comparison of low-Reynolds number k-ε turbulence models in predicting fully developed pipe flow. *Chemical Engineering Science*, **50**, 1923-1941 (1995).
Huang, Y.-N. and Rajagopal, K. R., On a generalized nonlinear k-ε model for turbulence that models relaxation effects. *Theoret. Comput. Fluid Dynamics*, **8**, 275-288 (1996).
Humphrey, J. A. C. and To, W. M., Numerical simulation of buoyant, turbulent flow–I. Free and mixed convection in a heated cavity. *Int. J. Heat and Mass Transfer*, **29**, 593-610 (1986).
Ince, N. Z. and Launder, B. E., On the computation of buoyancy-driven turbulent flows in rectangular enclosures. *Int. J. Heat and Fluid Flow*, **10**, 110-117 (1989).
Incropera, F. P. and DeWitt, D.P., *Fundamentals of Heat and Mass Transfer*. John Wiley, New York (1990)
IMechE, *Computational Fluid Dynamics for the Environmental and Building Service Engineer – Tool or Toy* ? Mechanical Engineering Publication Limited for IMechE, London (1991)
Jones, P. J. and Whittle, G. E., Computation fluid dynamics for building air flow prediction – Current status and capabilities. *Building and Environment*, **27**, 321-338 (1992).
Jones, W. P. and Launder, B. E., The prediction of laminarization with a two-equation model of turbulence. *Int. J. Heat and Mass Transfer*, **15**, 310-314 (1972).
Jones, W. P. and Launder, B. E., The calculation of low-Reynolds-number phenomena with a two-equation model of turbulence. *Int. J. Heat and Mass Transfer*, **16**, 1119-1130 (1973).

Kaizuka, M. and Iwamoto, S., A numerical calculation on the distribution of surface temperature and thermal comfort index caused by radiation interaction in a heated room. *Trans. SHARE*, No. **33**, 103-112 (1987).

Karniadakis, G. E., Orszag, S. A. and Yakhot, V., Renormalization group theory: Simulation of transition and turbulent flow over a backward-facing step. In *Large Eddy Simulation of Complex Engineering and Geophysical Flows* (eds B. Galperin and S. A. Orszag), Cambridge University Press, 349-366 (1993).

Kawamura, H. and Kawashiba, N., An application of a near-wall k-$\tilde{\varepsilon}$ model to the turbulent channel flow with transpiration and to the oscillatory flow around a square cylinder. In *Proc. 2nd Int. Symposium on Turbulent, Heat and Mass Transfer* (eds K. Hanjalic and T. W. J. Peeters), 379-389, Delfta University, the Netherlands (1997).

Kim, J., Moin, P. and Moser, R., Turbulence statistics in fully developed channel flow at low Reynolds number. *J. Fluid. Mech.*, **177**, 133-166 (1987).

Kim, J. and Moin, P., Application of a fractional-step method to incompressible Navier-Stokes equations. *J. Comp. Phys.*, **59**, 308-323 (1985).

Krambeck, F. J., Shinnar, R. and Katz, S., Stochastic mixing models for chemical reactors. *I&EC Fundamentals*, **6**, 276-288 (1967).

Lai, Y. G. and So. R. M. C., On near-wall turbulence flow modelling. *J. Fluid Mech.*, **221**, 641-673 (1990).

Lam, C. K. G. and Bremhorst, K., A modified form of the k-ε model for predicting wall turbulence. *ASME J. Fluid Engineering*, **103**, 456-460 (1981).

Launder, B. E. and Sharma, B. I., Application of the energy dissipation model of turbulence to the calculation of flow near a spinning disc. *Lett. Heat and Mass Transfer*, **1**, 131-138 (1974).

Landahl, M. T. and Mollo-Christensen, E., *Turbulence and Random Processes In Fluid Mechanics*. Cambridge University Press, Cambridge (1986).

Launder, B. E. and Spalding, D. B., *Mathematical Models of Turbulence*, Academic Press (1972).

Launder, B. E. and Spalding, D. B., The numerical computation of turbulent flows. *Computer Method in Applied Mechanics and Engineering*, **3**, 269-289 (1974).

Launder, B. E., Reece, G. J. and Rodi, W. Progress in the development of a Reynolds-stress turbulence closure. *J. Fluid Mech.*, **68**, 537-566 (1975).

Launder, B. E., Low-Reynolds-number turbulence near walls, *Report TFD/86/4*, UMIST, Department of Mechanical Engineering, Manchester (1986).

Launder, B. E., On the computation of convective heat transfer in complex turbulent flows. *ASME J. Heat Transfer*, **111**, 1112-1128 (1988).

Launder, B. E., Second moment closure: present ... and future?. *Int. J. Heat and Fluid Flow*, **10**, 282-300 (1989).

Launder, B. E. and Shima, N., Second-moment closure for the near-wall sublayer: development and application. *AIAA J.*, **27**, 1319-1325 (1989).

Launder, B. E., Advanced turbulence models for industrial application. In ERCOFTAC Series **2**, *Turbulence and Transition Modelling* (eds M. Hallbäck, D. S. Henningson, A. Johansson and P. H. Alfredsson), 193-232, Kluwer Academic Publishers (1995).

Le, H. and Moin, P., Direct numerical simulation of turbulent flow over a backward facing step. *Report TF-58*, Thermosciences Division, Department of Mechanical Engineering, Stanford University (1994).

Leonard, A., Energy cascade in large-eddy simulations of turbulent fluid flows. *Adv. Geophys.* **18**A, 273-248 (1974).

Leonard, B. P., A stable and accurate convective modeling based on upstream interpolation. *Comp. Meth. Appl. Mech. Engng.*, **19**, 59-98 (1979).

Leonard, B. P. and Drummond, J. E., Why you should not use 'Hybrid', 'Power-law' or related exponential schemes for convective modelling–There are much better alternatives. *Int. J. Numerical Methods in Fluids*, **20**, 421-442 (1995).

Lesieur, M and Métais, O., New trends in large-eddy simulations of turbulence. *Annu. Rev. Fluid*

Mech., **28**, 45-82 (1996).
Levenspiel, O., *Chemical Reaction Engineering - An Introduction to the Design of Chemical Reactors*, John Wiley & Sons, Inc., London (1962).
Li, Y., *Simulation of Flow and Heat Transfer in Ventilated Rooms*. Ph. D. Thesis, Royal Institute of Technology, Stockholm, Sweden (1992).
Liddament, M. W., The role and application of ventilation effectiveness in design. In *Proceeding of International Symposium on Room Air Convection and Ventilation Effectiveness*, 59-75, University of Tokyo (1992)
Lilly, D. K., The representation of small-scale turbulence in numerical simulation experiments. In *Proc. IBM Sci. Comput. Symp. Environ. Sci.,* IBM data Process Div., White Plains, N. Y. 195-210 (1967).
Lilly, D. K., A proposed modification of the Germano subgrid-scale closure method. *Phys. Fluids A*, **4**, 633-635 (1992).
Liu, F., and Zheng, X., Staggered finite volume scheme for solving cascade flow with a k-ω turbulence model. *AIAA J.*, **32**, 1589-1596 (1994).
Liu, S., Meneveau, C. and Katz, J., On the properties of similarity subgrid-scale models as deduced from measurements in a turbulent jet. *J. Fluid Mech.*, **275**, 83-119 (1994).
Lockwood, F. C. and Papadopoulos, C. A new method for the computation of particulate dispersion in turbulent two-phase flows. *Combustion and Flame*, **76**, 403-413 (1989).
Lu, W. and Howarth, A. T. Numerical analysis of indoor aerosol particle deposition and distribution in two-zone ventilation system. *Building and Environment*, **31**, 41-50 (1996).
Lumley, J. L., Towards a turbulent constitutive relation. *J. Fluid Mech.*, **41** (2), 413-434 (1970).
Lumley, J. L., Computation modelling of turbulent flows. *Adv. Appl. Mech.*, **18**, 123-177 (1978).
Lund, T. S., Ghosal, S. and Moin, P., Numerical experiments with highly-variable eddy viscosity models. In *Engineering Applications to Large Eddy Simulation* (eds U. Piomelli and S. Ragab), 7-11, ASME, New York (1993).
Markatos, N. C., Computer simulation techniques for turbulent flows. *Encyclopaedia of Fluid Mech.*, **6**, *Complex Flow Phenomena and Modeling* (ed. N. P. Cheremisinoff), 1222-1274 (1987).
Mansour, M. N., Kim, J. and Moin, P., Near-wall k-ε modeling. *AIAA J.*, **27**, 1068-1073 (1988).
Mason, P. J. and Callen, N. S., On the magnitude of the subgrid-scale eddy coefficient in large-eddy simulations of turbulent channel flows. *J. Fluid Mech.*, **162**, 439-462 (1986).
Mellor, G. L. and Herring, H. J., A survey of the mean turbulent field closure models. *AIAA J.*, **11**, 590 (1973).
Meneveau, C. and Lund, T. S., Dynamic model with scale-dependent coefficients in the viscous range. In *Proc. of the Summer Program 1996*, Centre for Turbulence Research, Stanford University, 275-290 (1996).
Meneveau, C., Lund, T. S. and Cabot, W., A Lagrangian dynamic subgrid-scale model of turbulence. *J. Fluid Mech.*, **319**, 353-385 (1996).
Moin, P., Squires, W., Cabot, W. and Lee, S., A dynamic subgrid-scale model for compressible turbulence and scalar transport. *Phys. Fluids A*, **3** (11), 2746-2757 (1991).
Moin, P. and Jimenéz, J., Large eddy simulation of complex turbulent flows. *AIAA Paper*, AIAA-93-3099, Orlando (1993).
Mundt, E., *The Performance of Displacement Ventilation Systems: Experimental and Theoretical Studies*. Ph. D. Thesis, Royal Institute of Technology, Stockholm (1996).
Myong, H. K., and Kasagi, N., A New proposal for a k-ε turbulence model and its evaluation, 1st Report, Development of the model. *Trans. Japan Soc. Mech. Engrs.*, Series B, **54**, 3003-3009 (1988).
Nallasamy, M., Turbulence models and their applications to the prediction of internal flows: A review. *Computer & Fluids*, **15**, 151-194 (1987).
Nagano, Y., and Tagawa, M., An improved k-ε model for boundary layer flows. ASME *Journal of Fluid Engineering*, **112**, 33-39 (1990)
Nagano, Y. and Shimada, M., Rigorous modeling of dissipation-rate equation using direct simulations. *JSME International Journal B*, **38**, 51-59 (1995).
Nauman, E. B., Residence time distributions and micromixing. *Chem. Engng Commun.*, **8**, 53-131

(1981).
Nielsen, P. V., Airflow simulation techniques - Progress and trends. In *Proceedings 10th AIVC Conference*, **1**, 205-223 (1989).
Nielsen, P. V., *Displacement Ventilation: Theory and Design*. Aalborg University, Aalborg (1993)
NIOSH, *Guidance for Indoor Air Quality Investigations*, Cincinnati, Ohio, NIOSH, U. S. A..
Paolucci, S. and Chenoweth, D. R., Transition to chaos in a differentially heated vertical cavity. *J. Fluid Meh.*, **201**, 379-410 (1989).
Park T. S. and Sung, H. J., A nonlinear low-Reynolds-number k-ε model for turbulent separated and reattaching flows–I. Flow field computations. *Int. J. Heat and Mass Transfer*, **38**, 2657-2666 (1995).
Patankar, S. V., *Numerical Heat Transfer and Fluid Flow*. McGraw-Hill, Washington (1980).
Patel, V. C., Rodi, W. and Scheuerer, G., Turbulence models for near-wall and low Reynolds number flows: A review. *AIAA J.*, **23**, 1308-1319 (1984).
Patel, V. C., and Yoon, J. Y., Application of turbulence models to separated flow over rough surfaces. *ASME Journal of Fluid Engineering*, **117**, 234-241 (1995).
Peng, S-H. and Peterson, F., An investigation of indoor thermal sensation for Swedish people. *Report*, Department of Heating and Ventilation, Royal Institute of Technology, Stockholm (1993a).
Peng, S-H., Displacement ventilation: A case study. *Report*, Department of Heating and Ventilation, Royal Institute of Technology, Stockholm (1993b).
Peng, S-H., Analytical method for buoyant convective flow calculations. *Report*, Department of Heating and Ventilation, Royal Institute of Technology, Stockholm (1993c).
Peng, S-H. and Peterson, F., New wall functions for the numerical simulation of air flow in ventilated rooms. In *Proceedings of European Conference on Energy Performance and Indoor Climate in Buildings*, **3**, 913-918, Lyon, France (1994a).
Peng, S-H., Remarks on computer programming for numerical calculation of indoor air flows. *Report*, Department of Heating and Ventilation, Royal Institute of Technology, Stockholm (1994b).
Peng, S-H. Indoor air flow and indoor air flow simulation: A review and evaluation. *Climate and Buildings*, No. **2**, 5-98 (1994c).
Peng, S-H. and Peterson, P., Convection from a cold window with simulated floor heating by means of a transiently heated flat unit. *Energy and Buildings*, **23**, 95-103 (1995).
Peng, S-H., Investigation of draft risk due to cold window in a climate chamber. In *Proc. of 7th Int. Conf. on Indoor air Quality and Climate*, **1**, 245-250, Nagoya, Japan (1996a).
Peng, S-H., Davidson, L. and Holmberg, S., Performance of two-equation turbulence models for numerical simulation of ventilation flow. In *Proc. of 5th Int. Conf. on Air Distribution in Rooms*, **2**, 153-160. Roomvent '96, Yokohama, Japan (1996b).
Peng, S-H., Davidson, L., and Holmberg, S., The two-equation turbulence k-ω model applied to recirculating ventilation flows, *Report* **96/13**, Department of Thermo and Fluid Dynamics, Chalmers University of Technology, Gothenburg, Sweden (1996c).
Peng, S-H., Davidson, L., and Holmberg, S., A modified low-Reynolds-number k-ω model for internal flows in ventilated enclosures, *Report* **96/26**, Department of Thermo and Fluid Dynamics, Chalmers University of Technology, Gothenburg, Sweden (1996d).
Peng, S-H., Davidson, L., and Holmberg, S., Application and modifications of two-equation turbulence k-ω model for recirculating ventilation flows. *Arbetslivsrapport* **1996:20**, National Institute for Working Life, Stockholm, Sweden (1996e).
Peng, S-H. Holmberg, S. and Davidson, L., On the assessment of ventilation performance with the aid of numerical simulations. *Building and Environment*, **32**, 497-508 (1997a).
Peng, S-H. and Davidson, L., Towards the determination of regional purging flow rate. *Building and Environment*, **32**, 513-525 (1997b).
Peng, S-H., Davidson, L. and Holmberg, S., A modified low-Reynolds-number k-ω model for recirculating flows. *ASME Journal of Fluid Engineering*, **119**, 867-875 (1997c).
Peng, S-H. and Davidson, L., Computation of turbulent buoyant flow in enclosures with low-Reynolds-number k-ω models. Submitted to *Int. J. Heat and Fluid Flow* (1997d).

Peng, S-H. and Davidson, L., A proposed subgrid-scale model in large eddy simulation for turbulent thermal convection flow. *Report* **97/21**, Department of Thermo and Fluid Dynamics, Chalmers University of Technology, Gothenburg, Sweden (1997e).

Peng, S-H. and Davidson, L., Comparison of subgrid-scale models in LES for turbulent convection flow with heat transfer. To be presented at *2nd EF Conference Turbulent Heat Transfer*, Manchester, U.K., May 31-June 5 (1998a).

Peng, S-H. and Davidson, L., Large eddy simulation for turbulent buoyant flows induced by differentially heated vertical walls. *Report* **98/8**, Department of Thermo and Fluid Dynamics, Chalmers University of Technology, Gothenburg, Sweden (1998b).

Peng, S-H. and Davidson, L., Numerical study of personal exposure to contaminants and draft risk in a workshop with displacement ventilation. To be presented at *6th Int. Conf. on Air Distribution in Rooms*, Stockholm, Sweden, June 14-17 (1998c).

Peng, S-H., New scales for assessing ventilation performance. To be presented at *6th Int. Conf. on Air Distribution in Rooms*, Stockholm, Sweden, June 14-17 (1998d).

Piomelli, U., Moin, P. and Ferziger, J. H., Model consistency in large eddy simulation of turbulent channel flows, *Phys. Fluids*, **31**, 1884-1891 (1988).

Piomelli, U., Applications of large eddy simulations in engineering: An overview. In *Large Eddy Simulation of Complex Engineering and Geophysical Flows* (eds B. Galperin and S. A. Orszag), Cambridge University Press, 121-137 (1993).

Piomelli, U. and Liu, J., Large-eddy simulation of rotating channel flows using a localized dynamic model. *Phys. Fluids*, **7** (4), 839-848 (1995).

Piomelli, U and Chasnov, J. R., Large eddy simulation: Theory and applications. In ERCOFTAC Series, **2**, *Turbulence and Transition Modelling* (eds M. Hallbäck, D. S. Henningson, A. Johansson and P. H. Alfredsson), 269-336, Kluwer Academic Publishers (1995).

Prandtl, L., Überdie ausgebildete Turbulenz. *ZAMM*, **5**, 136-139 (1925)

Prandtl, L., Bemerkungen zur Theorie der freien Turbulenz. *ZAMM*, **22**, 241-243 (1942).

Reynolds, W. C., Computation of turbulent flows. *Ann. Rev. Fluid Mech.*, **8**, 183-208 (1976).

Reynolds, W. C., The potential and limitations of direct and large eddy simulations. In *Whither turbulence? Turbulence at the Crossroads*, Lecture Notes in Physics (ed. J. L. Lumley), **357**, 313-343 (1989).

Reynolds, O., On the extend and action of the heating surface for steam boilers, *Proc. Lit. Phil. Soc.*, **14**, 7-12 Manchester(1884).

Rhie, C. M. and Chow, W. L., Numerical study of turbulent flow past an airfoil with trailing edge separation. *AIAA J.*, **21**, 1527-1532 (1984).

Riffat, S. B., Cheong, K. W., Adam, N. and Shao, L., Measurement and computational fluid dynamics modelling of aerosol particles in buildings. *Indoor Environment*, **4**, 289-296 (1995).

Roache, P. J., Perspective: A method for uniform reporting of grid refinement studies. *ASME Journal of Fluid Engineering*, **116**, 405-413 (1994).

Robinson, B. A. and Tester, J. W., Characterization of flow maldistribution using inlet-outlet tracer techniques: an application of internal residence time distributions. *Chem. Engng Sci.*, **41**, 469-483 (1986).

Rodi, W., A new algebraic relation for calculating the Reynolds stresses. *ZAMM*, **56**, 219-221 (1976).

Rodi, W., *Turbulence Models and Their Application in Hydraulics – A State of the Art Review*. Institute for Hydromechanics, University of Karlsruhe, Germany (1980).

Rodi, W., and Mansour, M. N., Low Reynolds number k-ε modelling with the aid of direct simulation data, *J. Fluid Mech.*., **250**, 509-529 (1993).

Rodi, W., Simulation approaches for turbulent flows. *ECCOMAS '94*, Published by John Wiley & Sons Ltd., Germany (1994).

Rodi, W., Comparison of LES and RANS calculations of the flow around bluff bodies. In *Proc. 3rd Int. Colloq. on Bluff Body Aerodynamics & Applications*, Blacksburg, Virginial, (1996).

Rogallo, R. S. and Moin, P., Numerical simulation of turbulent flows. *Ann. Rev. Fluid. Mech.*, **16**, 99 (1984).

Rotta, J., Statistische Theorie nichthomogener Turbulenz I. *Z. für Physik*, **129**, 547-572 (1951).
Sandberg, M., The multi-chamber theory reconsidered from the viewpoint of air quality studies. *Building and Environment*, **19**, 221-233 (1984).
Sandberg, M., Blomqvist, C. and Mattsson, M., Turbulence characteristics in rooms ventilated with a high velocity jet. In *Proc. of 12th AIVC Conference*, **2**, Ottawa, Canada (1991).
Savill, A. M., One-point closures applied to transition, In ERCOFTAC Series, **2**, *Turbulence and Transition Modelling* (eds M. Hallbäck, D. S. Henningson, A. Johansson and P. H. Alfredsson), 233-268, Kluwer Academic Publishers (1995).
Schumann, U., Subgrid scale model for finite difference simulation of turbulent flows in plane channel and annuli. *J. Comput. Phys.*, **18**, 376-404 (1975).
Schumann, U., Realizability of Reynolds-stress models. *Phys. Fluids*, **20**, 721-725 (1977).
Schumann, U., Direct and large eddy simulation of turbulence − Summary of the state of the art. *Introduction to the Modelling of Turbulence*, VKI for Fluid Dynamics, Belgium, March 18-21 (1991).
Schumann, U., Subgrid length-scales for large-eddy simulation of stratified turbulence. *Theoret. Comput. Fluid Dyn.*, **2**, 279-290 (1991).
Shih, T.-H. and Lumley, J. L., Kolmogorov behaviour of near-wall turbulence and its application in turbulence modelling. *Comp. Fluid Dyn.*, **1**, 43-56 (1993).
Shih, T.-H., Zhu, J. and Lumley, J. L., A new Reynolds stress algebraic equation model. *NASA TM* 106644 (1994).
Shih, T.-H., Constitutive relations and realizabity of single-point turbulence closures. In ERCOFTAC Series, **2**, *Turbulence and Transition Modelling* (eds M. Hallbäck, D. S. Henningson, A. Johansson and P. Alfredsson), 155-192, Kluwer Academic Publishers (1995).
Skåret, E., Ventilation efficiency - A survey of concepts of ventilation effectiveness, *SINTEF Report* STF15 A84057, Trondhem, Norway (1984).
Smagorinsky, J., General circulation experiments with the primitive equations, Part I. The basic experiment. *Monthly Weather Review*, **91**, 99-152 (1963).
Smagorinsky, J., Some historical remarks on the use of nonlinear viscosities. In *Large Eddy Simulation of Complex Engineering and Geophysical Flows* (eds B. Galperin and S. A. Orszag), Cambridge University Press, 3-36 (1993).
So, R. M. C., Zhang, H. S. and Speziale, C. G., Near-wall modelling of the dissipation rate equations. *AIAA J.*, 29, 2069-2076 (1991).
Spalart, P. R., Direct numerical simulation of a turbulent boundary layer up to R_θ = 1400. *J. Fluid Mech.*, **187**, 61-98, (1988).
Spalding, D. B., A note on mean residence-times in steady flow of arbitrary complexity. *Chem. Engng Sci.*, **9**, 74-78 (1958).
Speziale, C. G., Calilean invariance of subgrid scale stress models in the large eddy simulation of turbulence. *J. Fluid Mech.*, **156**, 55-62 (1985).
Speziale, C. G., On nonlinear k-l and k-ε models of turbulence. *J Fluid Mech.*, **178**, 450-475 (1987).
Speziale, C. G., Turbulence modelling in non-inertial frames of reference. *Theor. Comput. Fluid Dyn.*, **1**, 3 (1989)
Speziale, G. C., Analytical methods for the development of Reynolds-stress closure in turbulence. *Ann. Rev. Fluid. Mech.*, **23**, 107-157 (1991).
Speziale, C. G., Abid, R. and Anderson, E. C., Critical evaluation of two-equation models for near-wall turbulence, *AIAA J.*, **30**, 324- 325 (1992).
Speziale, C. G. and Abid, R., Near-wall integration of Reynolds stress turbulence closures with no wall damping. *AIAA J.*, **32**, 1974-1977 (1995).
Stone, H., Iterative solution of implicit approximations of multidimensional partial differential equations. *SIAM J. Num. Anal.*, **5**, 530-558 (1968).
Sundell, J., On the association between building ventilation characteristics, some indoor environment exposures, some allergic manifestations and subjective symptom reports. *Indoor Air*, Supplement No. **2** (1994).

Tennekes, H. and Lumley, J. L., *A First Course in Turbulence*. The MIT Press, Massachusetts (1978).
To, W. M. and Humphrey, J. A. C., Numerical simulation of buoyant, turbulent flow–I. Free convection along a heated, vertical, flat plate. *Int. J. Heat and Mass Transfer*, **29**, 573-592 (1986).
Turner, S. and Binnie, P. W. H., An indoor air quality survey of twenty-six Swiss office buildings. In *Proceedings Indoor Air '90*, **4**, 27-32, Ottawa, Canada (1990).
van Doormaal, J. P. and Raithby, G. D., Enhancements of the SIMPLE method for predicting incompressible fluid flows. *Numerical Heat Transfer*, **7**, 147-163 (1984).
van Driest, E. R., On turbulent flow near a wall. *J. of Aeronaut. Sci.*, **23**, 1008-1015 (1956).
van Leer, B., Towards the ultimate conservative difference scheme: Monotonicity and conservation combined in a second order scheme. *J. Comput. Phys.*, **14**, 361-370 (1974).
Wallin, S. and Johansson, A. V., A new explicit algebraic Reynolds stress turbulence model including an improved near-wall treatment. In *Flow Modelling and Turbulence Measurements VI*, 399-406 (1996).
Wilcox, D. C., Reassessment of the scale-determining equations for advanced turbulence models. *AIAA J.*, **26**, 1299-1310 (1988).
Wilcox, D. C., Simulation of transition with a two-equation turbulence model. *AIAA J.*, **32**, 247-255 (1994).
Wilcox, D. C., *Turbulence Modelling for CFD*. DCW Industrial, Inc. La Cañada, California (1993).
Wong, V. C., A proposed statistical-dynamic closure method for the linear or non-linear subgrid-scale stresses *Phys. Fluids*, **4** (5), 1080-1082 (1992).
Wong, V. C. and Lilly, D. K., A comparison of two dynamic subgrid closure methods for turbulent thermal convection. *Phys. Fluids*, **6** (2), 1016-1023 (1994).
Yang, Z., and Shih, T. H., New time scale based on k-ε model for near-wall turbulence, *AIAA J.*, **31**, 1192-1198 (1993).
Yakhot, V. and Orszag, S. A., Renormalization group analysis of turbulence: I. Basic Theory. *J. Scientific Computing*, **1**, 3-50 (1986).
Yokhot, A., Orszag, S. A., Yakhot, V. and Israeli, M., Renormalization group formulation of large-eddy simulation. *J. Scientific Computing*, **4**, 139-158 (1989).
Yakhot, V., Orszag, S. A., Thangam, S., Gatski, T. B. and Speziale, C. G., Development of turbulence models for shear flow by a double expansion techniques. *Phys. Fluids A*, **4**(7), 1510 (1992).
Yoshizawa, A. and Horiuti, K., A statistically-derived subgrid-scale kinetic energy model for the large eddy simulation of turbulent flows. *Journal of the Physical Society of Japan*, **54**, 2834-2839 (1985).
Yoshizawa, A. Large eddy simulation of turbulent flows. *Encyclopaedia of Fluid Mechanics*, **6** (ed. N. P. Cheremisinoff), 1277-1297, (1987).
Yuan, X., Moser, A. and Suter, P. Wall functions for numerical simulation of turbulent natural convection along vertical plates. *Int. J. Heat and Mass Transfer*, **30**, 4477-4485 (1993).
Zang, Y., Lund, Street, R. L. and Koseff, J., A dynamic mixed subgrid-scale model and its application to turbulent recirculating flows. *Phys. Fluids A*, **5**, 3186-3196 (1993).
Zvirin, Y. and Shinnar, R., Interpretation of internal tracer experiments and local sojourn time distributions. *Int. J. Multiphase Flow*, **2**, 495-520 (1976).